Molecular toxicity of nanomaterials

Thesis

submitted in fulfilment of the requirements for the degree of

Doctor of Philosophy

to

The University of the Basque Country/Euskal Herriko Unibertsitatea

By

SIMON PAUL JEREMIE POLY

2013

Universidad del País Vasco
Euskal Herriko Unibertsitatea

CIC nanoGUNE
nanoscience cooperative research center

Thesis Supervisor

Prof. Dr. Félix María Goñi Urcelay

Biophysics Unit

Universidad del País Vasco/ Euskal Herriko Unibertsitatea and Consejo Superior de Investigaciones Científicas.

Universidad del País Vasco Euskal Herriko Unibertsitatea

AUTORIZACION DEL DIRECTOR DE TESIS

PARA SU PRESENTACION

Dr. Félix M. Goñi Urcelay, con N.I.F. 15 232 184C, como director de la tesis doctoral: "Molecular toxicity of nanomaterials", realizada en el Departamento de Bioquímica y Biología Molecular y cicNanogune por el doctorando D. Simon Poly, autorizo la presentación de la citada tesis doctoral, dado que reúne las condiciones necesarias para su defensa.

En Leioa, a 11 de marzo de 2013

EL DIRECTOR DE LA TESIS

Fdo.: _____

Universidad del País Vasco Euskal Herriko Unibertsitatea

CONFORMIDAD DEL DEPARTAMENTO

El Consejo del Departamento de Bioquímica y Biología Molecular, en reunión celebrada el día de de 2013, ha acordado dar la conformidad a la admisión a trámite de presentación de la tesis doctoral titulada "Molecular toxicity of nanomaterials", dirigida por el Dr. D. Félix María Goñi Urcelay, y presentada por D. Simon Poly ante este departamento.

En Leioa, a….. de ……. de 2013.

Vº Bº DIRECTOR DEL DEPARTAMENTO SECRETARIA DEL DEPARTAMENTO

Fdo.: __J.L. Nieva Escandón Fdo.: H. Ostolaza Etxabe

Universidad del País Vasco Euskal Herriko Unibertsitatea

ACTA DE GRADO DE DOCTOR
ACTA DE DEFENSA DE TESIS DOCTORAL

DOCTORANDO: D. SIMON POLY.

TITULO DE LA TESIS: “Molecular toxicity of nanomaterials”.

El tribunal designado por la Subcomisión de Doctorado de la UPV/EHU para calificar la tesis doctoral arriba indicada y reunido en el día de la fecha, una vez efectuada la defensa por el doctorando y contestadas las objeciones y/o sugerencias que se le han formulado, ha otorgado por_____la calificación de:

unanimidad ó mayoría

APTO o NO APTO

Idioma/s de defensa (en caso de más de un idioma, especificar apartados o porcentaje defendido en cada idioma):

_____

En _____a _____de _____de _____

EL/LA PRESIDENTE/A, EL/LA SECRETARIO/A,

Fdo.: Fdo.:

Dr/a: _____ Dr/a:

_____

VOCAL 1º, VOCAL 2º, VOCAL 3º,

Fdo.: Fdo.: Fdo.:

Dr/a: _____Dr/a:_____Dr/a:_____

EL/LA DOCTORANDO/A,

Fdo.: _____

A la fin, toutes choses viennent se fondre en une seule, et au milieu coule une rivière.

Norman Mc LEAN. La Rivière du sixième jour (USA, 1976)

1. Declaration

I solemnly declare that this thesis is exclusively the work of M. Simon Poly. All results, figures, and data presented within this thesis were performed by M. Simon Poly at CIC nanoGUNE.

2. Resumen y Abstract

En los últimos 20 años un nuevo tipo de materiales, los nanomateriales, han aparecido en la vida cotidiana y han atraído amplia atención debido a sus propiedades peculiares. Los nanomateriales, obtenidos a partir del desarrollo de la nanociencia, tienen propiedades particulares procedentes de sus dimensiones nanométricas. Ellos representan un nuevo paso en la ingeniería de los procesos de reducción del tamaño de los productos y traen nuevas capacidades y conocimiento a materiales de uso cotidiano.

Las inusuales propiedades ópticas, mecánicas y magnéticas de los nanomateriales permiten su uso potencial para la optimización de dispositivos biomédicos. Nanomateriales como los grafenos podrían ser utilizados en la detección microbiana y dispositivos de diagnóstico. Después de haber cambiado químicamente la superficie del grafeno uno puede utilizarlo para desarrollar nuevas tecnologías, por ejemplo biomédicas. Además, se sabe que las hojas de óxido de grafeno son altamente tóxicas para las bacterias y se podrían utilizar dentro de superficies bactericidas para productos de higiene y envases de alimentos.

Del mismo modo se ha demostrado que otro nanomaterial, las nanopartículas de semiconductor, llamadas puntos cuánticos (quantum dots, QD), absorben la luz UV y emiten luz fluorescente con una longitud de onda media dependiente de sus tamaños. El acoplamiento de las propiedades ópticas atípicas de QD y de la posibilidad de unirlas covalentemente con moléculas de seguimiento específico en su superficie las pueden hacer utilizables como marcadores para seguir una sola molécula adentro de una célula in vivo o ex vivo.

QD son más brillantes y más estables que las sondas fluorescentes convencionales, por lo tanto, han demostrado una amplia aplicabilidad a la imaginería medica como colorantes fluorescentes específicos. Además, acoplados a una molécula diana, pueden ser utilizados para lograr imágenes de células con alta sensibilidad. Su tamaño extremadamente pequeño permite la adquisición de muchas imágenes de planos focales y la reconstrucción de imágenes en 3D que representan la distribución de las moléculas de interés dentro de las células in vivo o ex vivo. Gracias a la alta resolución y la capacidad de seguimiento en tiempo real de la fluorescencia de los QD, el movimiento de una molécula de interés puede ser seguido durante largos períodos de tiempo. También esto será posible gracias a la capacidad de unir

anticuerpos, estreptavidina, péptidos, aptámeros, o ligandos de pequeño tamaño en la superficie QD de una manera altamente controlada.

Debido a su pequeño tamaño, su alta capacidad de dispersión, y la ausencia de drenaje linfático en los tumores, los QD pueden usarse para suministrar moléculas de silenciación de genes en células cancerosas.

Sin embargo, estudios recientes han demostrado que los nanomateriales presentan posibles riesgos para la salud humana. Estos riesgos para la salud son, fundamentalmente, dependientes de los materiales utilizados en su preparación, pero también el tamaño extremadamente pequeño de los nanomateriales y sus grandes superficies resultan en una alta capacidad para ser inhalados, ingeridos, o de absorberse atreves de la piel. Los nanomateriales incorporados en materiales compuestos en dispositivos biomédicos implantados directamente podrían ser liberados en el tejido vivo y su alta penetración y distribución en los organismos vivos generan otro peligro potencial. Por ejemplo, se ha demostrado que las nanopartículas son capaces de trasladarse lejos de su lugar de entrada a través de la sangre y de depositarse en sitios distantes como el riñón, que parece ser incapaz de eliminarlos.

Se ha demostrado recientemente que algunos nanomateriales inducían toxicidad en las células in vitro. Esta toxicidad parece originarse de la gran superficie en relación con el volumen de las nanopartículas, eso hace que las nanopartículas pueden ser muy reactivas, y en algunas situaciones catalíticas. En el interior de los medios acuosos, algunos QD han demostrado que pueden liberar iones de metales pesados que son tóxicos por fotólisis o hidrólisis cuando su revestimiento de polímero está dañado o imperfecto. Por ejemplo, algunos estudios han demostrado que las nanopartículas de CdSe no son estables en medios biológicos. Estas nanopartículas liberan iones tóxicos de cadmio en el medio circundante debido a su fotólisis o hidrólisis. La presencia de una baja cantidad de iones cadmio puede ser altamente tóxica para las células en cultivo.

También, debido a la alta reactividad de la superficie de los nanomateriales, estos pueden catalizar la formación de especies reactivas de oxígeno (ROS) a partir de las moléculas ambientes. La presencia de ROS puede conducir a la muerte de las células por necrosis a través de la ruptura de la membrana celular debido a la peroxidación de los lípidos que la constituyen. También la presencia de ROS puede conducir a la muerte de las células por apoptosis, a través de los daños generados por ROS sobre las proteínas, lípidos, y el ADN de las células.

La generación de iones tóxicos y de radicales libres tóxicos en la superficie del nanomaterial crea dos toxicidades celulares: una directa y otra indirecta. Los mecanismos de toxicidad conectados con estas dos toxicidades han sido ampliamente estudiados y son bien conocidos actualmente.

Recientemente, otro nivel de toxicidad fue descubierto; este nivel puede ser calificado de toxicidad molecular de los nanomateriales. Se demostró que diversos nanomateriales, como las nanopartículas de óxido de hierro, las nanopartículas de óxido de zinc, las nanopartículas de dióxido de titanio, los nanotubos de carbono, y las nanopartículas de óxido de cobre, eran capaces de inducir daños en el ADN cuando interactúan físicamente. El proceso por el cual el daño ocurre no está claro por el momento, pero podría originarse de la valencia de la superficie de estos nanomateriales y intervenir a través de un fenómeno de oxidación de la molécula de ADN.

Sin embargo, se demostró que la presencia de nanomateriales en los fluidos biológicos podría crear inestabilidad en la estructura de las biomoléculas. La capacidad de los nanomateriales de adsorber a biomoléculas sobre su superficie, debido a su gran área superficial, fue demostrada claramente. Pero un análisis reciente de las capas de biomoléculas, recubriendo la superficie de las nanopartículas de oro, han mostrado que éstas presentan una estructura tridimensional ligeramente modificada por comparación a las biomoléculas dispersas.

Este efecto ha sido cuestionado y aunque algunos estudios han demostrado tales efectos de los nanomateriales sobre las biomoléculas, otros no han mostrado ningún efecto de los nanomateriales en las mismas biomoléculas.Un efecto modificador de los nanomateriales sobre las biomoléculas podría ser muy preocupante para ciertas proteínas, cuyo replegamiento puede conducir a la aparición de elementos tóxicos en el organismo.

Estas proteínas son llamadas material amiloide y son péptidos y proteínas que nativamente o bajo ciertas condiciones pueden someterse a un replegamiento de su estructura interna que conduce a una mayor tendencia a la agregación. Esta agregación, también llamada fibrilizacion amiloide, presenta un alto grado de organización y genera agregados y fibras micrométricas que son tóxicos para las células.

Desgraciadamente, recientes artículos científicos han demostrado que algunas nanopartículas parecen ser capaces de mejorar la fibrilizacion de péptido amiloide

como el péptido A□ (1-42). En cuanto a proteínas estables este efecto no fue todavía demostrado para todos los tipos de nanopartículas. Y la razón de esta diferencia de efecto no es conocida actualmente. Los pequeños agregados solubles de Aβ son conocidos por ser extremadamente tóxicos para las células. Se demostró que eran capaces de generar ROS en el medio circundante y de oxidar directamente los lípidos de la membrana celular. Esta oxidación y la presencia de óxido reactivo pueden explicar la muerte de las células: directamente por necrosis a través de una brecha en la membrana o indirectamente por apoptosis inducida por los oxidantes. Los materiales amiloide están implicados en un gran número de enfermedades degenerativas, también llamadas proteopatías, para las cuales no hay curas conocidas. Entre esas proteopatías uno puede encontrar la enfermedad de Alzheimer (AD) o la enfermedad de Parkinson, dos enfermedades cuya incidencia se prevé que aumentará drásticamente en las próximas décadas. La posibilidad de que la presencia de nanomateriales en el medio ambiente juegue un papel en la incidencia de estas proteopatías tiene que ser investigada. Una de las formas para clarificar esta posible relación es analizar el efecto de los nanomateriales sobre péptidos y proteínas implicados en estas enfermedades in vitro.

En este estudio hemos demostrado que el efecto de los nanomateriales en la estabilidad de estructura de proteínas se debe a la carga presente en la superficie de los nanomateriales. En efecto, nuestra hipótesis de trabajo era que la fuerza principal que causa el comportamiento pro-amiloidosis fuera la carga presentada en la superficie de las nanopartículas. Con el fin de probar esto, hemos desarrollado nanopartículas de la misma composición química, forma, estructura superficial, y tendencia de agregación, pero con un valor diferente de carga en su superficie. Estas nanopartículas fueron incubadas con diferentes biomoléculas: el Aβ que es un péptido amiloide fuertemente inestable, la insulina, una proteína que es inestable sólo bajo condiciones muy desestabilizadores, y la albúmina de suero bovino (BSA), una proteína grande conocida por su estabilidad bajo condiciones de desestabilización. Al analizar al mismo tiempo la estructura de estas biomoléculas, la distribución de tamaño en diferentes mezclas, y la presencia de estructuras intermoleculares especificas de amiloide, hemos sido capaces de comprender la acción de la carga de las nanopartículas sobre la agregación de los péptidos y proteínas.

En esta tesis hemos demostrado que diferentes proteínas reaccionan de manera específica a la misma carga en la superficie de un nanomaterial definido. Curiosamente, hemos demostrado que la presencia de cargas positivas en la superficie de los QD inhibe la formación de agregados amiloideos de Aβ y favorece la formación de una capa de péptidos no estructurados en esta superficie. También la presencia de cargas positivas en la superficie de los QD indujo una agregación débil de insulina o BSA en esta superficie pero no indujo el replegamiento amiloide de estas proteínas. Por oposición, la presencia de carga negativa en la superficie de los QD parece mejorar la fibrilizacion amiloide de Aβ y de insulina. También, las cargas negativas inducen la agregación de BSA en la superficie de los QD, pero parecen no tener ningún efecto sobre la estructura interna de BSA. Este efecto de aumento por las cargas negativas parece ser dependiente de la estabilidad interna de las biomoléculas. Sorprendentemente, los QD que llevan cargas negativas débiles parecen inducir o mejorar la agregación amiloide de proteínas relativamente estables, como la insulina, mientras que los péptidos inestables, como Aβ, parecen estar más influenciados por las cargas fuertemente negativas.

Al modificar el radio de los QD, demostrábamos que el efecto de los nanomateriales sobre la estructura de la proteína es dependiente no sólo de la carga presente en su superficie sino además de la distribución de estas cargas en la superficie. De hecho la insulina parece agregarse a cualquier QD que lleva cargas negativas débiles pero sólo los QD que tienen un tamaño de núcleo de 3,3 nm parecen ser capaces de inducir el replegamiento de la proteína y de iniciar la formación de agregados amiloideos. Nuestra hipótesis para explicar este efecto es que las proteínas en suspensión no reaccionan frente a una carga específica presentada en la superficie de los QD sino a una distribución especifica de carga tridimensional.

Sobre la base de estos datos, hemos sido capaces de desarrollar un nuevo tipo de agente terapéutico basado en una distribución de carga controlada en la superficie de unos nanomateriales que permiten una interacción específica de esos nanomateriales y de proteínas especificas sin necesitar el uso de moléculas de reconocimiento. Anteriormente, se había demostrado que mediante una selección apropiada de los grupos químicos en la superficie de los QD se podría crear QD con un efecto de agregación no amiloide de péptidos inestables. Por lo tanto, se podría crear QD con la capacidad de agregar unos péptidos amiloideos tóxicos específicos, como Aβ, con el

fin de reducir su efecto tóxico en el organismo mediante sus eliminaciones por el sistema inmunitario.

Dado que se había demostrado antes que la presencia de cargas positivas en la superficie de los QD induce una agregación no amiloide de Aβ, hemos desarrollado un QD estable en medios orgánicos, capaces de interactuar fuertemente con un Aβ péptido, y con una capacidad limitada de endocitosis en las células vivas. En esta tesis hemos demostrado que nuestro producto estaba cumpliendo con estos tres objetivos, pero que tenía un potencial uso terapéutico limitado debido a su efecto sobre una otra proteína de prueba, la insulina. Nuestra hipótesis es que estos efectos secundarios se deben a la presencia de carga negativa débil, en la superficie de los QD, utilizada para estabilizarlos en tampón fisiológico y que ya se demostró que era capaz de inducir el replegamiento de la insulina amiloide. Sin embargo, este trabajo demuestra la viabilidad de tal sistema y uno se puede imaginar que un sistema similar, usando otros grupos químicos para estabilizar los QD o cambiando el esquema de las cargas débiles, podría ayudar en la eliminación de estos péptidos Aβ del organismo por los macrófagos y/o microglia. Además, mediante la sustitución de los QD por nanopartículas superparamagnéticas se podría pensar en eliminar específicamente estos péptidos de los organismos vivos.

El descubrimiento del efecto de repartición de las cargas en la superficie de los objetos de tamaño nanométrico sobre las biomoléculas circundantes abre el camino a una mejor comprensión de la toxicidad de los nanomateriales y al desarrollo de nuevos nanomateriales con una estabilidad in vivo mejorada para aplicaciones biomédicas (por ejemplo, suministro de fármacos, implantes biomédicos, y agentes de marcado). El desarrollo de recubrimientos nanoestructurados con tecnologías de control de la distribución de cargas podría mejorar el desarrollo de implantes bio-compatibles, y otros sistemas biónicos, reduciendo la necesidad de tratamiento con drogas inmunosupresoras. En efecto, si la superficie de los implantes se recubriera con una distribución controlada de cargas a la escala del nanómetro, que proporcionara propiedades immuno-furtivas y de prevención de la formación de agregados de proteína al contacto entre el implante y la materia orgánica, aumentaría la vida útil de tales sistemas y se prevendrían complicaciones para los pacientes, como la formación de trombos en la sangre.

Nanomaterials have attracted widespread attention due to their peculiar properties, originating from their nanometre-scale dimension. The unusual optical, mechanical, and magnetic properties of nanomaterials allow their application in the development of more efficient biomedical devices. However, recent studies have proved that due to the materials used in their preparation and to their nanometre-scale dimensions, nanomaterials present possible risks for human health. Indeed, it was demonstrated that some nanomaterials could induce cellular toxicity *in vitro* because of the seeding of toxic ions and to the generation of toxic free radicals at the nanomaterial surface. These direct and indirect cellular toxicity mechanisms of nanomaterials have been thoroughly studied and are currently well-known but another level of toxicity has been recently discovered, namely the molecular toxicity of nanomaterials. It has been demonstrated that the presence of nanomaterials in biological fluids could create instabilities in the structure of biomolecules. Various studies have shown such effects of nanomaterials on different biomolecules. Within this study we have demonstrated that the effect of nanomaterials on protein structure stability is due to the charge present at the surface of nanomaterials. We showed that different proteins will react differently with the same charge at the surface of nanomaterials. Interestingly, we demonstrated that the effect of nanomaterials on protein structure was dependent not only on the charge present at the surface of nanomaterials but more importantly on the distribution of charge at the surface. On the basis of these data, we were able to develop a new type of therapeutic agent based on controlled charge distribution at the surface of nanomaterials allowing specific interaction of nanomaterials and target protein without the need for coupled recognition molecules. This new agent is able to specifically interact with pathological proteins and aggregate them in a safe way in order to ease their removal from living organisms. Furthermore this discovery opens the way to a better understanding of nanomaterial toxicity and to new nanomaterial with increased *in vivo* stability for biomedical applications e.g. drug-delivery, biomedical implants, and tagging agents.

3. Acknowledgements

This work was supported by the French National Research Agency (Agence Nationale de Recherche, ANR) under grant ANR-08-BLAN-0185, NATO grant SfP-983207 Advanced Biochips and FP7 project NMP-2009-4.0-3-246479 NAMDIATREAM. Support of the Region Champagne-Ardenne and FEDER funding through project HYNNOV is also acknowledged.

4. Table of contents

1. Declaration 7
2. Abstract 8
3. Acknowledgement 15
4. Table of content 16
5. Introduction: 18
   5.1. Implications of protein and polypeptide structure instability: from physiological to pathological secondary structures 18
      5.1.1. The natural instabilities of amyloid peptides 20
      5.1.2. Necessity of protein structure stabilization and internal restructuration of the secondary structure 26
      5.1.3. Direct and indirect toxicities of amyloid soluble aggregates 30
   5.2. Nanomaterials: Definitions and relevant structures 34
      5.2.1. Nanomaterials 34
      5.2.2. Nanoparticles 37
      5.2.3. Quantum Dots 39
   5.3. Impact of nanomaterials on living beings 41
      5.3.1. Impact of nanomaterial-containing macro-objects 42
      5.3.2. Direct impact of nanomaterials 43
   5.4. Aim of the thesis 47
6. Materials and methods 48
   6.1. Materials 48
      6.1.1. Chemical table 48
      6.1.2. QD synthesis 50
   6.2. Methods 52
      6.2.1. Analytical techniques and tools 52
      6.2.2. QD solubilisation 58
      6.2.3. Protein and peptide preparation 60
7. Results 62
   7.1. PEGylated CdSe/ZnS quantum dots induced human insulin amyloid fibrillisation under physiological conditions 62
      7.1.1. Interactions of PEGylated QD with human insulin *in vitro* 62
      7.1.2. PEGylated QD induced Insulin aggregation 64
      7.1.3. QD-induced insulin aggregation displays similarities with amyloid fibrillisation phenomena 66
      7.1.4. Effect of QD concentration on QD-related insulin fibrillisation 72

7.1.5. Effect of temperature on QD-related insulin fibrillisation 74
7.1.6. Effect of pH on QD-related insulin fibrillisation 76
7.1.7. The effect of QD surface charges on QD-related insulin fibrillisation 78
7.1.8. The effect of surface charge distribution on the QD-related insulin fibrillisation 80
7.2. PEGylated CdSe/ZnS QD modify the kinetics of amyloid β (1-42) peptide fibrillisation and of bovine serum albumin aggregation under physiological conditions 82
7.2.1. QD interact with Aβ and BSA to form aggregates 82
7.2.2. QD-Aβ interactions are dependent on QD surface charges 84
7.2.3. QD-BSA interactions are dependent on QD surface charges 86
7.2.4. QD induces changes in the kinetics of Aβ secondary structure modifications 86
7.2.5. QD induces no changes in the BSA secondary structure 89
7.2.6. Impact of QD on Aβ amyloid fibrillisation is charge-dependent 89
7.2.7. QD does not induce amyloid fibrillisation of BSA 92
7.3. The design of specifically generated PEGylated CdSe/ZnS quantum dots, invisible to insulin and capable of inhibiting Aβ amyloid fibrillisation under physiological conditions 93
7.3.1. The generation of electrically-neutral QD, containing specific surface charges. 93
7.3.2. The interaction of electrically-neutral QD with Aβ reduces amyloid fibrillisation 96
7.3.3. Interactions of electrically-neutral QD with insulin give rise to amyloid fibrillisation 102
8. General Discussion 108
8.1. Surface charge distribution effect on biomaterials is dependent of and specific for the studied biomaterial and incubation conditions 108
8.1.1. NPs effect on stable proteins 108
8.1.2. Nanoparticle effect on amyloid-prone peptide and protein 111
8.2. The use of nanomaterials as therapeutic agents against amyloidosis-related diseases 115
8.2.1. Controlling nanomaterial surface to modulate effect on amyloid protein and peptide 116
8.2.2. Modifying charge at the nanoparticle surface 117
9. Perspective 121
10. Conclusions 121
11. References 122

5. Introduction:

5.1. Implications of protein and polypeptide structure instability: from physiological to pathological secondary structures

The discovery of the link between the physiologically important protein structure-related dysfunctions or proteopathies and such diseases as Alzheimer's, Parkinson's Creutzfeldt-Jakob, or type II diabetes is one of the major research breakthroughs in medical research in the last 20 years. These diseases, like Alzheimer's, which is supposed to affect up to 1 in 85 people by the year 2050 [1], were described in the beginning of the 20th century and were not thought to originate from the same mechanism [2]. The identification of the general mechanism of appearance of these diseases has generated a profound reconsideration of the physiological roles of protein structure and is currently at the origin of a profound revision of previously agreed cellular renewal mechanisms [3].

The first well-characterized proteopathy was Parkinson's disease, whose symptoms were first described and identified as originating from a single disease in 1817 by the apothecary James Parkinson [4]. His analysis was based on the observation of apparent, progressive and recurrent symptoms in elderly patients. Further in the course of the 19th century, a more elaborated symptom description was carried out by several neurologists [5]. Discovery in the 19th century of abnormal protein aggregates called amyloid and developing in the brain, inside or outside of neuron bodies, opened a new era in proteopathy research [6]. Characterization, in the first half of the 20th century, of the anatomic structures affected by the proteopathy was followed by identification of biochemical changes in brain neurotransmission thus providing the first insight on the molecular mechanisms of the amyloidosis-related diseases [6]. Fundamental studies in the second half of the 20th century have clearly demonstrated the important role of protein secondary structure modifications in the mechanism of amyloidosis development. Then the discovery of the proteinaceous infectious particles or prions provided a clear proof for the possibility of self-propagating proteopathies [6].

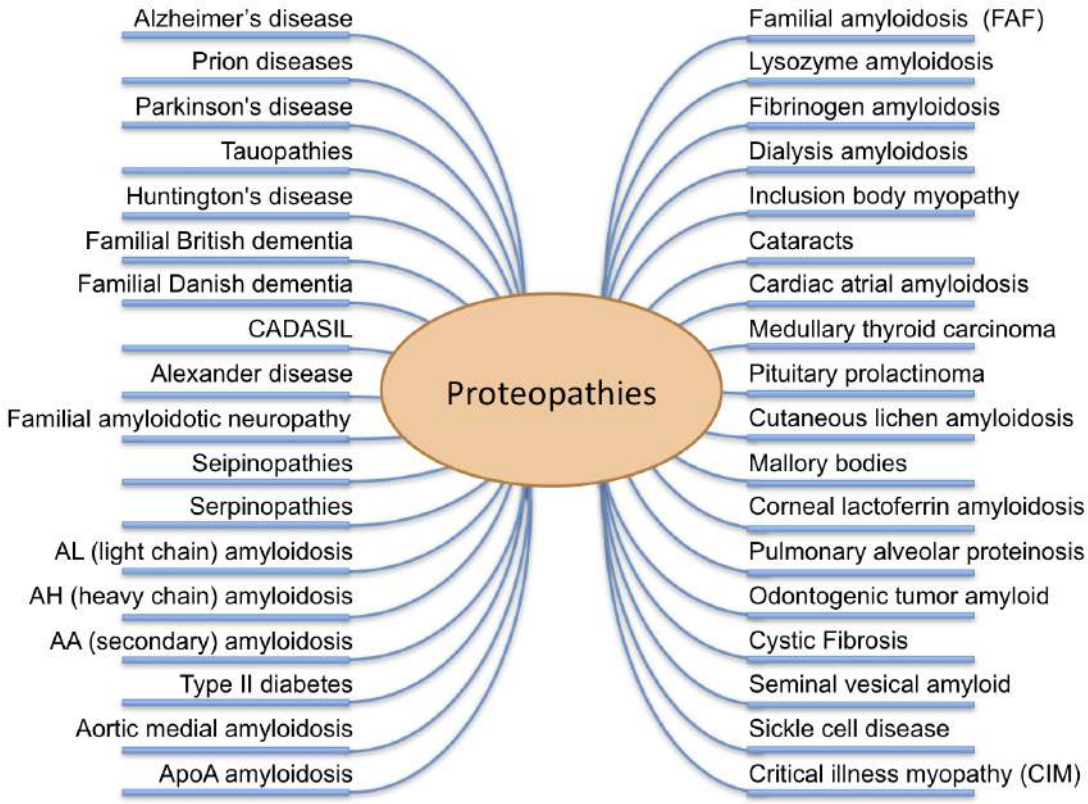

Figure 1. Diseases related to amyloid polymerization of identified proteins or peptides. Proteopathies are pathologies related to the natural protein refolding and polymerization events taking place in every human tissue. Some of these diseases can be classified either as genetic proteopathies, originated from mutations, or as spontaneous proteopathies, caused by environmental factors.

5.1.1. The natural instabilities of amyloid peptides

From the first observation of amyloid protein plaques in the brain of Alzheimer's patients to the identification of amyloid β-peptide (Aβ) as the main constituent of these plaques and then later the characterisation of inter-protein structural interactions inside the plaques, a long way has been walked [6]. Research has arrived to a point in which it is possible to relate the fundamental knowledge obtained on amyloid β-peptide pathological re-folding to numerous other protein folding diseases thus to link the mechanism behind the Alzheimer's disease to a large array of diseases [7]. Among these diseases some are impacting on an important part of the population (Figure 1) but others have limited epidemiologic repercussions. Nevertheless, all of them can be characterised by the protein or peptide constituting their pathological aggregates and by the event initiating the transformation from a physiological form of these molecules to a pathological form [8]. Different types of events that can possibly initiate the transformation of amyloid peptides or proteins from a physiological form to a pathological one are summarized in figure 2. In some cases, the protein or peptide pathological refolding is due to the instability of the protein or peptide under physiological conditions [9]. These peptides or proteins will partially unfold and refold into well-characterized β-cross structure, responsible for their aggregating behaviour and consequently for cellular toxicity [9]. In these cases, the important point will be to identify the event leading to the appearance of the pathological peptide or protein in the physiological compartment.

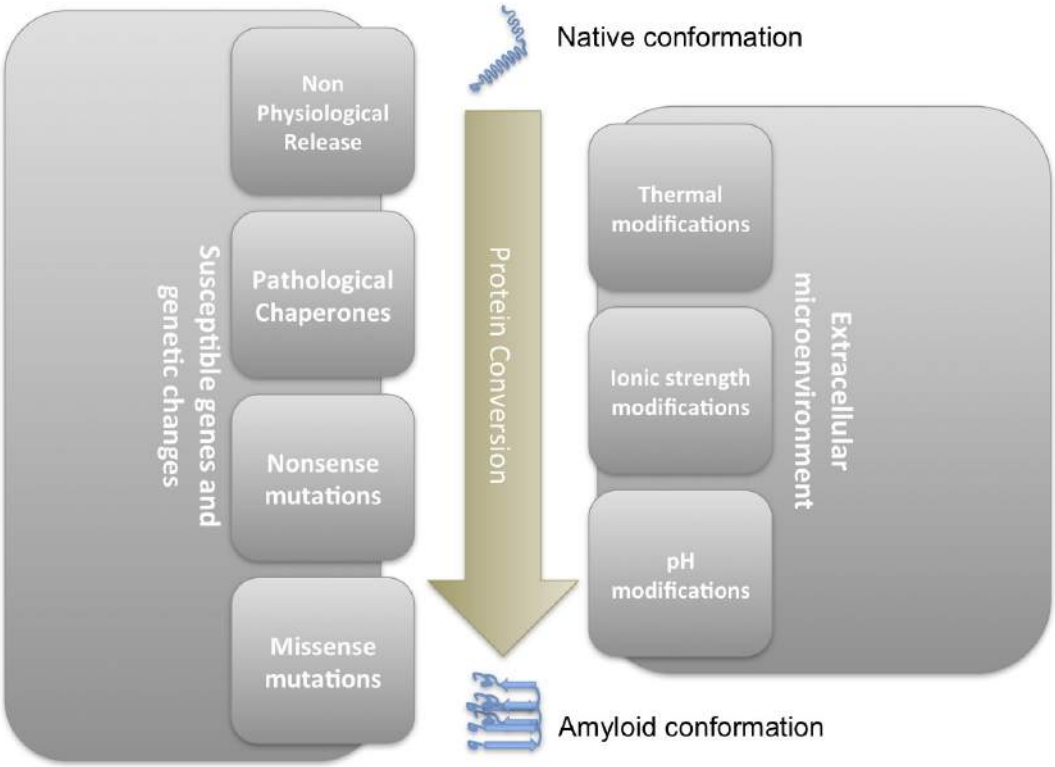

Figure 2. Different destabilization factors could induce the refolding of amyloidosis-prone proteins or peptides. Two general categories of destabilization factors were identified: genetic (left) and environmental (right) factors. Genetic factors include (1) non-physiological release of amyloid proteins or peptides in the extracellular media, (2) the effect of pathological chaperones on amyloid proteins or peptides, (3) nonsense mutations, and (4) missense mutations of amyloid proteins or peptides. Destabilizing environmental factors include modifications of temperature, ionic strength, and pH of the microenvironment of amyloid proteins or peptides.

5.1.1.1. Non- physiological release of amyloid peptides and pathological chaperons

In the case of the peptide-related amyloid diseases, the appearance of amyloid peptides is mostly related to the non-physiological release of these peptides. This non-physiological release can be generated by proteolysis, as in the case of the Alzheimer's disease [10]. In this case the amyloid β-peptide constituting amyloid plaques is liberated in the extracellular medium by the cleaving of a transmembrane protein, APP for Amyloid Precursor Protein, by an enzyme called β-secretase [10]. This proteolysis may originate from different mutations of the APP gene reinforcing interactions of APP protein with β-secretase, but also could emanate from environment-related events, like an excess of membrane lipid rafts due to a high level of cholesterol, that can ease the interaction between APP protein and β- or γ-secretase [11].

A good example of proteins with so-called native instability is α-synuclein. It can be misfolded by the influence of a mutated protein acting as a kind of chaperone during its synthesis [12]. The α-synuclein protein is a natively unfolded protein, which represents 1 % of all protein of the cytosol in neuron cells [13]. It has different functions in the neuronal tissue involving antioxidant and molecular chaperone activities [14, 15]. After synthesis, the α-synuclein population is composed of three differently folded forms of the protein in equilibrium: the mainly unfolded form, the α-helix folded form, and the β-sheet folded form [16]. The activity of pathological chaperones as well as environment modifications can lead to an increase in the β-sheet folded, aggregation-prone, form of α-synuclein resulting in the appearance of toxic intracellular aggregates [16]. These aggregates are able to polymerize and to form fibrils constituting the so-called Lewy body characteristic of Parkinson's disease [17].

5.1.1.2. Environment-induced instability of amyloid proteins

The study of amyloid diseases revealed that proteins potentially implicated in the formation of amyloid-like fibrils do not all present a natively aggregation-prone behaviour [18]. In some cases such aggregation is induced, on natively functioning proteins, by an outside event. The main difference between these proteins and the ones we discussed previously is that this destabilising event occurs after synthesis and acts more on the thermodynamic surrounding environment than on the primary structure of proteins [9].

Environmental modifications may create a secondary structure protein destabilization by modifying the thermodynamic equilibrium inducing the appearance of different protein variants [19]. Thermodynamic environment modifications can be induced by different parameters, temperature, ionic strength, and surface tension being the best documented ones (figure 2). The characterization of the environment effect on amyloid processes was permitted by the discovery of *in vitro* amyloid fibrillisation [20].

Temperature variations are well-known to induce structure modifications, so-called thermal unfolding, proceeding from a total unfolding of the protein due to changes in hydrogen bonds without peptide bond alteration [21]. This phenomenon transforms a protein with an organised secondary structure into an unfolded state at an ambient temperature higher than the so-called melting temperature of this protein. The protein thermal unfolding results in the loss of its 3D structure, and consequently the loss of molecular affinities and functions, functions which are issued from the protein structure. But the temperature can also induce an amyloidosis in certain proteins or peptides like insulin. In those cases the increase in temperature generates a destabilisation of the protein or peptide secondary structure which, without been strong enough to unfold, will allow its refolding to an amyloidosis-prone conformation of the protein [22].

Amyloid refolding can also rise from the ionic tension of the media surrounding the protein. Indeed, an important modification of the ionic forces creates a microenvironment in which the protein charges are modified. These modifications induce a necessity for the protein to refold itself to ensure its stability. One of the clearer examples of this is the case of amylin (IAPP). IAPP is released at the same time as insulin by the pancreatic β-cells with a ratio of 1 amylin for 100 insulin. It is a synergistic partner of insulin in the regulation of plasma glycaemic control. Upon

overexpression this polypeptide has been shown to be responsible for death of pancreatic β-cells. When released by the cell, the pentapeptides FLVHS and NFLVH that are the core self-recognizing and assembling peptides of the IAPP protein change their secondary structure and form a β-sheet structure, responsible for the amyloid-related toxicity [23]. This toxicity occurs through the bacterial-like permeabilization of the lipid bilayer by amyloid aggregates [24]. It has been shown that the amyloidicity of IAPP is due to the absence of ionic strength near the anionic cell membrane of pancreatic β-cells [25]. This absence creates an abnormal environment near the cell membrane that enhances the instability of IAPP peptides and leads to their refolding in an amyloid form [25]. Refolded peptides are later going to aggregate and form small soluble aggregates [25]. These aggregates are able to interact with the pancreatic β-cell membrane and to cause peroxidation of membrane lipids [24]. Peroxidation of membrane lipids induces membrane stiffening, leading to membrane disintegration and cell degeneration [24].

The induction or enhancement of amyloid fibrillisation can also be related to the repartition of charges at the surface of the membrane and the interphase behaviour of the membrane surface. Indeed, in some cases the destabilisation of amyloid proteins is due to the presence in the microenvironment of a hydrophobic surface, of hydrophobic areas on a polar surface or of any media barriers. The case of insulin is here revealing. As a matter of fact it has been shown that insulin amyloid fibers can be observed at the catheter surface after blood dialysis. This phenomenon originates from the hydrophobic surface of the catheter. When insulin is put in contact with a hydrophobic surface it tends, driven by thermodynamic equilibrium, to present its hydrophobic interior domain to the catheter surface. This first energetic destabilisation generates enough internal thermodynamic potential to push insulin to refold toward a β-cross organisation. This new folding of insulin enables its polymerization in amyloid fibers [26].

5.1.1.3. Mutation-induced instabilities

Interestingly in some cases environment changes are only one element of the equation giving rise to the amyloid behaviour. Indeed, in order for a physiologically folded protein to refold in an amyloid-prone form an "inside" protein destabilising event is needed, most often a mutation of the protein gene. Two different kinds of genetic mutations can give rise to the amyloid-prone form of a protein: Nonsense mutations which lead to shorter forms of proteins, and missense mutations which change the nature of one of the protein amino acid residues.

The nonsense mutation shortening the protein can radically change the thermodynamic initial folding of the protein. Indeed, in the case of α-synuclein, shorter mutants and duplicate fragment-genes have been identified and shown to be more pro-amyloidosis than the original protein [27]. The α-synuclein protein is known to be a natively unstructured soluble protein with three domains: an amphipathic N-terminal, a hydrophobic core, and a proline rich C-terminal. Inside the hydrophobic core, the peptide VGGAVVTGV has been shown to be responsible for amyloid behaviour and β-stacking of α-synuclein [28]. But when in contact with the cell membrane α-synuclein adopts an α-helix-rich folding in order to interact with the lipid part. Nevertheless, this protein can also fold to adopt a β-sheet-rich conformation, known for its amyloid-prone behaviour and responsible for appearance of protein plaques inside neurones, also-called Lewy bodies and characteristic of Parkinson's disease [17]. As described above, the actual proportions of these three forms of the same protein are highly dependent on the protein environment, but the appearance of truncated forms of α-synuclein can also be induced by the presence of nonsense mutations at the position 30, 46, or 53, especially in familial forms of Parkinson's disease [29]. In this disease β-sheet-rich conformers represent the majority of α-synuclein proteins and pro-polymerisation behaviour induces different pathological phenomena inside neurones [12].

Various modifications of amino acid residues lead to so-called missense mutations that can drastically change the behaviour of proteins giving them a more pro-amyloidosis primary structure. This type of mutations can also cause the appearance of interaction domains in non-amyloidogenic proteins and enhance amyloidosis behaviour in them. For example, numerous mutations in the gene coding for APP were identified as Aβ amyloidosis enhancers. Indeed, these mutations increase the

affinity of the γ-protease enzyme for APP thus the quantity of fragment 1-42 amyloid β-peptide released [30]. Very few peptides of this form, know to be very amyloidosis-prone, are released physiologically but in the case of certain Alzheimer's disease familial predispositions, two missense mutations in positions 595 and 596 have been shown to be responsible for a 6 to 8-fold increase in the neuronal Aβ production [30]. This increase in the Aβ 1-42 peptide production enhances the rate of the cytotoxic amyloid aggregate formation by accelerating the reaction of association between Aβ peptides [30].

The significance of missense and nonsense mutations in the amyloid behaviour was described by us earlier and has been limited to direct correlations between the mutation and the protein amyloid behaviour. However any missense and nonsense mutations can also have an effect on the protein amyloid behaviour through the regulation of their environment. Indeed, even if not directly linked, a mutation in the oxidation cleaning cell mechanism will always induce a modification of the intracellular environment contributing to the amyloidosis of physiological proteins. For example it is well known that the nitration of α-synuclein by nitric oxide (NO) induces folding toward β-sheet-rich conformers [12].

5.1.2. Necessity of protein structure stabilization and internal restructuration of the secondary structure

After having discussed the general causes of the amyloidosis behaviour of proteins, it is now time to clarify fundamental common molecular mechanisms explaining the amyloid protein and peptide highly structured fibrillisation. As we have noted before, this phenomenon may result from a thermodynamic destabilisation and tend to the stabilisation of the protein structure through its refolding but we have not refined our description of the secondary structure refolding and its implications on the protein behaviour. One common point of all amyloidosis protein behaviour is that the destabilisation of the protein secondary structure, by an outside or inside event, induces the necessity for the structure to change in order to satisfy thermodynamic laws [31]. In order to satisfy the latter, two mechanisms of stabilisation can be stated: an internal restructuration, through a secondary structure refolding, and the association with another protein. Figure 3 represents a summary of the different steps

of refolding and polymerisation occurring to amyloid proteins or peptides after any previously described destabilization events.

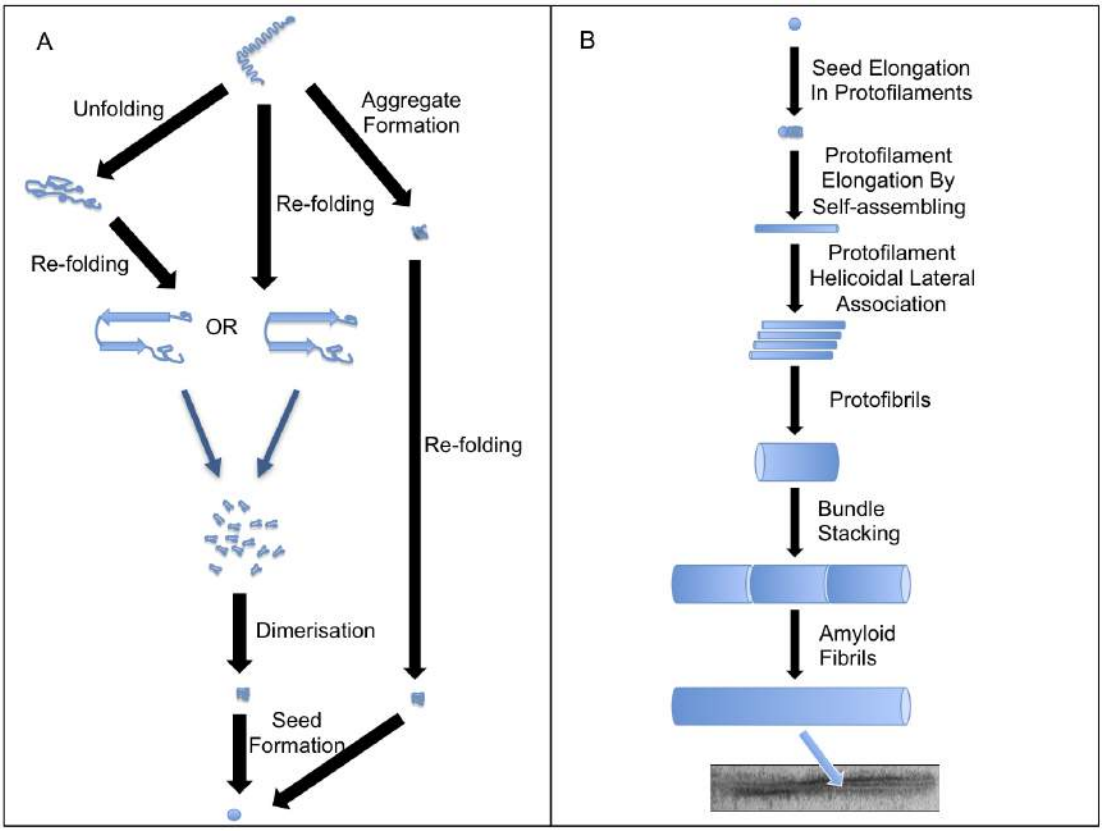

Figure 3. Amyloid fibrillisation from amyloidosis-prone proteins or peptides refolding to the formation of highly organized amyloid fibers. Panel A: Various ways of seed nucleation exist to explain the appearance of amyloid seed aggregates from amyloidosis-prone proteins or peptides. On one way, under certain conditions (pH or ionic strength stress, mutations, posttranslational modifications, etc.) proteins or peptides lose their native conformation and unfold. Subsequently, unfolded proteins or peptides can re-fold consequently to a β-sheet-rich conformer (left branch). Another possible way is constituted by the formation of β-sheet-rich conformer directly from the native state without unfolded intermediates (central branch). Finally, the aggregation of proteins or peptides can be the initial step, followed after aggregation by the formation of β-structures within aggregates and leading to further nucleation (right branch). Panel B: The common pathway of amyloid fiber formation. During the next stage of amyloid polymerization, proteins or peptides form dimers that further associate to form small soluble aggregates also known as amyloid seeds. Protofilaments are further formed from these seeds by terminal addition of a refolded amyloidosis-prone protein or peptide. Then, protofilaments helicoidally associate to form protofibrils. Protofibrils stick together, thus forming amyloid fibrils that associate with other proteins and form amyloid plaques, tangles, or Lewy's bodies observed in tissues or cells of patients

The internal restructuration is immediate and induced by destabilising events and consists mainly of the protein secondary structure folding or refolding toward a β-sheet-rich conformation [32]. As the protein folds or refolds itself under the effect of internal or external factors, the 3D structure of the protein is going to change, driven by the electrostatic potential of amino acid residues and by the ionic strength force applied by the surrounding environment [33].

The effect of the protein amino acid residue sequence and charge has been analysed thoroughly. It has been shown that after destabilisation of the secondary structure of α-helix-rich proteins the refolding of those will lead to the formation of more β-sheet-rich conformers without any change of the protein primary structure [32]. Nevertheless, the rate of the amyloid protein conversion from a native to a pathological form is dependent on the protein amino acid sequence, thus on the original intrinsic stability of the protein [33]. Conformational changes from disordered to β-sheet occur more slowly than the subsequent oligomerization. The presence of β-sheet secondary structure is mandatory for the next events of amyloid fibrillisation. So one of the main points of this phenomenon is to identify why certain amino acid sequences can so easily lead to two different secondary structures. To explain this occurrence the hypothesis was developed that a specific sequence of amino acid residues existed in the amyloidosis-prone protein [34]. This or these sequences should be able to form either an α-helix or a β-sheet depending on the protein microenvironment. A tetrapeptide sequence and a pentapeptide sequence were identified as containing both aromatic amino acid residues and positively charged amino acid residues and can be found inside different amyloid proteins or peptides [35]. Positively charged amino acid residues are known to associate mainly to give rise to α-helix secondary structure and aromatic amino acid residues are known to prefer formation of β-sheet secondary structure [36]. Also the presence of these sequences has been shown to be sufficient to give rise *in vitro* to β-sheet structures and to an intermolecular structure, the so-called β-cross, highly characteristic of amyloid fibrillisation [37]. These sequences were thus considered as the origin of the β-sheet forming behaviour of amyloid proteins and peptides. But recent studies have shown that some amyloid proteins can present high amyloidosis tendencies without the presence of these amino acid sequences and that other proteins presenting these amino acid sequences do not present an amyloidosis-prone behaviour [38]. The

current doctrine is that these sequences should not be seen as mandatory to any amyloid process but more as potential risk factors of proteopathy [38].

Once α-helix-rich amyloid proteins and peptides have unfolded their secondary structure and some of their amino acid residues have formed β-sheet secondary structure, amyloid-prone proteins and peptides see their secondary structure evolving again. Indeed, it has been shown that β-sheets, previously formed inside one amyloid protein or peptide, are going to associate together in an antiparallel way, this organisation being mandatory for the continuation of the amyloid polymerization process [39]. This new structure of amyloidosis-prone proteins induces a stabilisation of in their secondary structure by allowing the association of amino acid aromatic residues in their β-sheet [40]. The antiparallel association of β-sheet structures is mainly driven by the need for hydrophobic-cored proteins to satisfy the thermodynamic equilibrium arising from the polar water surrounding [41]. By enhancing the stability of β-sheet-rich amyloidosis-prone proteins or peptides this mechanism decreases the probability of a return to α-helix-rich conformers in case of disappearance of the environmental destabilising event [42]. It has been shown that under physiological conditions and for certain proteins there are certain mechanisms which prevent the β-sheet association by use of obstructer molecules which are able to interact with β-sheet positively charged residues [43]. These obstructer molecules are low-molecular weight negatively charged peptides or negatively charged domains of chaperone molecules and have been shown to be able to suppress the amyloid behaviour of amyloidosis-prone proteins *in vitro* [42]. Nevertheless in the absence of obstructer molecules the amyloidosis-prone proteins and peptides will achieve this β-sheet association and will continue to evolve by interacting with other refolded proteins or peptides.

The interactions between β-sheet-rich conformers take place almost immediately after the end of the protein internal refolding and also participate in the stabilisation of amyloidosis-prone protein or peptide conformers [39]. It has been shown that they result in the parallel association of β-sheet secondary structure driven by hydrophobic interactions and lead to a very stable cross-β intermolecular structure [42].

The cross-β structure arises between two amyloidosis-prone proteins or peptides after their refolding and gives rise to very stable dimer molecules. These dimers have been shown to be soluble and to have a low toxicity under physiological conditions

for cells *in vitro* but also emerge as initial seeds for the amyloid polymerization process which will occur if environment conditions are not stabilised or if the number of β-sheet-rich conformers in the environment reaches a certain stage [44]. Some proteins and peptides are natively unstable and in order to regain their stability they need to homodimerize. Homodimers that arise from this process are highly prone to auto-association by stacking in protofilaments and therefore can be considered as seeds of amyloid fibrils [45].

Until this point amyloidosis-prone proteins or peptides that we have described previously were still lowly toxic and could stay in this form for long periods of time as in the α-synuclein case in which there is, physiologically, a balance between different conformers of amyloidosis-prone proteins [12]. But if environment conditions continue to sustain the generation of β-sheet-rich conformers, the so-called amyloid aggregates appear inside or outside of originator cells [46]. The first aggregates to arise from β-sheet-rich conformers are dimers of proteins or peptides. They appear from the charge repulsion by refolded proteins to form dimers in parallel β-sheet arrangement with amino acids of adjacent chains in register [47]. Dimers are stabilized by intermolecular hydrophobic interactions and serve as a platform for the formation of larger assemblies of β-sheet-rich conformers of amyloidosis-prone proteins or peptides [48, 49]. Indeed, these dimers play the role of a seed by inducing the destabilisation of surrounding natively fold proteins [50] through a "dock-and-lock" mechanism in which the "locking" step is due to sequential conformational changes, each increasing the affinity of the monomer for the fibril until a condition of irreversible binding is reached [51].

5.1.3. Direct and indirect toxicities of amyloid soluble aggregates

Amyloidosis-prone protein aggregates, around 100 nm in length, are soluble in physiological media but larger amyloid fibers are known to be hydrophobic [52]. For a long time the dogma was that the cytotoxicity of amyloid aggregates, fibers and plaques was related to their hydrophobic behaviour and that by solubilising them it should be possible to limit the progression of associated neurological diseases. Recently it has been demonstrated that small soluble aggregates of β-sheet-rich conformers are responsible for amyloidosis toxicity [53]. The modus operandi of this cytotoxicity has also been described for most of amyloidosis-prone proteins and

peptides and seems common to all of them [54]. Differences of symptoms observed between different amyloidosis-related diseases are more related to the place of origin of β-sheet-rich conformers than to the kind of proteins involved [9]. This amyloid soluble aggregate cytotoxicity has been linked to two main effects of aggregates: first the direct toxicity of aggregates through induction of membrane instability and secondly the indirect toxicity through activation of the cell apoptosis mechanisms.

The direct toxicity of amyloid soluble aggregates is mainly due to their capacity to interact with the cell membrane where they originated and to induce its peroxidation, leading to cell membrane disruption and to cell death by necrosis [55]. The cell membrane peroxidation phenomenon has been elucidated and revolves around peroxidation of cell membrane lipids [56]. This peroxidation induces saturation of the hydrophobic part of cell membrane phospholipids thus decreasing the fluidity of the membrane and increasing the possibility of a cell membrane fracture, which can cause cell material intercellular leakage or cell necrosis [57]. Contrary to what was previously believed the contact of amyloid soluble aggregates cannot induce cell death in a way that could be described as direct and mechanical but through its capacity to generate hydrogen peroxide, a free radical highly reactive to cell membrane lipids [58]. This mechanism, which requires a certain amount of amyloid soluble aggregates, can be slowed down by antioxidant enzymes thus allowing the time to put in place other mechanisms of amyloid cell death [59]. These mechanisms have been described as the indirect amyloid toxicity and act mainly on stress-induced pathways.

As shown in the previous paragraph, once in contact with amyloid soluble aggregates, cell membrane phospholipids are going to be oxidized and their physico-chemical properties changed, reducing the cell membrane fluidity thus increasing the probability of deadly cell membrane fracture. But at the same time peroxidation of cell membrane phospholipids induces another series of mechanisms leading to cell death. The toxicity mechanism induced by the peroxidation of phospholipids is controlled by cell programming, and therefore leads to cell apoptosis [60]. The two cell death mechanisms have in common that they are both induced by cell membrane phospholipid peroxidation [61]. The indirect cell death mechanism uses a large variety of secondary messengers and cell mechanisms to arrive to the same final result: cell apoptosis [62]. Here we will limit ourselves to detail the best described and understood of those mechanisms, the reduction system pathway. Upon

peroxidation of cell membrane phospholipids certain mechanisms are going to be put in place to ensure the reduction of oxidised phospholipids in order to stabilise the cell membrane fluidity thus decrease the risk of membrane rupture [59, 63]. Moreover phospholipid oxidation increases the formation of several reactive unsaturated aldehydes, all of which are well-recognized neurotoxic agents [61]. Even if the activation of this mechanism lowers the probability of a direct mechanical cell death it also induces the indirect cell death. As a matter of fact the activation of the so-called mitochondrial regulation of apoptosis can be eased by the presence of nitric oxide (NO) in the cytosol, yet this element is known to be at the same time one of the key-factors of the phospholipid reduction mechanism [12]. NO has also been shown to react with superoxides leading to the formation of peroxynitrite, a powerful oxidant and nitrating agent [64]. Peroxynitrite *in vivo* is known to react with carbon dioxide resulting in the formation of carbonate radical and nitrogen dioxide, two free radicals [64]. The free radical effect is considered to be dose-dependent and to induce different mechanisms of defence depending on the amount of radicals present in the cytosol [64]. The degree of indirect toxicity due to amyloid soluble aggregates can be classified in three tiers depending on the level of oxidative stress induced. Different levels of oxidative stress correspond to different response pathways with the higher being cytotoxicity. (A) In the first tier of the oxidative stress response, the anti-oxidant defence is activated and induces the creation of phase II detoxication enzymes. (B) If the level of oxidative stress still rises then the inflammatory response is put in place. (C) Ultimately the oxidative stress level rise can induce the mitochondrial release of pro-apoptotic molecules responsible for setting in motion the apoptosis mechanism [59].

In summary, amyloid soluble aggregates are highly toxic both in direct and indirect ways for their surrounding cells. We identified amyloid-related diseases as presenting large protein aggregates inside or outside the tissues. These large amyloid aggregates have been shown to be strongly hydrophobic, antigenic and surprisingly lowly toxic to surrounding or containing cells [52]. These recent findings support the hypothesis that this form of amyloid aggregates could be a storage solution put in place by organisms to dispose of highly toxic soluble amyloid aggregates. The effect of amyloid aggregates and fibers on cell viability is summarized in figure 4 together with the action of different factors on the amyloidosis process and the possible therapeutic target against amyloidosis.

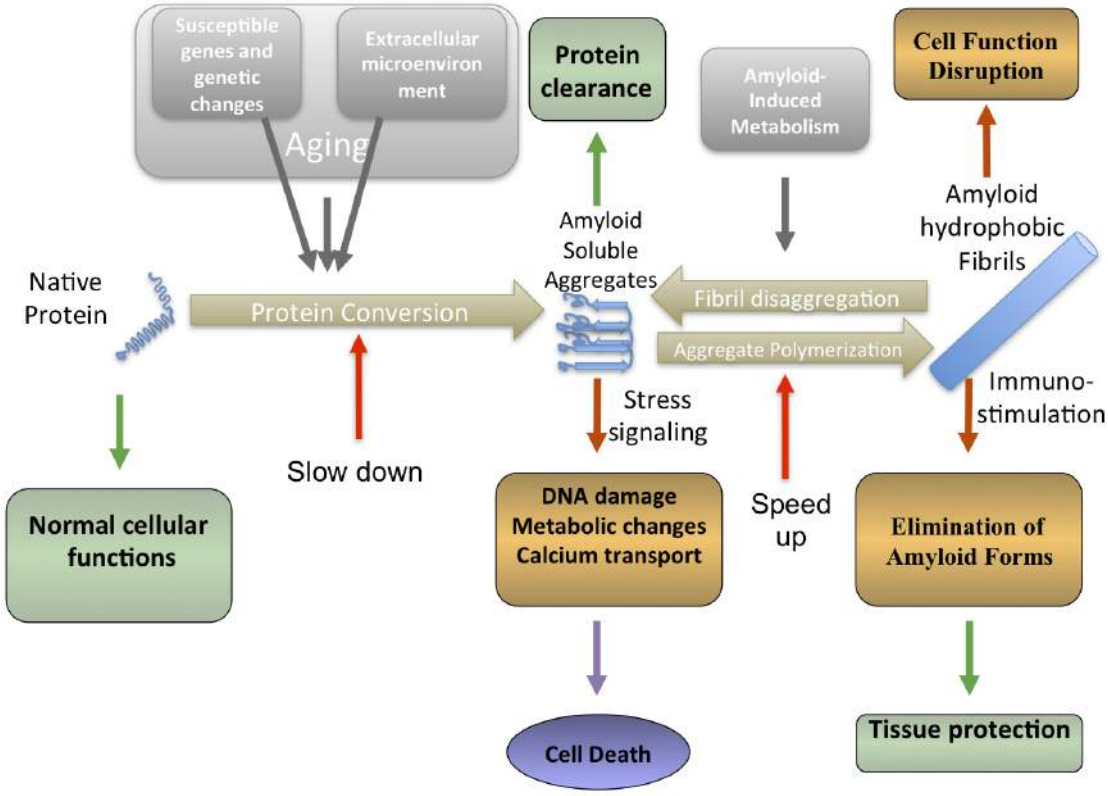

Figure 4. Dysfunctions of cellular and tissue metabolism that may be caused by amyloid polymerization. The refolding of amyloidosis-prone proteins and seed formation are irreversible. Although amyloid seed aggregates are soluble and can be eliminated from tissues, they interfere with intracellular metabolism, induce different disturbances of the membrane structure, and are responsible for most of the amyloid toxicity. The polymerization of seeds into fibers is reversible under the effect of some molecules generated by cells in response to the appearance of amyloid fibers. These large fibers are hydrophobic, cannot be removed from tissues, and disturb cell functions, although their immunogenicity may permit the immune system to eliminate them, hence protect tissues.

5.2. Nanomaterials: Definitions and relevant structures

The identification of proteopathy mechanisms and origins corresponds chronologically with the development of Nanoscience and the appearance of nanomaterials.

5.2.1. Nanomaterials

In the latter 20 years a new kind of materials has made its appearance in everyday life, nanomaterials. Nanomaterials are issued from the development of nanoscience. They represent a new step in the process of downsizing engineering products. Because their diameter range is below 100 nm, they bring new and unknown capacities to everyday materials [65]. Previously, it was accepted that material properties originated from the chemical nature of materials. Properties of nanomaterials do not only originate from their chemical nature but also from their size and shape [65]. This new relation between nature and properties of materials has forced the specialists to rethink the definition of materials for Nanoscience.

5.2.1.1. Definition

Since the difference in properties between materials and nanomaterials originates from a scaling effect, nanomaterials have been defined as materials with at least one of their dimensions inferior to 100 nm [65]. This definition of nanomaterials has been enlarged to encompass materials containing at least 1% of unbound, aggregated, or agglomerated submicrometre-sized particles [65]. These particles can be natural, accidental, or manufactured. Nanomaterials are commonly divided into two categories: fullerenes and inorganic nanoparticles. Fullerenes are constituted mainly of a monoatomic layer of carbon atoms, displaying many forms: spherical, cylindrical, or ribbon-like [65]. Nanoparticles are submicrometre-sized crystals of metals, semiconductors, or oxides [65].

5.2.1.2. Specificity

As we said before, nanomaterial specificities arise from their size. Indeed due to the submicrometre size, the ratio between the number of atoms present at their surface

over the total number of atoms is very high. This over-representation of surface atoms combined with the relatively low number of atoms present in nanomaterials induces variation in the properties at the nanoscale [65]. Nanomaterials present chemical, optical, mechanical, electrical, and thermal characteristics different from the bulk material that constitutes them. If the mechanisms explaining the properties of nanomaterials are the same in fullerenes and in nanoparticles, the resulting properties are different.

For the fullerenes, their mono-atomic organization generates particular mechanical strength, thermal and electrical properties, different from the ones observed in macro-scale carbonated structures [66]. For example, cylindrical fullerenes, also called carbon nanotubes, present a very strong mechanical strength in their longitudinal direction [67]. The same carbon nanotubes have demonstrated superconductivity with relatively high transition temperatures in their longitudinal direction [68]. They are very good thermal insulators in their radial direction but excellent thermal conductors in their longitudinal direction [69, 70]. They also present very good temperature stability in vacuum [71]. The surface of fullerenes is in theory chemically stable but addition of active chemical groups to their surface increases largely their reactivity [72]. On the contrary addition of other atoms inside fullerenes increases their chemical stability [72]. This theoretical stability of carbon nanotubes explains their solubility in apolar liquid and insolubility in polar liquid. Other fullerenes, like the bulky ball, present similar properties with the exception of ribbon-like fullerenes, also-called graphenes, which have the electrical properties of semi-metal or zero-gap semiconductors [73]. These atypical properties of fullerenes explain the development of various methods of use and applications in the recent years.

The other group of nanomaterials, the nanoparticles, present also particular mechanical, electrical, magnetic, optical, and chemical properties but contrary to fullerenes the properties of nanoparticles are directly dependent on their size. Indeed, with the decrease of the number of atoms in nanoparticles one can observe the appearance of atypical properties [65]. For example, the reduction of the number of atoms in semiconductor particles induces the appearance of quantum confinement generating unexpected visual effects [74]. Similarly, in some metal particles, the decrease in the number of atoms generates the appearance of surface plasmon resonance phenomena [75]. Size-dependent properties also concern magnetic particles

which, below a certain size, can present a superparamagnetic phenomenon [76]. In terms of mechanical properties, metal particles below 50 nm demonstrate different malleability and ductility than bulk materials, thus they are considered as super-hard materials [77]. The temperature stability of nanoparticles is improved by their surface effect, reducing the melting point of nanoparticles as compared to bulk materials [78]. Likewise, thermal magnetization phenomena are increased in ferroelectric materials below 10 nm in size [76]. The capacity of metal and semiconductor nanoparticles to be in suspension in different solvents, despite their important density difference, is as well dependent on particle size and originates from the strong interaction of nanoparticles with the solvent [79]. In a similar way the very high surface area to volume ratio of nanoparticles generates an important driving force for the diffusion of nanoparticles in solvents [79]. Finally the size of nanoparticles induces a strong reactivity of their surface, which leads to an important tendency of nanoparticles to aggregate in solvents [79]. These atypical size-tuneable properties of nanoparticles, as in the case of fullerenes, have generated multiple applications.

5.2.1.3. Applications

As discussed above, nanomaterials have atypical properties, different from those of their bulk material, and due to their submicrometre sizes. These properties explain the manifold applications of nanomaterials in various fields. The difference in properties between fullerenes and nanoparticles induces a difference in the applications of the two kinds of nanomaterials. We will now detail some of these applications of nanomaterials, first briefly of fullerenes and then in more detail of nanoparticles.

Fullerenes, due to their mechanical, electrical, thermal, and chemical properties have demonstrated a large applicability in the electronic industry for different components [80]. For example, graphene could be used in electronic transistors because of its high carrier mobility and low noise [81]. The use of graphene has also been predicted to generate ultracapacitor plaques because of its large surface area to volume ratio allowing a greater energy storage density [82]. Graphene could also be used to create transparent electrodes because of its high electrical conductivity, high optical transparency, mechanical strength, and flexibility [83]. Transparent electrodes could be used in applications such as touch screens. Also electrodes made of graphene could be used for DNA sequencing in nanopore-based electronic DNA sequencers [84].

Similarly graphene electrodes could be used for single molecule gas detection. Graphene is intrinsically insensitive but by functionalising its surface and by measuring local changes in electrical resistance one can detect adsorbed molecules. The sensitivity of graphene originates from its high electrical conductivity and low noise [85]. Since the optical absorption of graphene can be changed by tuning its Fermi level, then graphene can be used to create optical modulators [86]. Similarly, graphene could be use to produce inexpensive, flexible solar cells because of its capacity to be produced in large surfaces and because of its electric properties [87]. Graphene could also be used in microbial detection and diagnostic devices. By chemically changing its surface one could develop microbial detectors for medical diagnostics [88]. Interestingly, sheets of graphene oxide have been shown to be highly toxic for bacteria. This capacity opens the possibility to use graphene in bactericide surfaces for hygiene products and food packaging [89].

5.2.2. Nanoparticles

Nanoparticles are nanometre-sized single crystals, which can be found as individual particles in suspension, in composite materials as nanoclusters or in the solid state as nanopowders [65]. The first man-made nanoparticles date back from the Middle Age in the form of a lustre technique using a ceramic glaze containing a dispersion of silver and copper nanoparticles. The empirical methods of copper and silver nanoparticle synthesis were developed in the Arabic world to bypass the religious prohibition on the use of gold in artistic representation [90]. The first rational description of the process of oxidation and reduction involved in nanoparticle formation is credited to Michael Faraday [91]. Nanoparticles made of metal or semiconductor present atypical size-dependent properties different from the properties of their bulk material.

5.2.2.1. Characteristics

Nanoparticles display properties that are different from both bulk material and atomic structures. These properties originate from the high proportion of atoms at the surface of nanoparticles. Their large surface area dominates the contribution from their small inner core. This characteristic is mainly responsible for the strong diffusion capacity

of nanoparticles, their high tendency to accumulate, and their capacity to display surface plasmon resonance [65, 75, 79].

On the contrary, phenomena of superparamagnetism and of quantum confinement, which are observed in some nanoparticles, are linked to their small number of atoms. For example, the quantum confinement phenomenon originates from the capacity of nanoparticles to confine their electrons. This phenomenon results in the high capacity of semiconductor nanoparticles, called quantum dots, to absorb UV light and their high photostability [92].

The presence of nanoparticles in bulk material generates composite materials, which inherit some of the properties of the nanoparticles composing them. This is mainly used to reinforce plastic polymer matrices or to create smart and functional textiles [77].

There are different methods to create nanoparticles, among them attrition, pyrolysis, thermal plasma torches, inert-gas condensation, radiation chemistry, sol-gel processes, and colloidal chemistry [93]. Here we shall concentrate on the colloidal chemistry technique. Dissolved metal ions, generated by oxidation of metal salts in solvent, are used before generating crystals by reduction at high temperature in a reducing atmosphere. This gives rise to a solid-liquid mixture containing distinct dispersed solid particles [94]. This technique allows the production of particles of metal or semiconductor with a typical size range from nanometre to micrometre. Particle shape depends on the interatomic structure of the particles. Amorphous particles would usually generate spheres whereas crystal shape depends on their particular crystal habit and can form spheres, rods, fibers, or cups [95]. Surface coating of nanoparticles controls their stability, solubility, and, in the case of nanoparticles used *in vivo*, their targeting [94].

5.2.2.2. Applications

Nanoparticles have a wide range of application due to their atypical properties. One of the more interesting uses of nanoparticles is in solar cells where their high capacity to absorb light and enhanced photostability would be useful in order to increase both efficiency and durability of solar cells [96]. Janus nanoparticles can also be used as solid surfactants and assemble at water/oil interfaces [97]. One of the most interesting applications of nanoparticles is in medicine as an *in vivo* drug delivery system. Indeed

nanoparticles are small enough so that they can easily penetrate the living tissue. Inside the living organism, nanoparticles can be targeted to specific sites within the body and even to specific cell organelles using coupled targeting molecules. The targeting molecules e.g. monoclonal antibodies, aptamers, streptavidin, or specific peptides, are covalently bound to the nanoparticles in controlled numbers. Once *in situ* nanoparticles can be magnetically or optically stimulated [98].

Another interesting application of nanoparticles is as imaging agents. Indeed some semiconductor nanoparticles, called quantum dots (QD), are able to absorb UV light and to emit fluorescent light whose wavelength depends on their size. By coupling this atypical optical properties of QD to the possibility to covalently bind a specific tracking molecule to their surface one can use QD as single molecule tracking agents for *in vivo* or *ex vivo* cellular imaging [99].

5.2.3. Quantum Dots

Quantum dots (QD) are crystals of semiconductor, with sizes ranging from 1 to 10 nm, which display atypical optical properties linked to their relatively small number of atoms. Indeed the low number of atoms in QD gives them the capacity to confine excitons and consequently to have electronic properties in between the bulk material and the discrete molecules [100]. In QD these electronic properties are directly dependent on the size of QD because the smaller the crystal, the larger the difference in energy between the highest and the lowest energy bands. For QD, this size-dependent band gap impacts directly on the optical properties of QD. In summary, the capacity of QD to emit radiation after excitation is directly dependent on the size of the crystal: the smaller the size, the higher the energy of radiation emission will be. This allows a direct control of the wavelength emission peak of QD fluorescence through the control of QD crystal size [92]. The same effect of quantum confinement in semiconductor nanomaterials can be observed in quantum wires and quantum wells [74]. The size of QD crystals is controlled during their process of fabrication by colloidal chemistry. The colloidal synthesis of QD requires precursor compounds dissolved in solvent, these precursors are reduced metal salts, together with organic surfactants. When heated in an oxidizing atmosphere, precursors form monomers, which assemble by nucleation processes to form the nanocrystals. Therefore, by controlling the quantity of precursors in the medium, the temperature and the duration

of heating, on can control the size and properties of QD crystals [93]. Other techniques for QD production were developed like viral assembly, electrochemical assembly, or bulk manufacturing, but the scalability of the colloidal synthesis made it the most promising technique for commercial applications [101].

5.2.3.1. Applications

QD applications are numerous and reach a large number of fields but they are all related to the atypical electronic properties of QD. Indeed QD, due to the quantum confinement effect, are similar to and could be used as single electron transistors [102-104].

Moreover QD could be implemented for quantum information processing. QD could be used in solid-state quantum computing due to the electron flow control that one could have when stimulated. QD could also be used to control and measure the electron spin. By coupling several QD in an entangled state one can generate a quantum bit, which can serve as the basis for quantum calculations thus quantum computers [102].

Another of the most important and controversial applications of QD is in the production of cheaper and more efficient solar cells. Because of the large bandgap energy of QD they can generate multiple excitons for each photon received and therefore increase the maximum theoretical efficiency of a solar cell. Also, through the same carrier multiplication phenomenon, the presence of QD in solar cells could limit the heat generated by cells and as a result increase the lifespan of current solar cells. Moreover the use of QD in solar cells could induce a decrease of solar cell price because of the scalability of QD manufacturing [105].

The application of QD in light emitting diodes (LED) as a light source originates from the capacity of QD to generate Gaussian-distributed light from little power and from the discovery of QD emitting monochromatic light. Indeed, by emitting light in specific Gaussian distributions, QD proved to be potentially more accurate renders of colours than current devices. Also QD require little power since they are already colour-filtered and their small sizes allow resolutions below what is humanly perceivable. Similarly the bright emission in the visible and near infrared regions of QD combined with their capacity to emit white light favour QD for the development of more efficient light sources [106].

Furthermore in optical applications QD, due to their sharper density of states, could also be use in diode lasers and amplifiers because of their superior transport and optical properties [107]. Similarly, due to their brightness and photostability QD have demonstrated a wide applicability to medical imaging as specific fluorescent dyes. Indeed QD are brighter and more stable than conventional fluorescent dyes and when coupled to a targeting molecule, they can be used to achieve highly sensitive cellular imaging. Their extremely small size allows the acquisition of many focal-plan images and the reconstruction of 3D images representing the distribution of targeted molecules and cells *in vivo* or *ex vivo*. Using high resolution and real time tracking of QD fluorescence the movement of a molecule of interest can be followed over extended periods of time. This is also made possible by the capacity to covalently bind targeting molecules at the surface of QD in a highly controlled fashion. Amongst the tracking molecules which have been coupled to QD one can find antibodies, streptavidin, peptides, aptamers, and small-molecule ligands [108].

Within biomedical applications, QD have also been used to deliver gene-silencing molecules into cancer cells. Indeed, QD can actively target tumour cells through their coupling to tracking molecules, or passively target tumour cells by accumulation inside tumours because of the absence of lymphatic drainage in tumours [109].

QD, like the other nanomaterials, have numerous applications and appear to be destined to become an important part of the biomedical toolbox. However one important issue remains, namely the potential toxicity of QD and other nanomaterials.

5.3. Impact of nanomaterials on living beings

Nanomaterials, because of their large surface area to volume ratio, have demonstrated unique properties as compared to bulk materials. These atypical properties have attracted attention on potential applications for nanomaterials both in material science and biomedical applications. For example, the broad excitation profile, narrow tuneable emission spectra of QD make them a promising tool for optical encoding and multiplexing biomedical applications. But the same quantum size effects also increase the reactivity of nanomaterials in liquid media. For example gold, which is known to be inert in bulk material, is highly active at nanometre dimensions [110]. This unusual reactivity of nanomaterials could generate toxic effects and make nanomaterials a potential threat to the environment and to human beings.

5.3.1. Impact of nanomaterial-containing macro-objects

5.3.1.1. Stability of the inserted nanomaterials inside macro-objects

Most of the man-made nanomaterials encountered in the environment are nanocomposites. Nanocomposites are solid combinations of a bulk matrix and nanomaterials, like carbon nanotube or metal nanoparticles, embedded homogeneously in the bulk matrix. Due to the large surface of the nanoparticles, the presence of a relatively low quantity of nanomaterials in nanocomposites brings new nanoscale-related properties to macroscale composites. These nanocomposites present improved electrical, thermal, optical, and mechanical properties, which make them attractive for a large range of industrial applications. By and large, nanocomposites are more resistant and durable then their bulk counterparts [111]. Nevertheless, nanocomposites are also sensitive to deterioration over time thus the issue arises of the release of nanomaterials to the environment.

5.3.1.2. Nanomaterial dispersion

When the nano-reinforcement is homogeneously dispersed in the matrix the quantity of released nanomaterial should be negligible but the high surface to volume ratio of nanomaterials increases their dispersion in the environment [112]. Moreover, the behaviour of nanomaterials is dependent on their size, shape, and surface reactivity with the environment. Some nanomaterials present a high tendency to aggregate, when others are perfectly soluble and monodisperse in polar liquids, like water [113]. Nevertheless the extremely small size of nanomaterials and their large surface area result in their capacity to be easily inhaled, swallowed, and adsorbed on the skin [114]. Also nanocomposites incorporated in implanted biomedical devices could directly release nanomaterials directly into living tissue [115]. The capacity of nanomaterials to disperse in the environment generates another potential hazard of nanomaterials, their permeation and distribution among living organisms.

5.3.1.3. Nanomaterial permeation and distribution in living organisms

The very small size of nanomaterials also means that they are more easily absorbed by living organisms than larger particles. As a matter of fact it has been demonstrated that nanoparticles can readily penetrate the animal skin [116]. Also nanomaterials can move easily into the lung tissue after inhalation [117]. Nanoparticles can also penetrate the body through the gastrointestinal tract [118, 119]. Once inside the living organisms, it has been demonstrated that nanoparticles are able to translocate far from their site of entry through the blood and to deposit in distant sites like the kidney, liver, bone marrow, and muscles [120]. Nanoparticles have even been identified as experimentally able to pass the blood-brain barrier of mice [121]. In comparison, very little is known about the excretion of nanoparticles from the living organism [120]. Since nanomaterials can readily enter the organism and the latter seems unable to remove them, one should have a look at the impact of the presence of nanomaterials in living organisms.

5.3.2. Direct impact of nanomaterials

As mentioned above nanomaterials, and more particularly nanoparticles, can readily penetrate living organisms, have a high capacity to distribute even into secluded organs, and cannot be excreted. Therefore the issue of the impact of nanoparticles in living organisms arises. Recent studies seem to demonstrate the toxicity of nanoparticles in living organisms. This toxicity appears to originate from the large surface area to volume ratio of nanoparticles. This makes the nanoparticles very reactive and in some situations even catalytic [122, 123]. Also some QD have been shown to release toxic heavy metal ions by photolysis or chemical quenching when their polymer coating is damaged or imperfect [124]. One of the key aspects of nanoparticle toxicity is the fact that nanoparticles are able to passively diffuse through the cell membrane. Because of this nanoparticles present a toxicity that can be characterised as acting at three levels: at the organ/tissue level, at the cellular level, and at the molecular level.

5.3.2.1. At the organ/tissue level

At the tissue level, nanoparticles are toxic because of their surface reactivity. It has been demonstrated that the presence of breathable nanomaterials, like carbon nanotubes, in the lung tract can generate mechanical damage to the tissue and chronic respiratory disease [125]. Once in the lung, the gastrointestinal tract or on the skin, nanoparticles because of their small size can access the blood stream and then be transported around the body and taken up by various organs and tissues. Once in these tissues, nanoparticles will generate a response by the immune system, resulting in inflammation, immune responses and allergic phenomena [126, 127]. This inflammation is due to the high reactivity of the nanoparticle surface. The activation of the immune system deteriorates the tissues in which it takes place because of stress signals generated by the immune cells. For example, the presence of nanoparticles has been shown to damage the cardiovascular system of mice [128]. Also it has been demonstrated that phagocytic cells can recognize and try to eliminate nanoparticles. However the durability of certain nanomaterials creates the risk of a weakening of the immune system against other pathogens because of the presence of nanoparticles monopolizing the immune system [126].

5.3.2.2. At the cellular level

At the cellular level, the presence of nanoparticles has been shown to be toxic. Metal oxide nanoparticles and semiconductor nanoparticles have been shown to be toxic for cultured cells. The main mechanisms of nanoparticle toxicity in cells have been identified as the direct toxicity of nanoparticles and the generation of reactive oxygen species (ROS) by nanoparticles. Previous studies have shown that CdSe nanoparticles are not stable in biological media [129]. These nanoparticles are seeding toxic cadmium ions in the surrounding media due to photolysis or hydrolysis under physiological conditions (temperature and pH). The presence of a low quantity of cadmium ions can be highly toxic for cultured cells [130]. A solution to this issue of nanoparticle stability is to coat them with stable polymer but this only delays nanoparticle destabilisation and does not improve their excretion from the organism.

Another main mechanism of nanoparticle toxicity is their capacity to generate toxic ROS in the surrounding media [131]. It has been demonstrated that because of the high reactivity of the nanomaterial surface, nanomaterials can catalyse the formation

of ROS from their surrounding molecules [131]. The presence of ROS can lead to cell death by necrosis through the rupture of the cellular membrane by peroxidation of its constituting lipids [132]. The presence of ROS can also lead to cell death by apoptosis because of the damage generated by ROS to proteins, membranes, and DNA [132]. Indeed, ROS can oxidize amino acid residues in proteins leading to protein conformational changes. Conformational changes in proteins can lead to their inactivation [133]. It has also been demonstrated that nanoparticles can easily penetrate the cell nucleus and produce ROS there. ROS can generate DNA damage leading to the initiation of apoptosis by the *TP53* gene [134].

5.3.2.3. At the molecular level

Iron oxide nanoparticles, zinc oxide nanoparticles, titanium dioxide nanoparticles, carbon nanotubes, and copper oxide nanoparticles have been found to experimentally induce DNA damage when physically interacting [135]. The process of damaging is not clear at present but could originate from the valency of nanomaterial surface and intervene through oxidation of the DNA molecule.

Another aspect of nanomaterial toxicity at the molecular level is related to its capacity to adsorb biomolecules onto the surface. It has been shown that nanoparticles, because of their large surface area, adsorb biomolecules in dispersion [136]. Previous studies have demonstrated that the biomolecules, coating the surface of gold nanoparticles in layers, present a slightly modified 3D structure [137]. This capacity to aggregate biomolecules at QD surface has been used to create magnetic nanoparticles that can be used to remove certain pathogenic biomolecules from the organism. For example, strategies for extraction of amyloid fibers from liquid phase have been developed using γ-Fe_2O_3 magnetic nanoparticles coupled to insulin fibers to ensure removal of free insulin fibers during dialysis [138]. Also the ability of nanoparticles to inhibit the fibrillisation of amyloid-prone proteins and to disaggregate amyloid fibers has already promoted their use as therapeutic agents [139]. Amyloid-prone proteins and peptides are biomolecules which natively or under certain conditions can undergo a internal structure refolding leading to an enhance aggregation tendency. This aggregation, also called amyloid fibrillisation, presents a high degree of organisation and generates aggregates and micrometre scaled fibers which are toxic for the surrounding cells.

Unfortunately, reports have also shown that some nanoparticles seem to be able to enhance amyloid fibrillisation of amyloid-prone peptide like amyloid β (1-42) peptide [140]. The cause of this difference of effect of nanoparticles on amyloid-prone protein and peptide is not currently known.

5.4. Aim of the thesis

Within the framework of this thesis we have tried to identify the factor responsible for the pro-amyloidosis behaviour of certain nanoparticles. These findings could be applied to the design of nanoparticles for therapeutic use against Alzheimer's disease with little secondary effects on other amyloid-prone proteins or peptides.

Our working hypothesis is that the main force causing pro-amyloidosis behaviour is the charge presented at the surface of nanoparticles. In order to test it, we have developed nanoparticles of the same chemical composition, shape, surface structure, and aggregation tendency but presenting a different charge value at their surface. These nanoparticles were co-incubated with three different biomolecules: amyloid β, a strongly amyloid-prone peptide, insulin, a protein that is amyloid-prone only under very destabilizing conditions, and bovine serum albumin, a large protein known for its stability under destabilizing conditions. By analysing at the same time the biomolecule structure, the distribution of size in different mixtures, and the presence of amyloid-specific intermolecular structure we have been able to understand the role of nanoparticle surface charge on the amyloid aggregation of peptides and proteins.

This thesis aims to demonstrate that the presence of positive charges at the surface of nanoparticles inhibits the formation of amyloid aggregates and favours the aggregation of unstable peptides in a safe form on the nanoparticle surface. The thesis also intends to show that the presence of negative charge at the surface of nanoparticles can enhance amyloid fibrillisation of surrounding biomolecules. Moreover, this enhancing effect seems to be dependent on the internal stability of biomolecules. Nanoparticles carrying weak negative charges seem to induce or to enhance amyloid aggregation of relatively stable proteins while unstable peptides seem more influenced by nanoparticles carrying strongly negative charges.

6. Materials and methods

6.1. Materials

6.1.1. Chemical table

Name	Purity	Supplier
Human insulin, recombinant expressed in yeast	> 27.5 units per mg	Sigma Aldrich
Albumin, Bovine Serum	98 %	Sigma Aldrich
Amyloid β (1-42) peptide	> 95 %	Istituto di Ricerche Farmacologiche Mario Negri
Thioflavin T	75 %	Sigma Aldrich
Congo red	> 85 %	Sigma Aldrich
D,L-cysteine hydrochloride hydrate	98 %	Sigma Aldrich
PEG-OH (HS-C11-EG6-OH)	> 95%	Prochimia
PEG-COOH (HS-C11-EG6-OCH2-COOH)	> 95%	Prochimia
PEG-NH_2 (HS-C11-EG6NH2)	> 95%	Prochimia

$(CH_3)_2Cd$	99.9 %	STREM
Elemental Se	> 99.99%	STREM
Trioctylphosphine Oxide (TOPO)	99%	Sigma Aldrich
Trioctylphosphine (TOP)	99%	FLUKA
Hexadecylamine (HAD)	98%	FLUKA
Hexamethyldisilthiane $((tms)_2S)$	> 98 %	FLUKA
Diethylzinc (DEZn)	95 %	STREM
NaH_2PO_4	99 %	Sigma Aldrich
Na_2HPO_4	> 99.5 %	Sigma Aldrich
KCl	> 99.5 %	Sigma Aldrich
HCl	36.5 – 38 %	Sigma Aldrich
NaOH	98 %	Sigma Aldrich
Chloroform	99.8 %	Sigma Aldrich
Methanol	99.93 %	Sigma Aldrich
Ultrapure water	18 mΩ	Millipore

6.1.2. QD synthesis

The QD synthesis protocol used here was adapted by Artemyev and Sukhanova from already proven protocols [141, 142]. Briefly, a solution of 80 mg elemental Se, 110 μl dimethylcadmium, and 1 ml Trioctylphosphine (TOP) was rapidly injected into a solution of 10 g trioctylphosphine oxide (TOPO) and 5 g hexadecylamine (HDA) that had been dried, degassed under vacuum at 180°C, purged with argon, and heated to 300°C under argon flow beforehand. After injection CdSe crystal cores are formed whose average size is 2 nm. Further growth of the CdSe cores to the desired size can be achieved by refluxing of the mix solution at 280°C. CdSe cores are harvested by cooling down, using chloroform, to 60°C, precipitation and washing with methanol, before drying.

The synthesis of the ZnS shell on CdSe cores requires the dispersion of the latter in a solution of 10 g TOPO and 5 g HAD which had been dried, degassed, purged, and heated beforehand as described above. After dispersion of the cores, a solution of 210 μL hexamethyldisilthiane ($(tms)_2S$) and 130 μl diethylzinc (DEZn) in 2 ml TOP was added drop-by-drop into the mix at 220°C under argon flow and vigorous stirring. The resulting dispersion is cooled down, using chloroform, to 60°C and CdSe/ZnS quantum dots are harvested by precipitation and washing with methanol before drying.

6.2. Methods

6.2.1. Analytical techniques and tools

6.2.1.1. CD spectrometry

Circular dichroism (CD) spectrometry is a technique of biomolecule structure analysis based on the difference of absorption, by optically active chiral molecules, of circularly polarized electromagnetic radiations. Optically active chiral molecules absorb more circularly polarized radiations that are rotating with their same orientation [143]. Therefore by analysing the amount of left-hand and right-hand circularly polarised radiations absorbed at each wavelength value, one can generate a CD spectrum specific of each optically active chiral molecule [144]. Therefore, by comparing the CD spectra of the sample with known CD spectra databases, one can identify optically active chiral molecules present in a sample [145, 146]. Furthermore, the CD spectrum can also reveal chemical interactions if these interactions impact on the chirality of molecules. Thus by following the CD spectrum evolution of a chiral dye dispersion under different conditions, one can estimate the interactions of this chiral dye with various molecules [147]. More complex molecular systems, e.g. protein secondary structure conformations (α-helix, β-sheet, β-turn, and random coil), possess chirality thus present specific CD spectra [148]. Therefore CD spectra also give information on the structure of proteins present in a sample [149, 150] .

Secondary structure analysis was carried out by measuring CD spectra using a J815 CD spectrometer (Jasco-Spain, Madrid Spain) at 10°C over a wavelength range of 180 to 250 nm. All measurements were carried out in solutions using 1 mm path length cells (Hellma 110-QS). Using 1 mm path length quartz cuvettes the aliquot samples were diluted ten times in the corresponding buffer. Each spectrum is an average of twenty measurements.

Amyloid fiber specific detection was performed by measuring Congo red CD spectra using the same apparatus at 10°C over a wavelength range of 350 to 600 nm. All measurements were carried out in solutions using 1 mm path length cells (Hellma 110-QS). Samples were diluted ten times in Congo red solution. Each spectrum is an average of twenty measurements.

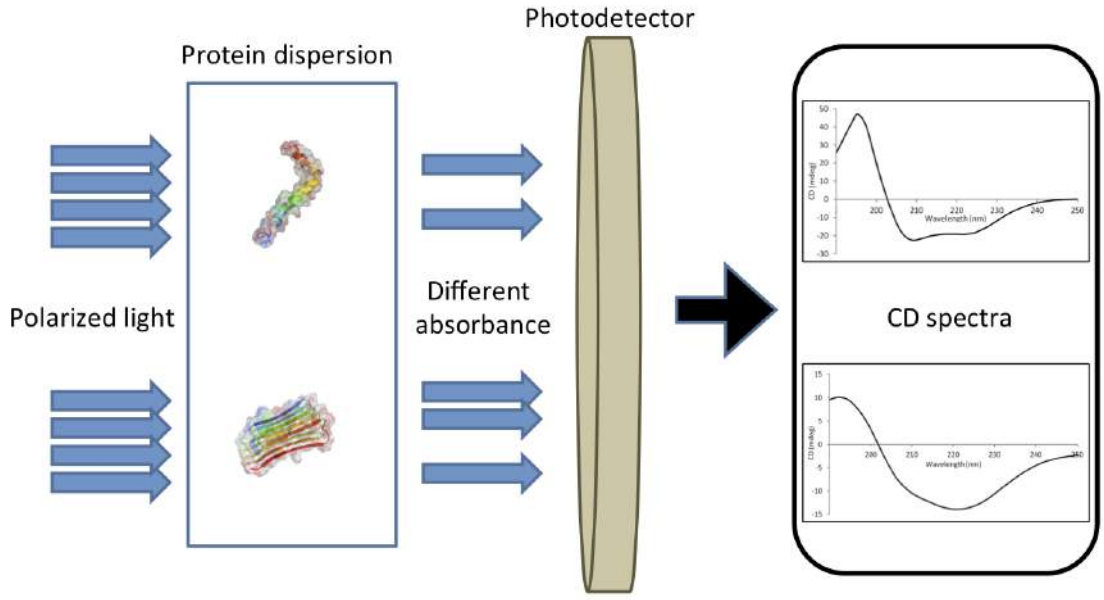

Figure 5. Circular dichroism is an analytical technique based on the difference of absorption of polarised light between orientated structures. In CD spectrometry the protein dispersion is excited at each wavelength with left-hand or right-hand polarised light. Upon passing through the quartz cuvette containing the protein dispersion one part of the polarized light is absorbed by proteins. The non-absorbed polarised light is detected by a photodetector and the resulting signals are converted into spectra representing the difference of absorption of left-hand and right-hand polarised light at each wavelength tested. These spectra are characteristic of the secondary structure organising the proteins inside the dispersion.

6.2.1.2. Dynamic Light Scattering

Dynamic light scattering (DLS) is based on the analysis of laser light scattering when particles in movement pass in front of the laser line. In DLS, and under certain conditions, the intensity of scattered light is dependent on the size of particles in suspension. Particles in suspension undergo Brownian motion and their speed of motion is dependent on their size, charge, polarity, and viscosity of the media. In DLS, the analysis of the speed of changes in the scattered light pattern can be translated into the average hydrodynamic radius of the dispersion particles [151, 152]. DLS analysis is very efficient in determining the hydrodynamic radius of monodisperse populations of particles in dispersion. The CONTIN algorithm is used to analyse polydisperse populations with DLS [153]. CONTIN analysis allows a minimum in size resolution of a factor of five between two different particle populations and a maximum in intensity difference of a factor of 10^5 [154, 155].

A periodic analysis of nanoparticle dispersions by DLS allows the study of nanoparticle stability in a certain buffer. Indeed if nanoparticles are not stable in a given buffer they will aggregate and therefore generate a new population of particles with a higher hydrodynamic radius than the initial population of nanoparticles [156].

Another application of DLS is the estimation of the zeta potential of a monodisperse population of particles in suspension. In order to estimate the zeta potential of a particle suspension, an electrical field is applied to the dispersion. Within the influence of this field the particles are put in movement. The direction and intensity of this movement is dependent on the charge carried at the surface of particles and on the size of particles therefore is dependent on the zeta potential of particles [157]. The speed and direction of particle movement under the influence of the electrical field is determined by analysis of the laser light scattering dynamics. The zeta potential was calculated from these electrophoretic measurement using the Smoluchowski approximation [158].

Nanoparticle average diameter was measured by DLS with a Nano ZS Zetasizer (Malvern, Worcestershire UK) at 25°C. Colloidal stability was evaluated as a function of time in pH6, pH7, or pH8 sodium phosphate buffers at 25°C.

The electrophoretic determination of zeta potential was performed under moderate electrolyte concentrations. Zeta-potential measurements of nanoparticle solutions were carried out at 25°C in 10 mM pH7 sodium phosphate buffers.

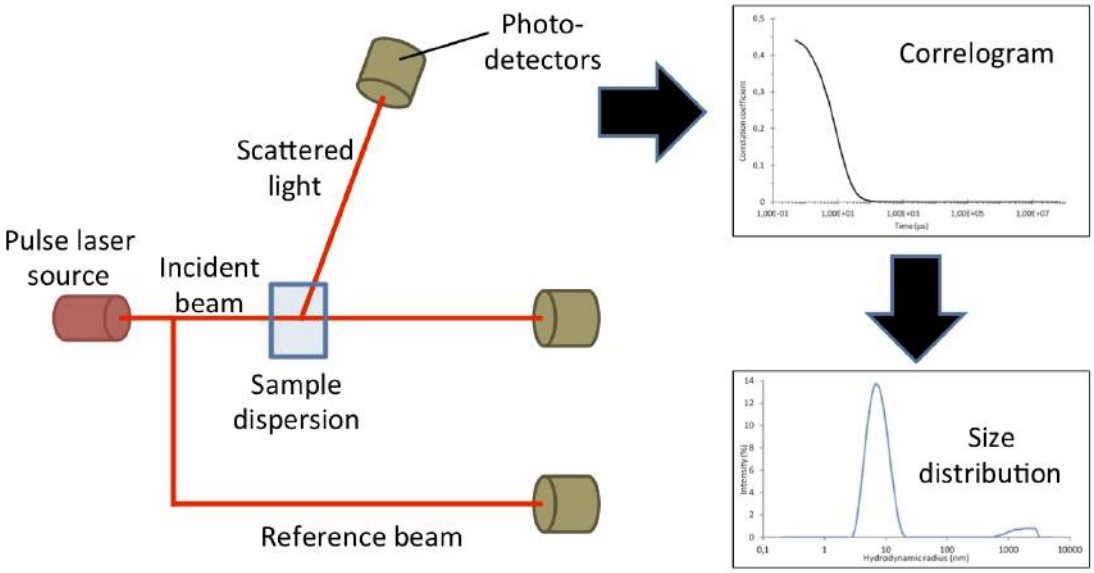

Figure 6. Dynamic light scattering is an optical method to analyse the size distribution of particles in suspension if their sizes range from 0.3 nm to 3 µm. The dynamic light scattering technique makes use of a 633 nm pulse laser split into two lines, one is a reference and the other is shined through a quartz cuve containing a dispersion. The laser light can be scattered by the particles in suspension. The intensity of light scattered by the particles is analysed through a photodetector fixed at an angle of 173° to the laser line. Upon analysis of the rate of change of the scattered light a correlogram of change of state upon time is generated. The rate of state change is dependent on the size and charge of the particles. Therefore it is possible to transform the correlogram into a representation of particle size distribution as a function of the percent total intensity of scattered light.

6.2.1.3. Fluorescence spectroscopy

Fluorescence spectroscopy is used to detect changes in fluorescence intensity and shifts of emission spectra induced by a modification of the fluorophore environment. These modifications of fluorescent dye optical properties are due to a change of the excited state charge distribution of the fluorophore. The excited state charge distribution is dependent on the interactions of the fluorescent dye with surrounding molecules, e.g. protein, or solvent. Fluorescence spectroscopy is measured by exciting the fluorescent dye at a specific wavelength and by measuring the emitted fluorescence light at different wavelengths. To avoid interference between excitation and emission light, the emission light is usually detected at 90° to the excitation light.

Fluorescence spectra were obtained using FP6600 spectro-fluorometer (Jasco). Before each fluorescence measurement, 30 µl aliquots were removed at different time periods, and diluted in 300 µl ThT solution. The ThT fluorescence was measured at 482 nm with an excitation wavelength of 440 nm in a semi micro quartz cuvette with a 1 cm optical path length (Hellma 115F-QS). Slit widths at excitation and emission were set respectively at 5 and 6 nm.

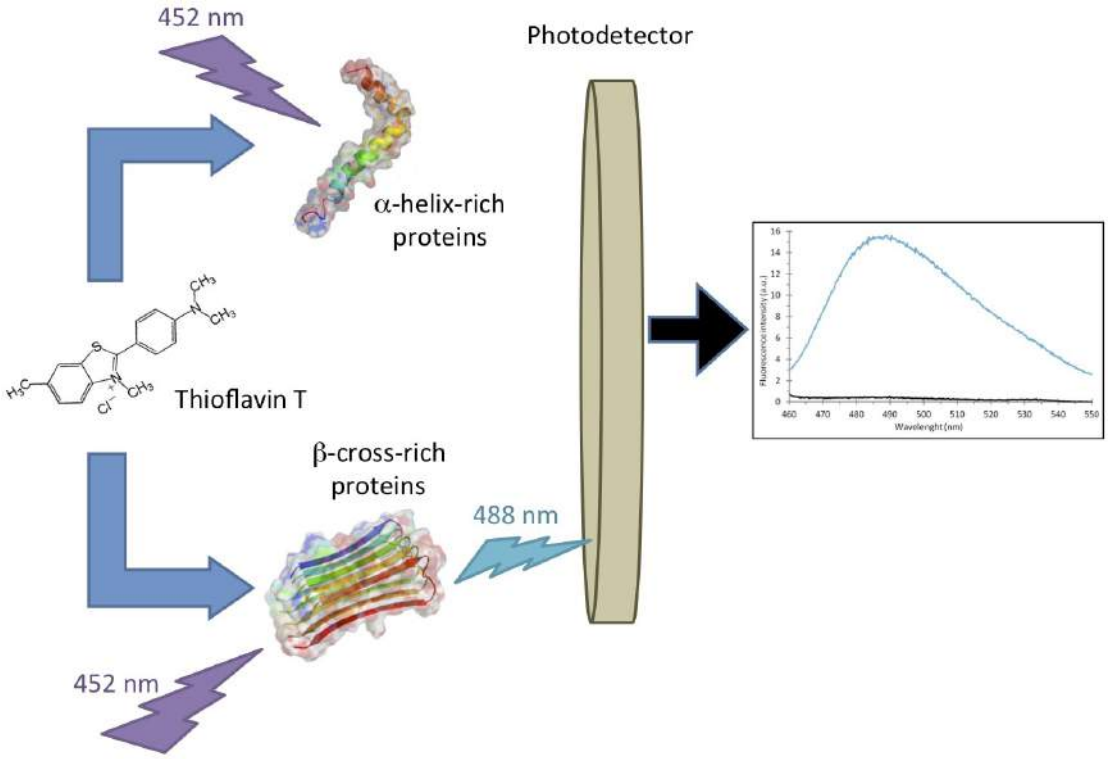

Figure 7. Spectro-fluorometry is an optical technique allowing the analysis of the light emitted by a specific molecule or particle upon excitation with a specific excitation wavelength. Here this technique is coupled to the use of the fluorescent dye thioflavin T (ThT). ThT changes its maximum of emission upon interacting with the β-cross amyloid-specific intermolecular structure. This capacity makes ThT a very good tagging agent of the amyloidosis process. ThT in the presence of β-cross-rich protein aggregates and excited at 452 nm will emit at 488 nm. This allows the use of ThT to follow the appearance and to quantify the β-cross intermolecular structure in protein dispersions.

6.2.2. QD solubilisation

After the synthesis of TOPO-capped hydrophobic QD, a modification to hydrophilic polyethylene glycol-capped (PEG) QD was carried out. First, chloroform was used to solubilize TOPO-capped QD. TOPO termination was removed by methanol washing, and replaced by D,L-cystein. After repeated methanol washing to remove the remaining TOPO-capped QD, QD dispersion was dried, for 2 minutes, in a concentrator plus (Eppendorf, Hamburg Germany). Cystein-solubilised QD were dispersed in ultrapure water, 1 M NaOH was added to improve QD solubilisation, and the dispersion was sonicated for 5 min using a Ultrasonic Cleaner 2510 sonication bath (Eppendorf) [159]. In order to minimize contamination by partially TOPO-capped QD the dispersions were centrifuged and filtered using Ultrafree-MC 0.2 μm-pore microcentrifuge filters (Sigma Aldrich, St. Louis USA).

PEG-OH, PEG-COOH, and/or PEG-NH_2 were used for surface ligand exchange of cystein-solubilised QD. An excess of low molecular weight mercapto-PEG was added to 1 ml cystein-solubilised QD in an alkaline dispersion and kept at 4°C overnight [160]. The excess PEG and D,L-cystein were removed by filtering the dispersion using Amicon Ultra-15 30 KDa Centrifugal Filter Units (Millipore, Billerica USA) and G-25 Sephadex columns (GE Healthcare, Little Chalfont UK).

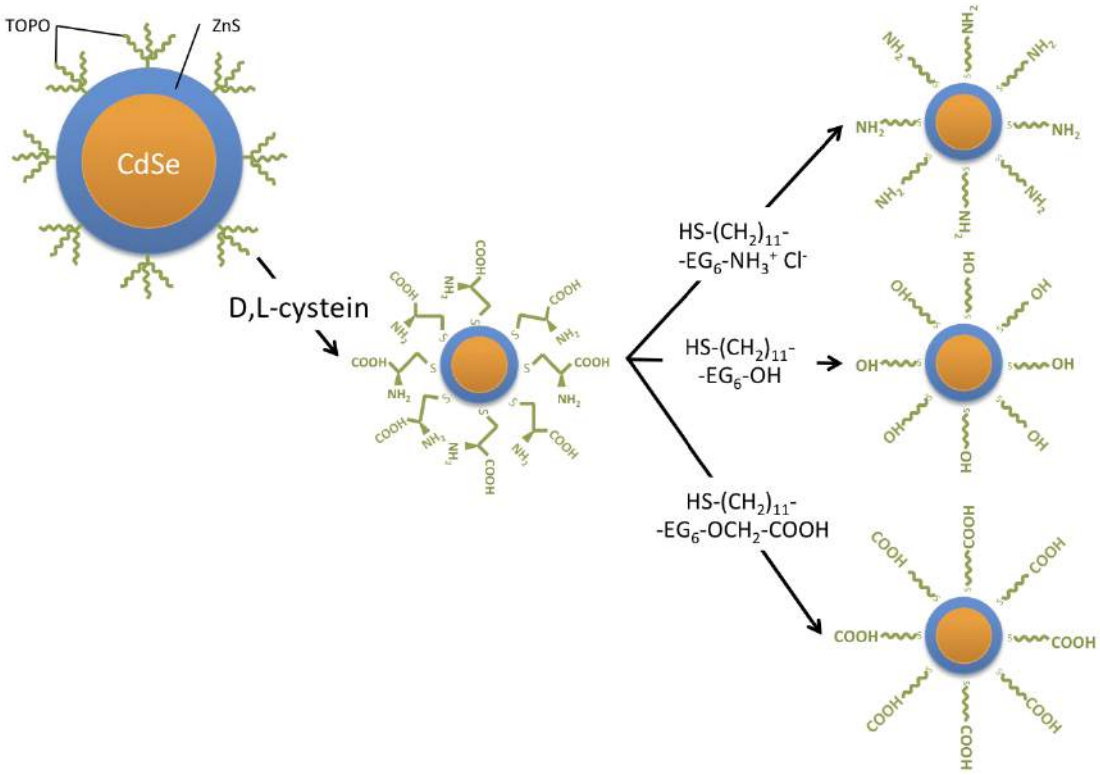

Figure 8. Solubilisation of QD CdSe/ZnS was carried out in two steps. First the layer of TOPO covering the QD was removed using methanol and replaced by D,L-cystein. Afterward, the cystein was exchanged for a low molecular weight polyethylene glycol (PEG) whose terminal chemical group has been selected. This technique ensures the high stability of CdSe/ZnS QD in aqueous buffers and the control of chemical groups distributed at the QD surface.

6.2.3. Protein and peptide preparation

6.2.3.1. Insulin solubilisation

Pure insulin dispersions were prepared solubilising 20 mg dehydrated human insulin in 1 ml 0.01 M HCl solution. The solution was then re-diluted in the appropriate buffer at 2 mg/ml and then incubated at different temperatures with or without CdSe/ZnS QD.

6.2.3.2. BSA solubilisation

Pure BSA dispersions were prepared solubilising 10 mg dehydrated BSA in 1 ml 10 mM sodium phosphate pH7 buffer. The solution was then re-diluted in 10 mM sodium phosphate pH7 buffer at 1 mg/ml and incubated at 37°C with or without CdSe/ZnS QD.

6.2.3.3. Aβ solubilisation

Pure Aβ dispersions were prepared by solubilising of 1 mg dehydrated human Aβ (1-42) peptide in 1 ml pure HFIP. The dispersion of Aβ in HFIP was stirred at room temperature until total solubilisation of the Aβ peptide powder (transparent dispersion without visible aggregates). HFIP was then evaporated under gentle nitrogen flux until only a yellow-coloured film was visible. 100 µl 10 mM sodium phosphate pH7 buffer were added. The solution was then re-diluted in 10 mM sodium phosphate pH7 buffer at 0.43 mg/ml and incubated at 37°C either with or without CdSe/ZnS QD.

6.2.3.4. Buffer preparation

10 mM sodium phosphate pH6 buffer was prepared by mixing 0.44 ml 0.1 M sodium phosphate dibasic, 4.56 ml 0.1 M sodium phosphate monobasic, and 45 ml Millipore ultrapure water. The buffer was then mixed thoroughly, filtered using Millex-LG 0.22 µm pore-size filter (Millipore), and degassed for 5 min using a Ultrasonic Cleaner 2510 sonication bath (Eppendorf).

10 mM sodium phosphate pH7 buffer was prepared by mixing 2.59 ml 0.1 M sodium phosphate dibasic, 2.41 ml 0.1 M sodium phosphate monobasic, and 45 ml Millipore ultrapure water. The buffer was then mixed thoroughly, filtered using a 0.22 µm filter (Millipore), and degassed for 5 min using a sonication bath (Eppendorf).

10 mM sodium phosphate pH8 buffer was prepared by mixing 4.6 ml 0.1 M sodium phosphate dibasic, 0.4 ml 0.1 M sodium phosphate monobasic, and 45 ml Millipore ultrapure water. The buffer was then mixed thoroughly, filtered using a 0.22 μm filter (Millipore), and degassed for 5 min using a sonication bath (Eppendorf).

Congo red dispersion was prepared and filtrated daily through a 0.22 μm filter (Millipore); it contains 0.1 g/l Congo red in 10 mM sodium phosphate pH7 buffer.

10 μM thioflavin T (ThT) working dispersion was prepared and filtered daily through a 0.22 μm filter (Millipore); it contains 16 μl 1 g/l ThT mother dispersion in 4.985 ml 10 mM sodium phosphate pH7 buffer. 1 g/l ThT mother dispersion was prepared every week by dissolving 1 mg of ThT powder in 1 ml 10 mM sodium phosphate pH7 buffer.

7. Results

7.1. PEGylated CdSe/ZnS quantum dots induced human insulin amyloid fibrillisation under physiological conditions

7.1.1. Interactions of PEGylated QD with human insulin *in vitro*

The incubation of different PEGylated QD with human insulin leads to an association between insulin and nanoparticles. Figure 9 represents the DLS analysis of different dispersions, and demonstrates that PEGylated QD are stable over a period of time of more than one week (Figure 9a). In the same way a dispersion of insulin alone shows no sign of aggregation over one week incubation in pH 7 buffer at 37ºC (Figure 9b). On the contrary analysis of a mixture of PEGylated QD with insulin shows a time-dependent evolution of size distribution in the dispersion and an experimental average size higher than the theoretical one and the one of PEGylated QD alone (Figure 9c). Analysis of PEGylated QD absorbance and fluorescence spectra confirms the stability of QD when mixed with insulin for longer than one week in physiological media. Interaction of insulin and PEGylated QD shows size-stable aggregates with most PEG but incubation with PEG-OH shows an aggregation process with aggregates of millimetre size after 24 h.

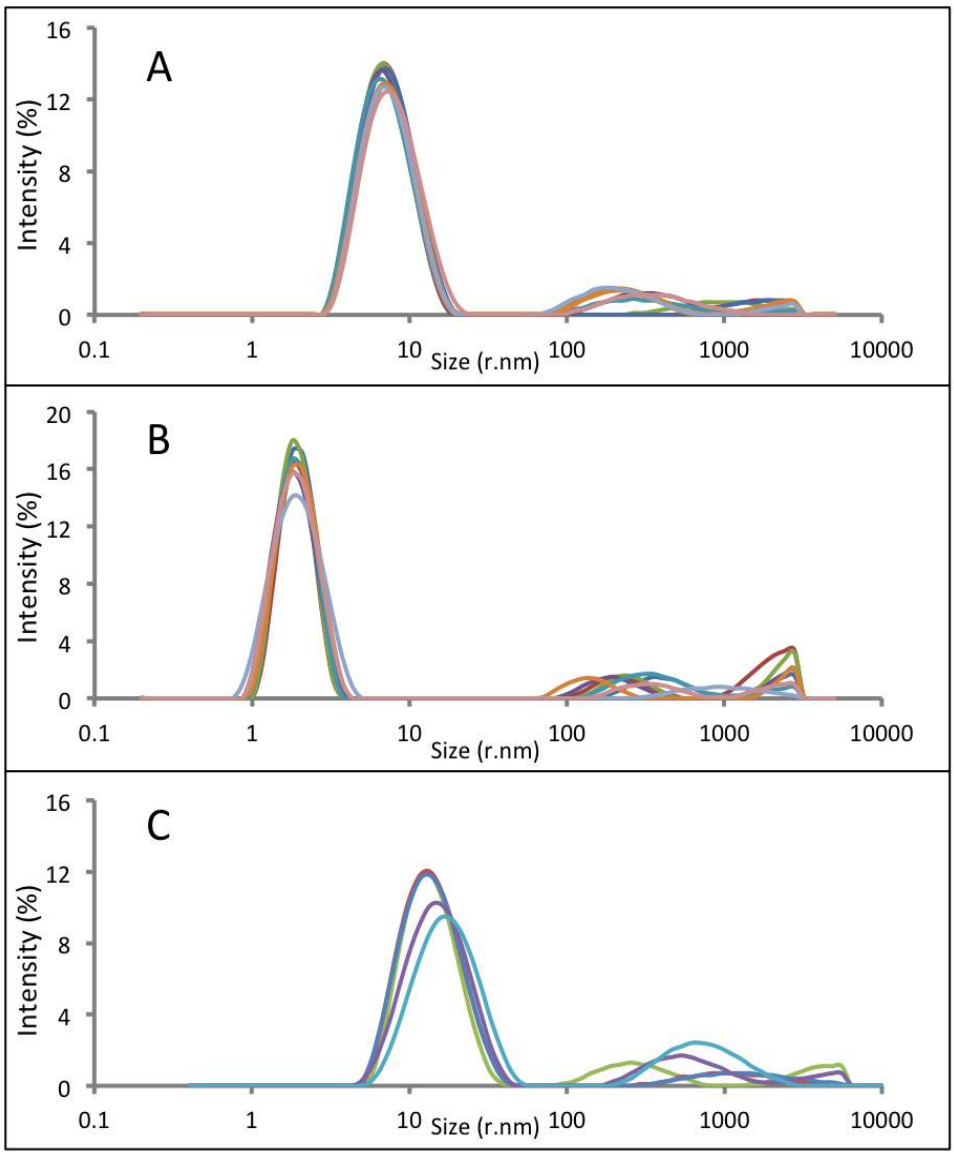

Figure 9. Size distribution of PEG-OH-coated CdSe/ZnS QD alone, insulin alone, and insulin in the presence of QD.

(A) Insulin was incubated at 2 mg/ml. (B) PEG-OH-coated CdSe/ZnS QD was incubated at 3.44 µM. The different dispersions were incubated in a 10 mM sodium phosphate pH 7 buffer at 37ºC over 7 days. DLS frequency curves were recorded after 0 (blue), 1 (red), 2 (green), 3 (violet), 4 (cyan), 5 (orange), 6 (grey), and 7 days (pink). (C) Insulin (2 mg/ml) was incubated in the presence of PEG-OH-coated CdSe/ZnS QD (3.44 µM), for 30 min. Frequency curves were recorded after 0 (blue), 5 (red), 10 (green), 20 (violet), and 30 min (cyan). (r.nm): hydrodynamic radius (in nm).

7.1.2. PEGylated QD induced Insulin aggregation

The process of aggregation, observed when insulin and PEG-OH QD were incubated in pH 7 buffer at 37°C, was demonstrated using dynamic size analysis (Figure 10). Through analysis of aggregate size evolution, one can observe that the size distribution of aggregates evolved rapidly after incubation (Figure 10a). Size distribution evolves continuously for 24 h with appearance of intermediate size aggregates of 0.05, 0.2, and 1 μm of diameter (Figure 10b). Insulin is known to form structurally defined fibers, amyloid fibers, but environmental conditions needed to induce this fibrillisation (at pH 2 and 60°C) are different from the ones observed in this study. Amyloid fiber specific parameters were analysed in order to characterize aggregates observed when insulin is incubated with PEGylated QD.

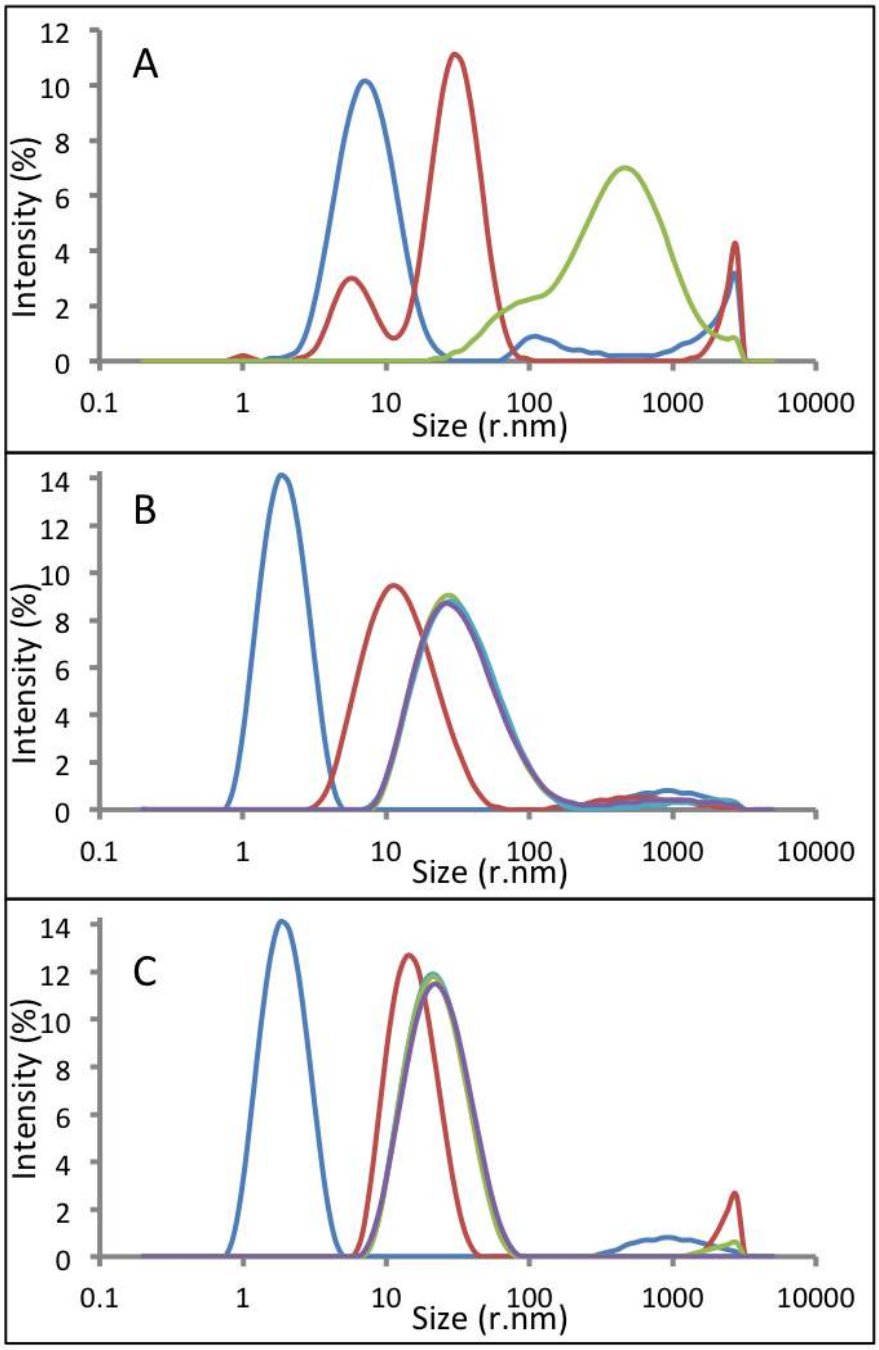

Figure 10. Insulin size distribution in the presence of PEG-OH-coated CdSe/ZnS QD, PEG-COOH-coated CdSe/ZnS QD, and PEG-NH_2-coated CdSe/ZnS QD, monitored over 24 h.

Insulin (2 mg/ml) was incubated in the presence of 3.44 μM PEG-OH-coated CdSe/ZnS QD (A), PEG-COOH-coated CdSe/ZnS QD (B), and PEG-NH_2-coated CdSe/ZnS QD (C) in a 10 mM sodium phosphate pH 7 buffer at 37ºC. All dispersions were incubated for 24 h. (A) Dynamic light scattering frequency curves were recorded after 0 (blue), 12 (red), and 24 h (green). (B) Frequency curves represent insulin alone (blue), PEG-COOH-coated CdSe/ZnS QD alone (red) and mix of insulin and QD after 0 (green), 12 (violet), and 24 h (cyan). (C) Frequency curves represent insulin alone (blue), PEG-NH_2-coated CdSe/ZnS QD alone (red) and mix of insulin and QD after 0 (green), 12 (violet), and 24 h (cyan). (r.nm): hydrodynamic radius (in nm).

7.1.3. QD-induced insulin aggregation displays similarities with amyloid fibrillisation phenomena

Analysis of aggregates generated when insulin is incubated with PEGylated QD shows that insulin aggregation, induced by PEG-OH QD at pH 7 and 37°C, generates fibers presenting amyloid structural features. Indeed, by analysing the secondary structure of insulin one can see that the addition of PEGylated QD, with PEG-OH, induces a change in the far UV circular dichroism spectra of the dispersion, which can be interpreted as an insulin secondary structure change from a native form, rich in α-helix to a form rich in β-sheet (Figure 11a). The dispersion of PEGylated QD does not present any circular dichroism activity in the far UV and dispersions of insulin alone present stable circular dichroism spectra corresponding to the native α-helix form of insulin (Figure 11b) over the same period of incubation at pH 7 buffer and 37°C, which confirms that the aggregation process of insulin induced by PEGylated QD coated with PEG-OH is linked to a secondary structure change similar to the one occurring during amyloid fibrillisation. Insulin aggregation induced by PEGylated QD was investigated using amyloid specific dyes: Congo red or thioflavin T, in order to further demonstrate its relation with amyloid phenomena.

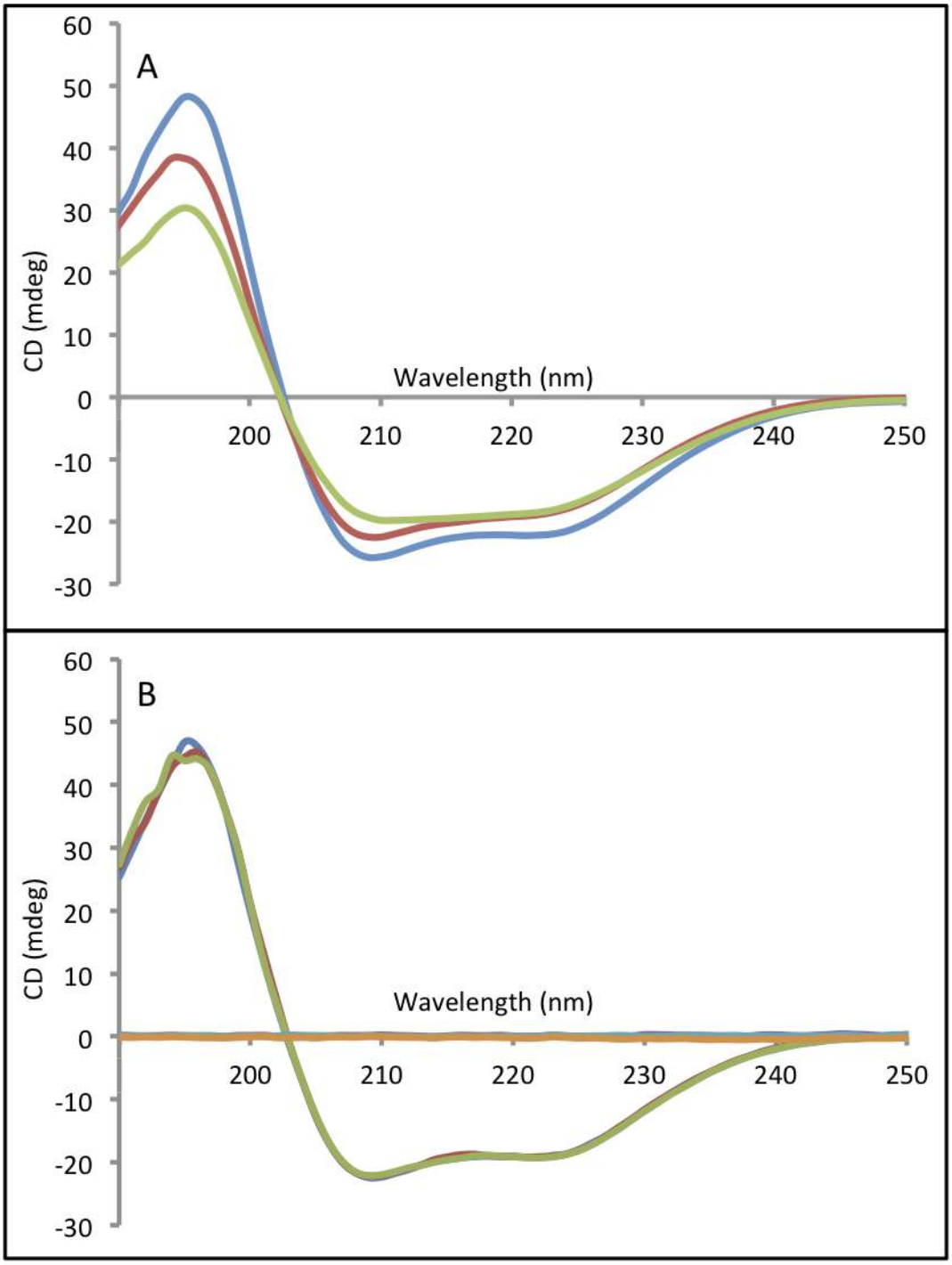

Figure 11. Change in insulin secondary structure in the presence of QD.

Far UV circular dichroism spectra of insulin (2 g/l) in the presence of 3.44 μM PEG-OH-coated CdSe/ZnS QD (A). Far UV circular dichroism spectra of pure insulin (2 g/l) and pure PEG-OH-coated CdSe/ZnS QD (3.44 μM) (B). Spectra of insulin in the presence of PEG-OH-coated CdSe/ZnS QD were recorded after 0 (blue), 12 (red), and 24 h (green). Spectra of pure insulin were recorded after 0 (blue), 12 (red), and 24 h (green), and spectra of pure PEG-OH-coated CdSe/ZnS QD were recorded after 0 (violet), 12 (cyan), and 24 h (orange). All experiments were performed in 10 mM sodium phosphate buffer pH 7 at 37ºC.

Congo red had been used for a long time as a tagging agent of amyloid cerebral deposits for the diagnostic of Alzheimer's disease [147]. It is known to interact with the cross-β structure of amyloid fibers and this interaction induces the appearance of a circular dichroism activity by the so-called extrinsic Cotton effect [161]. Congo red CD spectrometry confirms that insulin aggregation can be related to a secondary structure change but does not demonstrate its amyloid nature (Figure 12). Indeed a dispersion of QD alone presents no Congo red CD spectra induction over 36 h in pH 7 buffer at 37°C (Figure 12b). Figure 12b, representing the evolution of Congo red CD spectra of a dispersion of pure insulin, shows that the spectra do not change over incubation for 36 h in pH 7 buffer at 37ºC and stay similar to the spectra of monomeric insulin as described in the literature. On the contrary, insulin incubated with PEGylated QD, coated with PEG-OH, shows a decrease in Congo red circular dichroism spectra specific of monomeric insulin but without the appearance of an insulin amyloid fiber specific spectrum (Figure 12a). This result demonstrates the change of secondary structure already observed during analysis of insulin secondary structure by far UV CD spectrometry but is not sufficient to demonstrate the appearance of amyloid fibers of insulin in the dispersion. In order to clarify the nature of the protein structure change observed in these dispersions an amyloid specific fluorescent dye has to be used.

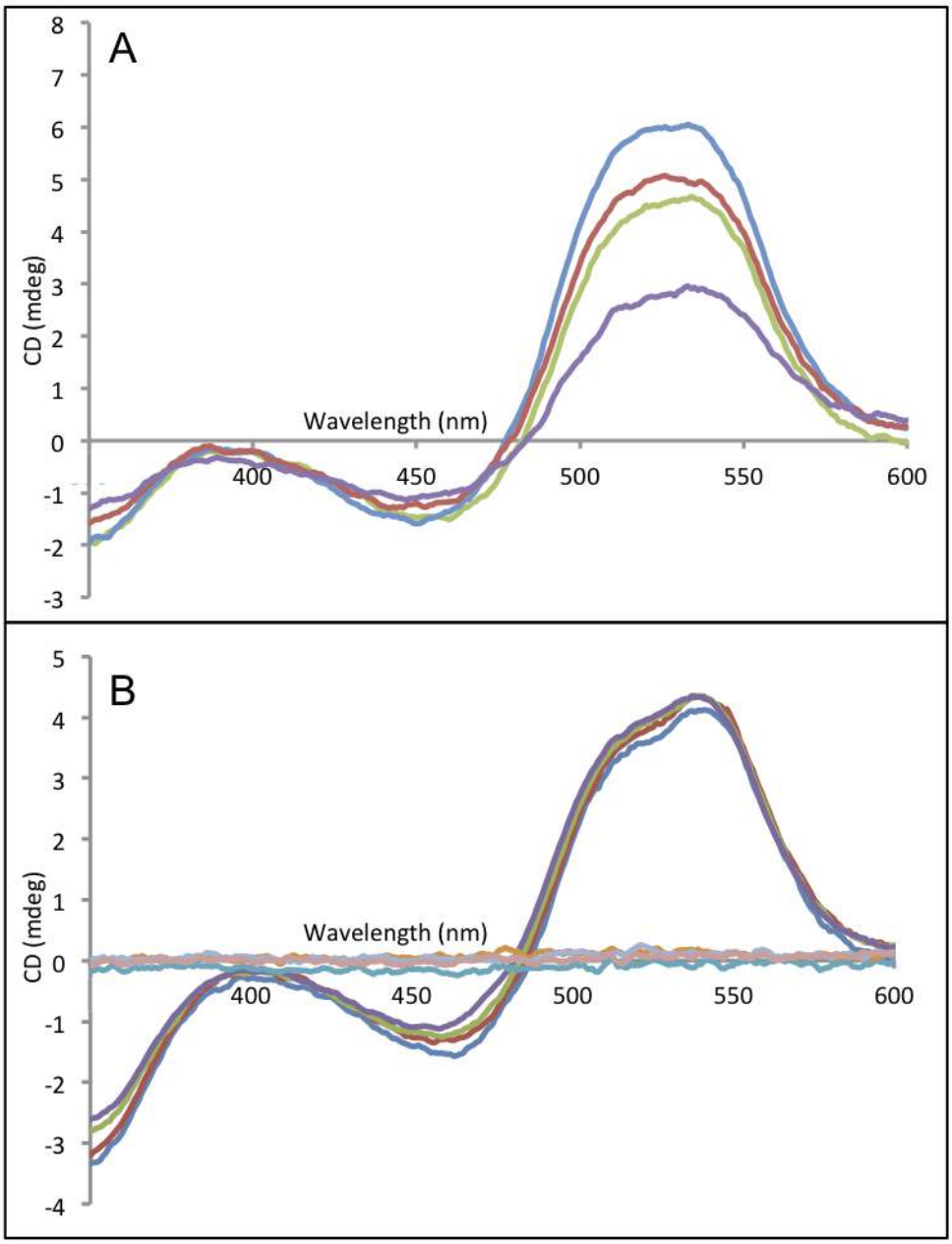

Figure 12. Insulin fibrillisation kinetics at 37ºC monitored by Congo red CD.

Insulin (2 g/l) was incubated in the presence of 3.44 μM PEG-OH-coated CdSe/ZnS QD (A). Spectra were recorded after 0 (blue), 12 (red), 24 (green), and 36 h (violet). 3.44 μM PEG-OH-coated CdSe/ZnS QD or 2 g/l insulin were incubated alone (B). For pure insulin, spectra were recorded after 0 (blue), 12 (red), 24 (green), and 36 h (violet). For pure QD, spectra were recorded after 0 (cyan), 12 (orange), 24 (grey), and 36 h (pink). All experiments were performed in 10 mM sodium phosphate pH 7 buffer at 37ºC.

Thioflavin T and derived dyes are currently used as specific tagging agents for amyloid fibers *in vitro* [162]. Thioflavin T, a fluorescent dye, has excitation and emission spectra which change when it interacts with a cross-β structure: its absorption maximum shifts from 350 nm to 438 nm and its emission maximum shifts from 450 to 482 nm [162]. Here ThT fluorescence assay confirms results obtained with Congo red: insulin aggregation, induced by PEGylated QD coated with PEG-OH, exhibits amyloid fibrillisation characteristics. Analysis of Figure 13 shows that when insulin is incubated in pH 7 buffer and 37°C there is no fluorescence at 482 nm, thus insulin does not form amyloid fibers over 30 h incubation. But if mixed with PEGylated QD then an increase in fluorescence is observed at 482 nm starting after 6 h and continuing over about 30 h. If the observed phenomenon of insulin amyloid fibrillisation is induced by PEG-coated QD then an increase in QD concentration should induce an accelerated amyloid fibrillisation and *vice versa*.

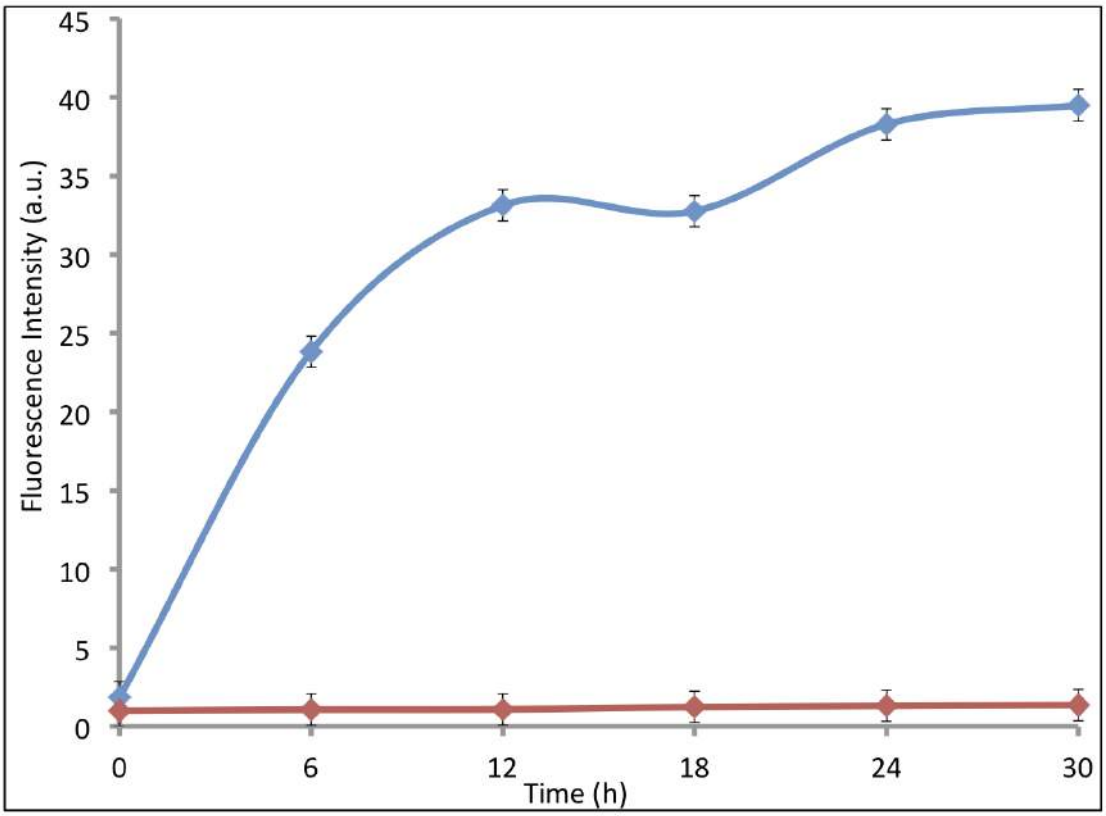

Figure 13. Insulin fibrillisation kinetics at 37ºC monitored by ThT fluorescence.

Human recombinant insulin (2mg/ml) was incubated in the absence (red) or in the presence (blue) of 3.44 μM PEG-OH-coated CdSe/ZnS QD in 10 mM sodium phosphate pH 7 buffer at 37ºC over 30 h.

7.1.4. Effect of QD concentration on QD-related insulin fibrillisation

In order to demonstrate the direct inducing effect of QD on insulin fibrillisation the effect of QD concentration in the dispersion has been studied. Analysis of different QD/insulin molar ratios in pH 7 buffer at 37°C shows that the phenomenon of insulin aggregation in the presence of PEG-OH-coated QD (QD-OH) is directly dependent on the QD/insulin molar ratio. Indeed, as shown in Figure 14 a higher QD/insulin ratio induces a faster protein refolding, which can be connected to insulin aggregation, and a lower ratio induces a slower insulin refolding. Again a dispersion of pure insulin shows no sign of protein refolding over 24 h at 37°C (Figure 14a). The role of QD-OH on insulin aggregation is thus demonstrated but the underlying mechanism has not been unraveled so far. The link between temperature and pH variations and the aggregation phenomenon has been investigated in order to elucidate its mechanism.

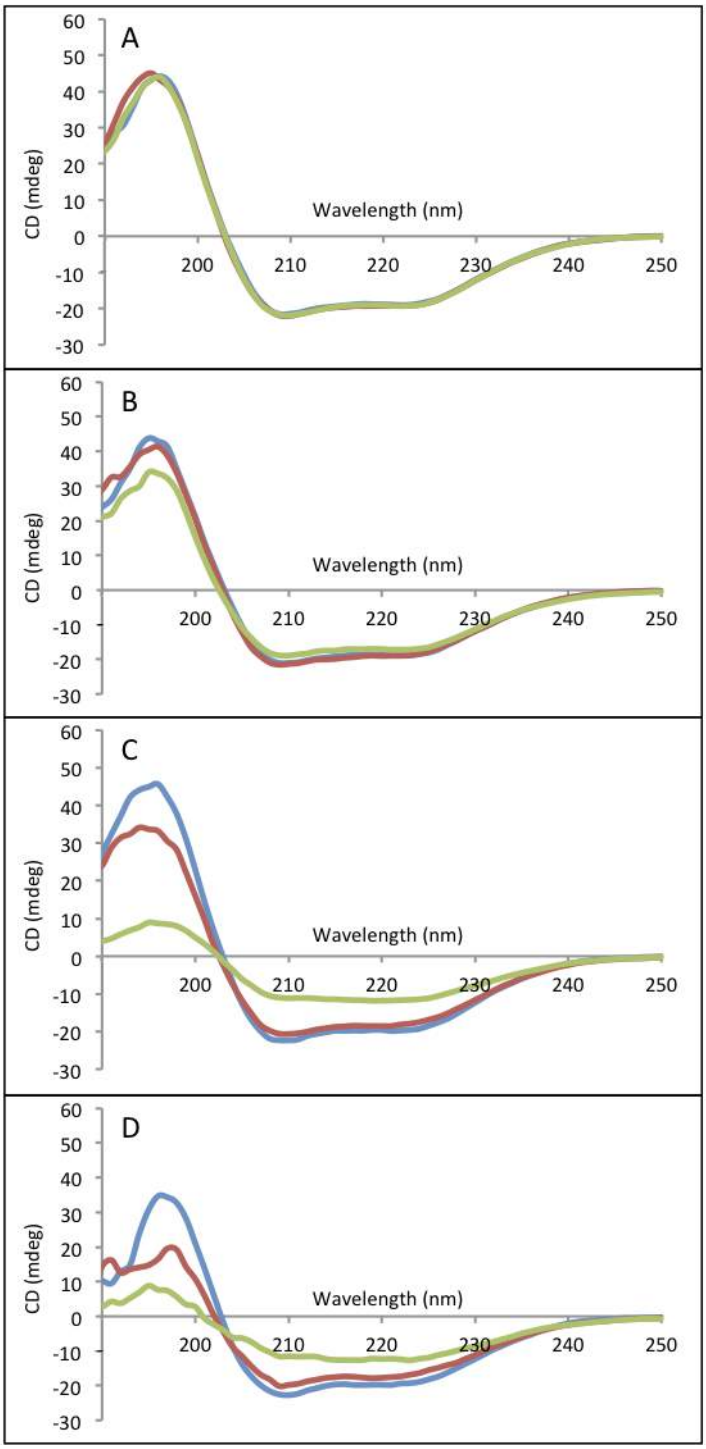

Figure 14. Change in insulin secondary structure in the presence of different concentration of QD.

Far UV circular dichroism spectra of insulin (2 mg/ml) in the absence (A) or the presence of different concentrations of PEG-OH-coated CdSe/ZnS QD: 13.76 μM (B), 3.44 μM (C), 0.86 μM (D). Dispersions were incubated for 24 h in a 10 mM sodium phosphate pH 7 buffer at 37ºC. For each condition, spectra were recorded after 0 (blue), 12 (red), and 24 h (green).

7.1.5. Effect of temperature on QD-related insulin fibrillisation

The effect of temperature on the previously observed phenomenon was investigated. It has already been shown that native insulin can form amyloid fibrils under certain *in vitro* incubation conditions: 60°C and pH 2 buffer [163]. It is known that in the case of the already described *in vitro* insulin fibrillisation, the effect of both temperature and pH are complementary to induce the secondary structure destabilisation needed to induce amyloid fibrillisation. An increase in incubation temperature or a decrease in pH has been shown to accelerate the process of insulin fibrillisation [163].

QD-OH and insulin were incubated in pH 7 buffer at 25, 37, or 50°C. Insulin fibrillisation was investigated using ThT fluorescence assay. Figure 15 shows that, when incubated at 25°C the dispersion shows no increase in the ThT specific fluorescence over 6 h incubation, incubation at 37°C causes a constant increase in the ThT specific fluorescence, and incubation at 50°C accelerates the rate of the specific fluorescence increase

Temperature-dependence supports the hypothesis that the role of QD-OH in the induction of insulin fibrillisation is linked to the destabilisation of insulin structure.

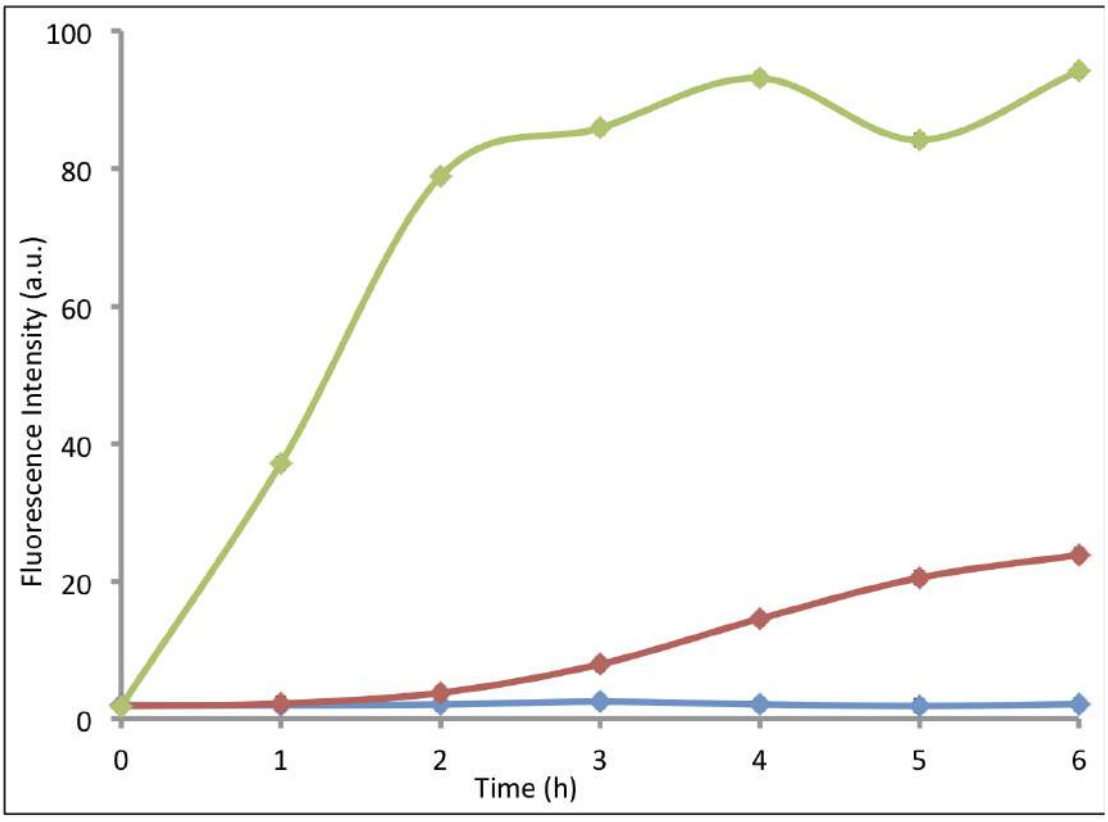

Figure 15. Insulin fibrillisation kinetics monitored through ThT fluorescence intensity.

Human recombinant insulin (2mg/ml) was incubated in the presence of 3.44 μM PEG-OH-coated CdSe/ZnS QD in a 10 mM sodium phosphate pH 7 buffer. The resulting dispersions were incubated at different temperatures for 6 h: 50ºC (green), 37ºC (red), or 25ºC (blue).

7.1.6. Effect of pH on QD-related insulin fibrillisation

Low pH was described to destabilize insulin without inducing a change in the secondary structure [163]. This effect is known to accelerate the *in vitro* insulin thermo-fibrillisation and to accelerate the aqueous solubilisation of solid insulin [163]. Here the impact of pH variations is investigated with the same aim: to identify the mechanism of insulin fibrillisation induction by QD-OH. Indeed, we postulate the hypothesis that if the presence of QD is acting as a destabilization agent then a decrease in pH of the mixture of QD and insulin should generate a faster insulin fibrillisation.

Three mixtures of QD-OH and insulin were incubated at 37°C in three different buffers of pH 6, 7, or 8. The effect of pH on insulin fibrillisation was investigated using ThT fluorescence assay. Figure 16 shows that the change in ThT fluorescence is faster at the higher pH.

These findings allow us to propose that QD-OH induced insulin fibrillisation is related to electrical charges present at the QD surface. Indeed, pH variations could induce charge changes at the surface of QD. Thus the link between QD surface charge variations and the QD-induced insulin amyloid fibrillisation has been studied.

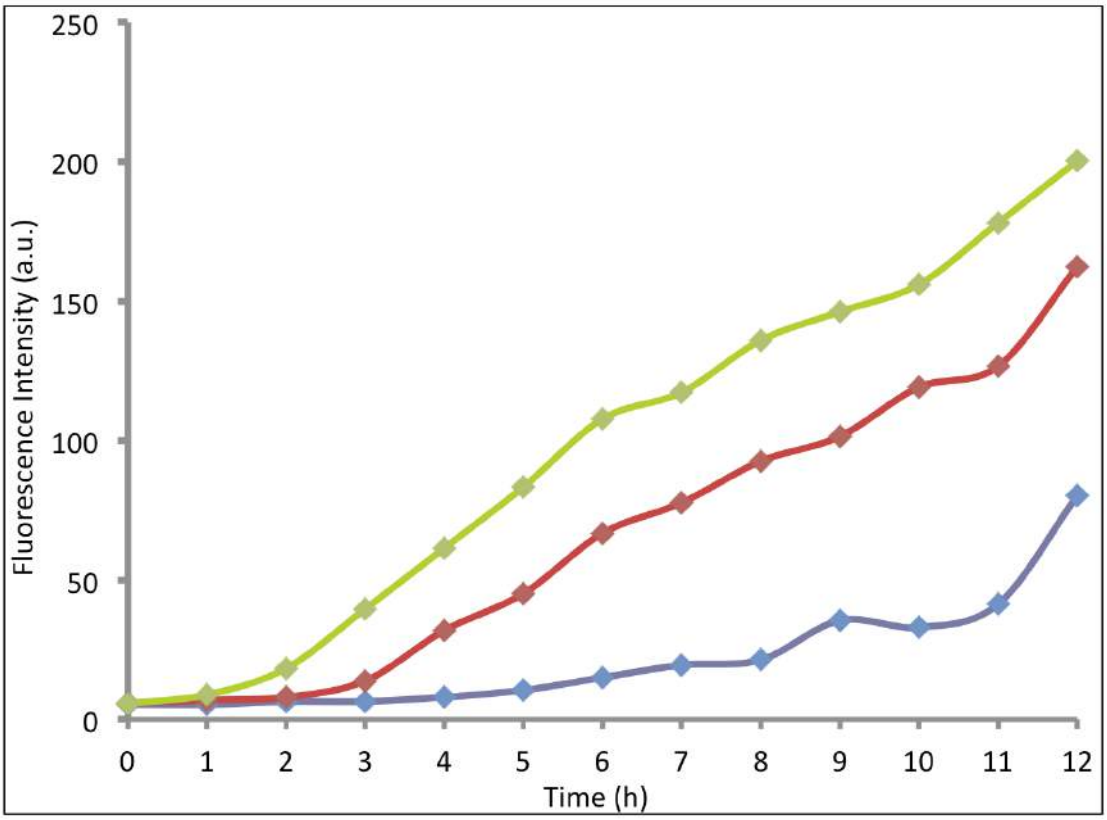

Figure 16. Insulin fibrillisation kinetics monitored through ThT fluorescence intensity.

Human recombinant insulin (2mg/ml) was incubated in the presence of 3.44 μM PEG-OH-coated CdSe/ZnS QD at 37ºC. Insulin and QD were incubated for 12 h in 10 mM sodium phosphate buffers with different pH: 8 (green), 7 (red), or 6 (blue).

7.1.7. The effect of QD surface charges on QD-related insulin fibrillisation

By analysing the effect on soluble native insulin of PEGylated CdSe/ZnS QD presenting different chemical functions, and so different charges at their surface, we demonstrate below that only QD with a weak negative charge are able to induce insulin aggregation. Indeed, figure 17 indicates that in the presence of PEG-COOH-coated QD (QD-COOH) (Figure 17B) or PEG-NH_2-coated QD (QD-NH_2) (Figure 17C) the insulin secondary structure remains unchanged for 24 h at pH 7. Meanwhile, Figure 17A shows that QD-OH, as previously described, induce a change in the secondary structure of insulin dispersion.

The zeta potential of PEGylated CdSe/ZnS QD dispersions in pH 7 buffer at 37°C shows that QD-OH present an average charge of -5.2 mV, QD-COOH present an average charge of -53.6 mV, and QD-NH_2 present an average charge of +18.4 mV (table 1).

Type of QD	Hydrodynamic radius (nm)	Zeta potential (mV)
QD-COOH	6.4 ± 1.9	-53.6 ± 5.4
QD-OH	5.8 ± 1.8	- 5.2 ± 6.6
QD-NH_2	6.4 ± 2.9	+ 18.4 ± 8.2

Table 1 Hydrodynamic radius and zeta potential of CdSe/ZnS QD coated with different PEG.

3.44 µM of CdSe/ZnS QD coated with PEG-COOH, PEG-OH, or PEG-NH_2 were incubated in 10 mM sodium phosphate pH 7 buffer at 37ºC and analysed after 10 min incubation. Hydrodynamic radius was calculated from the intensity-based particle size distribution, using the Rayleigh's approximation, to reflect the number-based particle size distribution. Zeta potential was calculated using the Huckel's approximation.

Thus low negative charges at the surface of nanoparticles are responsible for inducing the effect of PEGylated QD on insulin fibrillisation. These findings correlate with previous studies that show that gold nanoparticles with negative charges at their surface induce insulin fibrillisation. In this study negative charges are proposed to be the fibrillisation-inducing element of nanoparticles [164]. In order to explain our results, and in particular the requirement of a low negative charge, we formulate the hypothesis that the inducing effect of PEGylated QD could be related, not to the value of negative charges at the surface of QD but to the distribution pattern of charges.

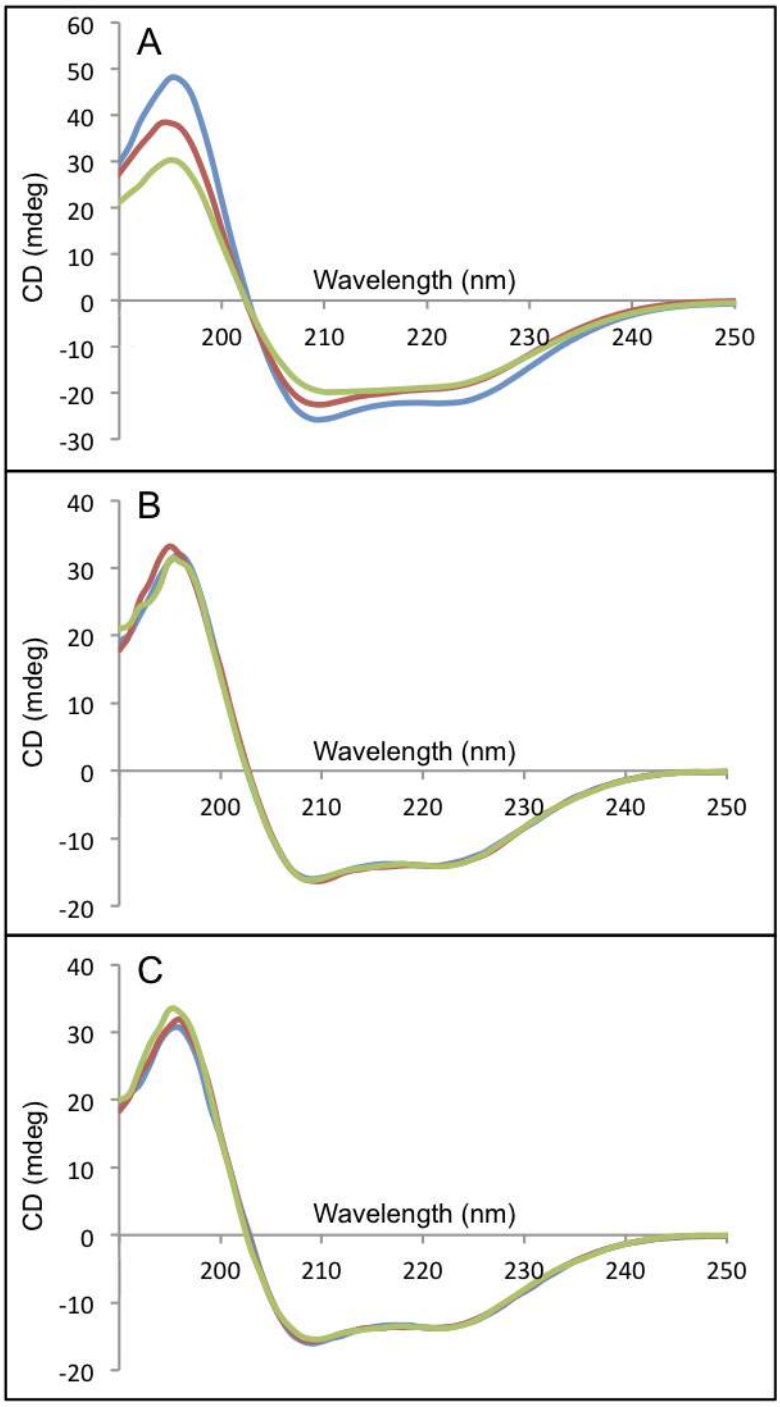

Figure 17. Change in insulin secondary structure in the presence of differently coated QD.

Far UV circular dichroism spectra of insulin (2 mg/ml) in the presence of 3.44 μM of differently coated CdSe/ZnS QD: with PEG-OH (A), with PEG-COOH (B), or with PEG-NH_2 (C). Dispersions were incubated for 24 h in a 10 mM sodium phosphate pH 7 buffer at 37ºC. For each condition spectra were recorded after 0 (blue), 12 (red), and 24 h (green).

7.1.8. The effect of surface charge distribution on the QD-related insulin fibrillisation

To analyse the effect of charge distribution at the surface of QD-OH we used QD of different size coated with the same amount of PEG-OH in order to generate a variation of the spacing between charges at the QD surface. Three different QD-OH were created using CdSe/ZnS core/shell QD with a respective core diameter of 2.5, 3.3, and 4.8 nm, and are named using their fluorescence emission maximum: respectively QD 530, QD 570, and QD 610. The newly created QD-OH hydrodynamic radius and zeta potential have been analysed by dynamic light scattering in order to ensure the purity of the QD dispersion and the value of the individual surface charge (Table 2).

Type of QD	Hydrodynamic radius (nm)	Zeta potential (mV)
QD 530	4.9 ± 1.5	- 2.5 ± 4
QD 570	5.8 ± 1.8	- 5.2 ± 6.6
QD 610	7.2 ± 2.4	- 12.3 ± 7.9

Table 2. Hydrodynamic radius and zeta potential of CdSe/ZnS QD with different core-sizes.

3.44 µM of CdSe/ZnS QD coated with PEG-OH and core-sizes of 2.5 (QD 530 nm), 3.3 (QD 570 nm), or 4.8 nm (QD 610 nm) were incubated in 10 mM sodium phosphate pH 7 buffer at 37ºC and analysed after 10 min incubation. Hydrodynamic radius was calculated from the intensity-based particle size distribution, using the Rayleigh's approximation, to reflect the number-based particle size distribution. Zeta potential was calculated using the Huckel's approximation.

Analysis of the effect of these three kinds of QD-OH on insulin for 3 days, at pH 7 and 37°C, shows that only QD 570 were able to induce secondary structure change (Figure 18B). Analysis of a dispersion of insulin and QD 570, by circular dichroism, demonstrates that the presence of QD 570 induces a change in secondary structure of insulin. Differences between spectra observed in Figure 18C can be considered as non-consistent and due to the noise created by the absorption spectrum of QD 610.

We conclude that the induction of insulin fibrillisation observed in this study is not related to the bulk value of charges at the QD surface but to a specific charge density at the QD surface thus to a specific presentation pattern of these charges to insulin.

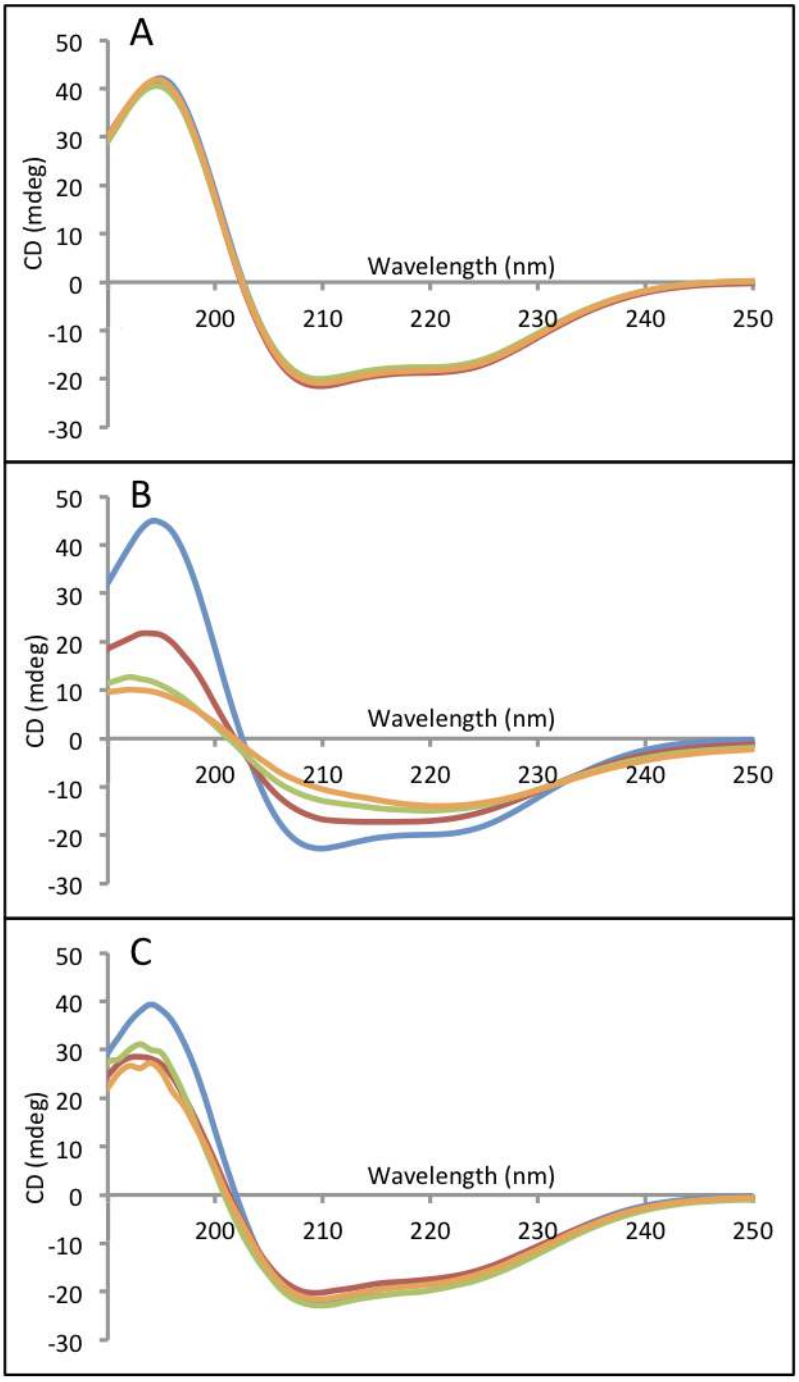

Figure 18. CD demonstrates changes in insulin secondary structure in the presence of QD of different sizes.

Far UV circular dichroism spectra of insulin (2 mg/ml) in the presence of 3.44 μM of PEG-OH-coated CdSe/ZnS QD with different core diameters: 2.5 (A), 3.3 (B), and 4.8 nm (C). Dispersions were incubated for 3 days in a 10 mM sodium phosphate pH 7 buffer at 37ºC. For each condition, spectra were recorded after 0 (blue), 1 (red), 2 (green), and 3 days (orange).

7.2. PEGylated CdSe/ZnS QD modify the kinetics of amyloid β (1-42) peptide fibrillisation and of bovine serum albumin aggregation under physiological conditions

Following our results on insulin we decided to analyse the effect of QD on an amyloidosis-prone peptide and, as a control, on a stable protein with the aim to clarify the role of QD surface charges on the peptide and protein structure previously identified on insulin.

Amyloid β (1-42) peptide (Aβ) was chosen as an amyloidosis-prone peptide for its role in Alzheimer's disease, its known structural unstability in physiological buffer, and its ability to form fully-matured amyloid fibers within a week of incubation at 37°C.

Bovine serum albumin (BSA) was chosen as the stable protein because of its relatively large size and structure stability, its easy availability, and its known pattern of aggregation without fibrillisation upon incubation at 37°C.

In order to assess consequences of the interaction of QD with peptides or proteins one should first clarify the capacity of QD to physically interact with peptides or proteins previously observed when QD and insulin were mixed together.

7.2.1. QD interact with Aβ and BSA to form aggregates

Physical interaction of QD with various proteins and peptides was studied using the dynamic light scattering technique. Results can be found in Figure 19. QD appears to interact with different proteins and peptides under physiological conditions.

Figure 19A shows that interactions of QD-OH and Aβ generate aggregates (green curve) larger than pure QD (red curve) and pure Aβ (blue curve). Similar results have been obtained using QD-COOH (Figure 19B) and QD-NH_2 (Figure 19C). These results demonstrate the capacity of QD coated with different chemical groups to interact with the Aβ.

Figure 19 also shows that QD can also interact with larger proteins like bovine serum albumin (BSA). Indeed, Figure 19D demonstrates that interactions of QD-OH and BSA generate aggregates (green curve) larger than pure QD-OH (red curve) and pure BSA (blue curve). Similarly interactions of QD-NH_2, or QD-COOH, with BSA also generate complexes larger than pure BSA or pure QD (Figure 19D and 19E). These results demonstrate the capacity of QD coated with various chemical groups to interact with BSA.

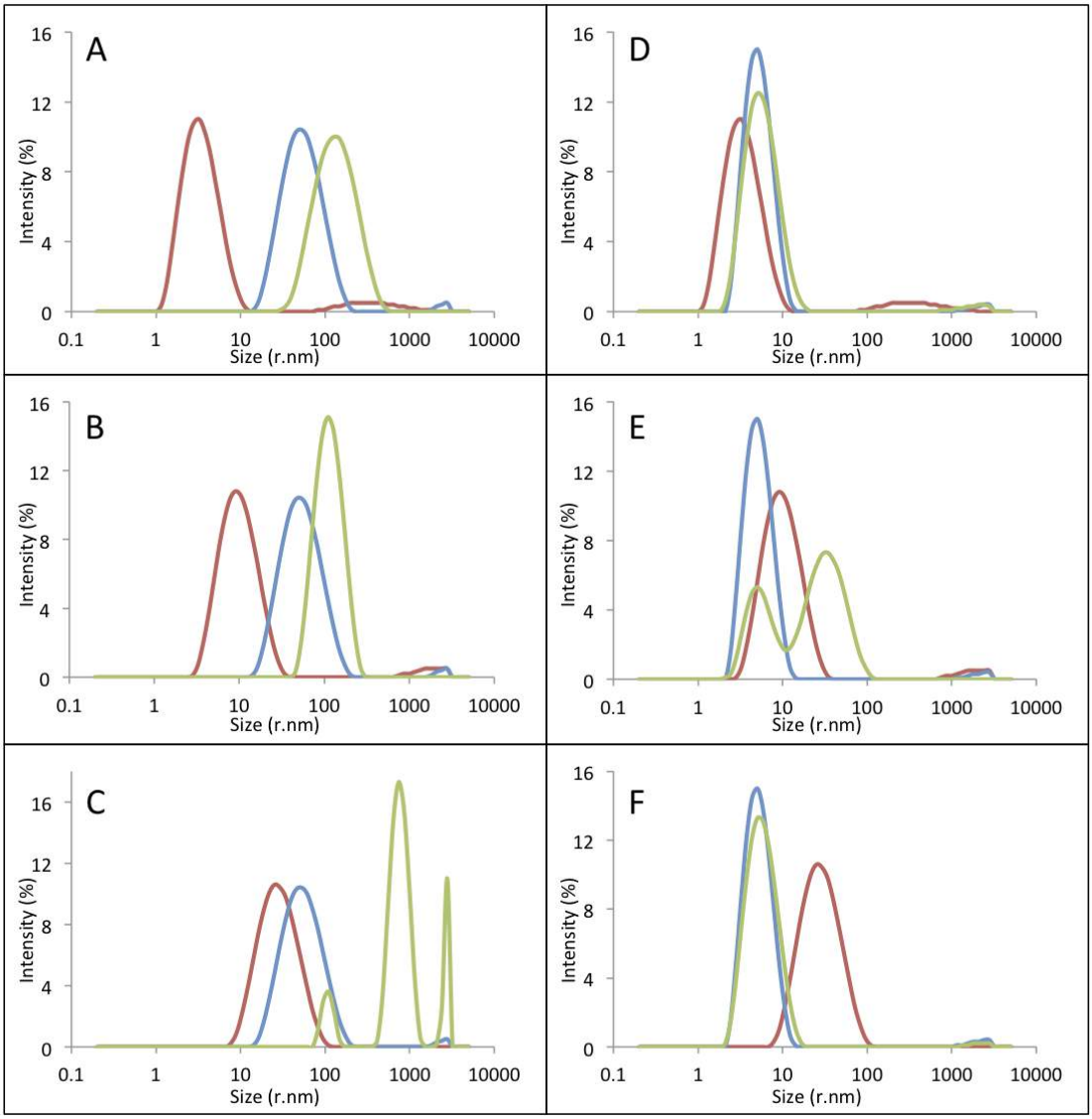

Figure 19. Size distribution of QD, amyloid β (1-42), bovine serum albumin alone, and their mixtures.

(A) Aβ (blue), QD-OH (blue), and mix of Aβ and QD-OH (green).

(B) Aβ (blue), QD-COOH (blue), and mix of Aβ and QD-COOH (green).

(C) Aβ (blue), QD-NH_2 (blue), and mix of Aβ and QD-NH_2 (green).

(D) BSA (blue), QD-OH (blue), and mix of BSA and QD-OH (green).

(E) BSA (blue), QD-COOH (blue), and mix of BSA and QD-COOH (green).

(F) BSA (blue), QD-NH_2 (blue), and mix of BSA and QD-NH_2 (green).

The dispersions were incubated in a 10 mM sodium phosphate pH 7 buffer, 37ºC, and with 300-rpm agitation over 1 hour. (r.nm): hydrodynamic radius (in nm).

Analysis of the capacity of QD to interact with Aβ and BSA confirms the observation made on insulin and demonstrates interactions between QD and proteins or peptides under physiological conditions.

Regarding this finding, since QD coated with different chemical groups are interacting with Aβ and BSA then the effect of charges at the surface of QD on peptides and proteins needs to be elucidated.

In order to investigate this aspect of the interaction of QD and peptides or proteins we used QD carrying at their surface specific chemical groups that, under physiological conditions, will give to the QD surface a neutral, negative, or positive charge.

The effect of QD surface charges on peptides or proteins was first investigated, using these specially designed QD, on the kinetics of the Aβ peptide aggregation through the analysis of size distribution evolution by DLS.

7.2.2. QD-Aβ interactions are dependent on QD surface charges

Dynamic light scattering was used to clarify the effect of QD surface charges on the kinetics of growth of Aβ aggregates. Changing electrical charges at the QD surface induces a change in the pattern and rate of Aβ aggregate growth (Figure 20).

OH groups, generating a quasi-neutral charge, at the surface of QD induce a slowdown of Aβ aggregate formation compared with a dispersion of pure Aβ (Figure 20A). QD presenting a negative charge due to COOH groups at their surface have a similar effect (Figure 20C).

On the contrary, the presence of QD with positively charged NH_3^+ groups at their surface in the Aβ dispersion seems to induce an extremely fast appearance of Aβ aggregates, of sizes above the limit of DLS detection (Figure 20D).

As previously shown with insulin the effect of QD on Aβ seems to be dependent on QD surface charge too. In order to extend our studies we have analysed the effect of QD on bovine serum albumin (BSA) because BSA is a much larger protein than insulin and is known to be resilient and sensitive to the presence of nanoparticles [165].

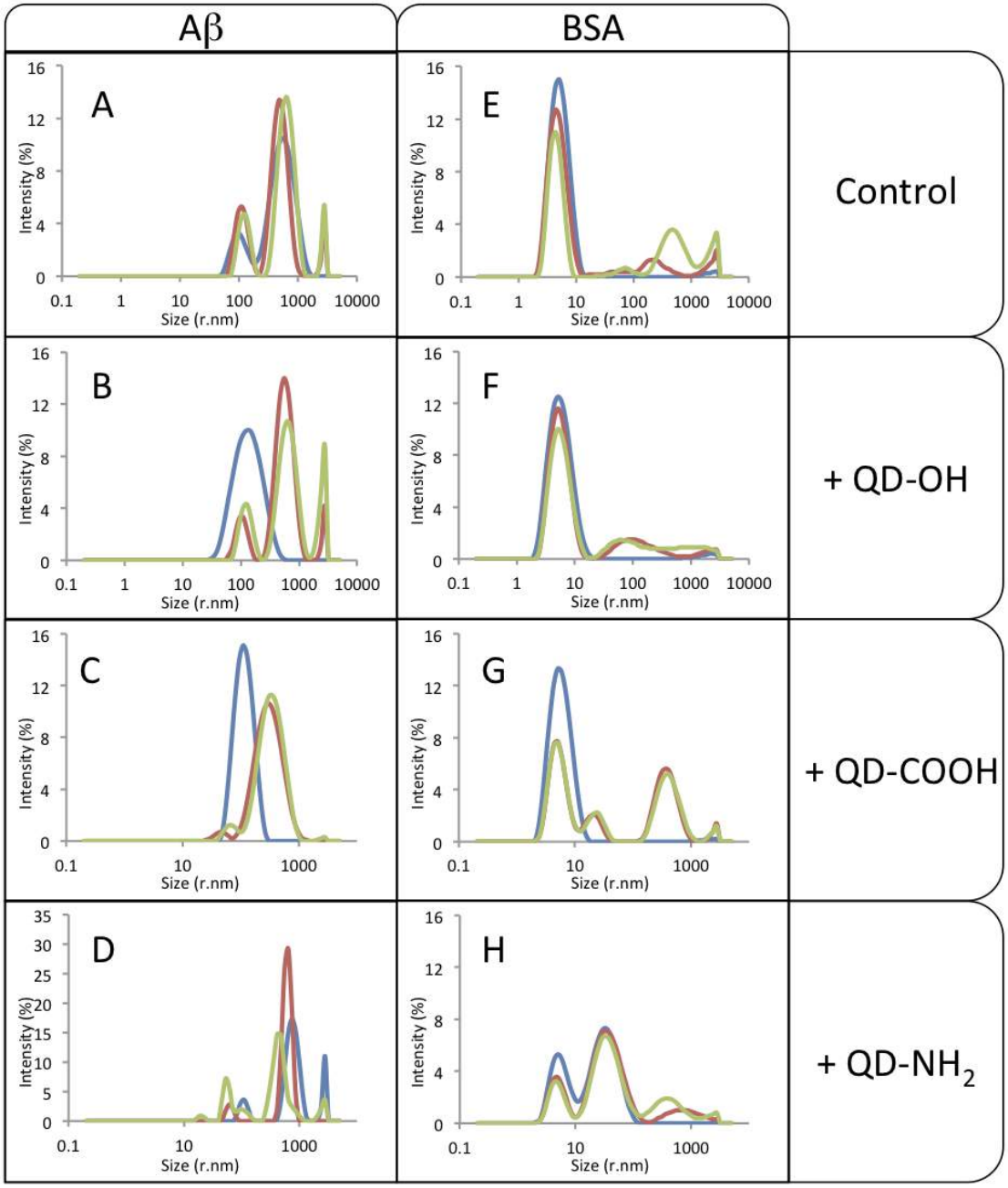

Figure 20. Change in amyloid β (1-42) peptide and bovine serum albumin aggregate size distribution in the absence or presence of various QD, monitored over time.

Aβ (0.5 g/l) in the absence (A) or in the presence of 1.11 μM QD-OH (B), 1.11 μM QD-COOH (C), or 1.11 μM QD-NH_2 (D). Dynamic light scattering was recorded after 0 (blue), 2 (red), and 4 days (green) incubation. All dispersions were incubated in 10 mM sodium phosphate pH 7 buffer, 37°C, and with 300-rpm agitation.

Bovine serum albumin (0.1 g/l) in the absence (E) or in the presence of 150 nM QD-OH (F), 150 nM QD-COOH (G), or 150 nM QD-NH_2 (H). Dynamic light scattering was recorded after 0 (blue), 2 (red), and 4 days (green) incubation. All dispersions were incubated in 10 mM sodium phosphate pH 7 buffer, 37°C, and with 300-rpm agitation. (r.nm): hydrodynamic radius (in nm).

7.2.3. QD-BSA interactions are dependent on QD surface charges

We analysed the effect of QD on the BSA aggregation kinetics under physiological conditions. Figure 20F shows that the aggregation kinetics of BSA is slower in the presence of QD-OH than for BSA alone (Figure 20E). Contrary to what was observed for Aβ, addition of QD-COOH to a BSA dispersion seems not to induce the stabilization of a particular population of BSA aggregates but to enhance the rate of aggregate growth (Figure 20G). Regarding QD-NH_2 (Figure 20H), its incorporation in the BSA dispersion under physiological conditions appears to induce a stronger interaction with BSA than other QD and to stabilise aggregates over time.

These findings suggest that the effect of QD on the BSA aggregation is clearly dependent on the QD surface charges, confirming our previous results on human insulin and amyloid β (1-12) peptides. However these results do not demonstrate any effect of QD on the specific process of aggregation like amyloid fibrillisation. Indeed, contrary to Aβ, which is known to form amyloid fibers while aggregating, BSA aggregation does not give rise to any fiber-like structures and is not known to present any modifications of the secondary structure.

In order to clarify if the impact of QD on the aggregate kinetics of Aβ and BSA is related to an amyloid fibrillisation mechanism, we investigated the effect of QD on the secondary structure of both biomolecules.

7.2.4. QD induces changes in the kinetics of Aβ secondary structure modifications

The investigation of the impact of various QD on the secondary structure of Aβ was performed using the circular dichroism technique (CD), the aim been to clarify if variations of the aggregation process previously observed when QD were present, originate from an amyloid process or from an aggregation process.

Analysis of various QD impacts on the Aβ secondary structure shows that QD does not change the pattern of the secondary structure modification present when Aβ form amyloid fibers but it shows that the presence of QD induces modifications in the rate of the observed changes. These modifications are dependent on charges at the QD surface.

QD-OH seem to induce a slower Aβ CD signal disappearance when mixed with the Aβ dispersion (Figure 21B) in comparison with pure Aβ (Figure 21A). Signal decrease is characteristic of the appearance of larger aggregates in the dispersion.

Indeed, as aggregate sizes reach 10 % of the wavelength of the incident radiation then the Mie model of light scattering and in particular the forward scattering effect is directly dependent on particle size.

QD-COOH in the Aβ dispersion seems to induce the stabilization of the CD signal over time (Figure 21C). The stabilized CD signal of Aβ is characteristic of β-sheet secondary structures. β-sheet secondary structures appear in Aβ after the refolding from initial α-helix-rich conformers. The β-sheet structure and the peptide refolding are characteristic of an amyloid fibrillisation process. By correlating these findings with the previous results one can argue that the stabilized population of aggregates observed during the DLS analysis may be constituted of β-sheet-rich Aβ conformers. In opposition to what was observed previously, Figure 21D shows that in the presence of QD-NH_2 the CD signal of Aβ disappears extremely fast.

These data support the hypothesis that the rapid appearance of micrometric aggregates, observed by DLS, is at the origin of the Aβ CD signal reduction observed here. The secondary structure analysis through CD confirmed that the presence of QD has an effect on the secondary structure of Aβ and this effect is dependent on QD surface charges.

The β-sheet spectrum observed when Aβ is incubated with QD-NH_2 could suggest that its aggregation is due to amyloid fibrillisation, however the disappearance of the CD signal and the poor signal quality prevent us from claiming that Aβ aggregation is due to amyloid fibrillisation. In order to clarify this point we will use an amyloid-specific fluorescence dye to confirm the presence or the absence of amyloid fibers within aggregates of Aβ.

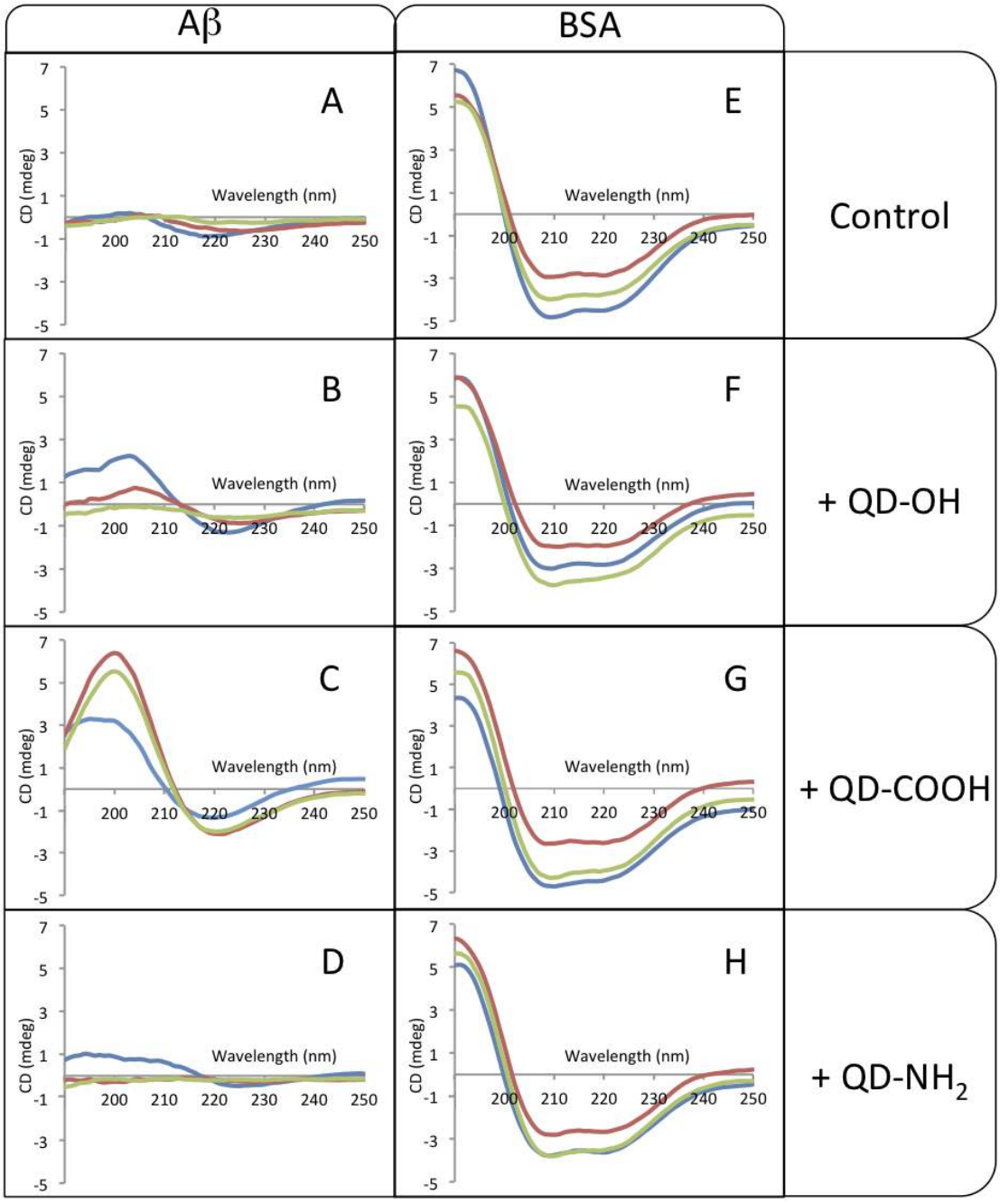

Figure 21. CD demonstrates changes in Aβ and BSA secondary structure in the presence of QD.

Far UV circular dichroism spectra of Aβ (0.5 g/l) were recorded in the absence (A) or in the presence of 1.11 μM QD-OH (B), 1.11 μM QD-COOH (C), or 1.11 μM QD-NH_2 (D). Spectra were recorded after 0 (blue), 2 (red), and 4 days (green). All dispersions were incubated in 10 mM sodium phosphate pH 7 buffer, 37ºC, and with 300-rpm agitation.

Far UV circular dichroism spectra of BSA (0.1 g/l) were recorded in the absence (E) or in the presence of 150 nM QD-OH (F), 150 nM QD-COOH (G), or 150 nM QD-NH_2 (H). Spectra were recorded after 0 (blue), 2 (red), and 4 days (green). All dispersions were incubated in a 10 mM sodium phosphate pH 7 buffer, 37ºC, and with 300-rpm agitation.

7.2.5. QD induces no changes in the BSA secondary structure

As for Aβ, the effect of QD on BSA has to be elucidated in order to determine if this was originated from an amyloid fibrillisation or from a common protein aggregation. Figure 20E showed that BSA was naturally aggregating under physiological conditions and that under the influence of QD the aggregation kinetics was modified. CD spectra as a function of incubation time revealed that there are no changes in the secondary structure of BSA during its aggregation when incubated without QD (Figure 21E). The CD spectrum of BSA when incubated with various QD displays no changes during incubation (Figure 21F, 21G, and 21H). This absence of changes can be interpreted as an absence of a secondary structure refolding, the protein refolding being needed in amyloid fibrillisation process to generate highly structured protein aggregates. This finding leads us to suppose that protein aggregation, observed when BSA is co-incubated with QD, is not due to an amyloid fibrillisation. Even if CD results revealed that when incubated with QD, the BSA CD spectrum varies in intensity, this intensity variation can be explained by the appearance of the same kind of aggregates observed during DLS analysis, as shown in Figure 20. This assumption is correlated with similar observed variations of the intensity when BSA is incubated in the absence of QD (Figure 21E).

The time stability of the α-helix characteristic spectrum observed when QD coated with different groups are incubated with BSA seems to demonstrate an absence of amyloid in BSA aggregation, however the absence of BSA aggregates formed via amyloid fibrillisation cannot be totally ruled out. In order to establish the presence or absence of these possible aggregates, an amyloid-specific dye was used.

7.2.6. Impact of QD on Aβ amyloid fibrillisation is charge-dependent

As suggested above the implication of amyloid fibrillisation in the aggregation process of Aβ cannot be completely demonstrated using only the circular dichroism technique. In order to ensure the presence of amyloid aggregates, we decided to use an amyloid-specific fluorescent dye, thioflavin T (ThT). ThT recognises a specific intermolecular structure in Aβ aggregates. This structure, called the β-cross, is composed of an assembly of two antiparallel β-sheet secondary structures. Interaction

with this structure by ThT changes its fluorescence emission maximum. Thus by monitoring the intensity of fluorescence at the new maximum wavelength one can follow the appearance of amyloid aggregates of Aβ in the absence or presence of various QD.

Figure 22A demonstrates that when Aβ is incubated in the absence of QD the level of ThT fluorescence remains high throughout the incubation process, demonstrating that Aβ aggregation observed during the incubation is due to amyloid fibrillisation.

When Aβ are incubated in the presence of QD-OH, the intensity of ThT fluorescence is important but lower than the one of pure Aβ. The normalised ThT fluorescence of Aβ+QD over pure Aβ, presented in Figure 22B, reveals the tendency of ThT fluorescence induced by the presence of various QD. Here the normalised data appear to show that the presence of QD-OH induces a slow down in the amyloid fibrillisation process of Aβ.

In contrast, in the presence of QD-COOH the intensity of ThT fluorescence is higher than the one displayed by Aβ alone. The normalisation shows, in this case, that the effect of QD-COOH on Aβ gives rise to an uninterrupted increase in ThT fluorescence. The effect of QD-COOH on Aβ amyloid fibrillisation can therefore be interpreted as an enhancement of aggregates or fibril formation.

The addition of QD-NH_2 to a Aβ dispersion and the incubation under physiological conditions generates a very low ThT fluorescence, after normalisation one can see that ThT fluorescence is decreasing during the incubation. Our interpretation of these findings is that QD-NH_2 inhibits amyloid fibrillisation of Aβ and that large aggregates, observed in figures 16D and 17D, when QD-NH_2 are incubated with Aβ amyloid aggregates are not formed but instead a common protein aggregation occurs. Indeed, the appearance of amyloid aggregates should induce a fast ThT fluorescence increase followed by a slow decrease in ThT fluorescence due to the sedimentation of the aggregates.

The effect of QD on Aβ aggregation with an amyloid-specific fluorescence dye is dependent on QD surface charges. For QD with positive surface charges (QD-NH_2) the process of peptide aggregation induced by QD is not amyloid-related.

The same fluorescence dye technique has also been used to clarify the generation of amyloid aggregates or fibers of BSA when incubated in the absence or presence of various QD.

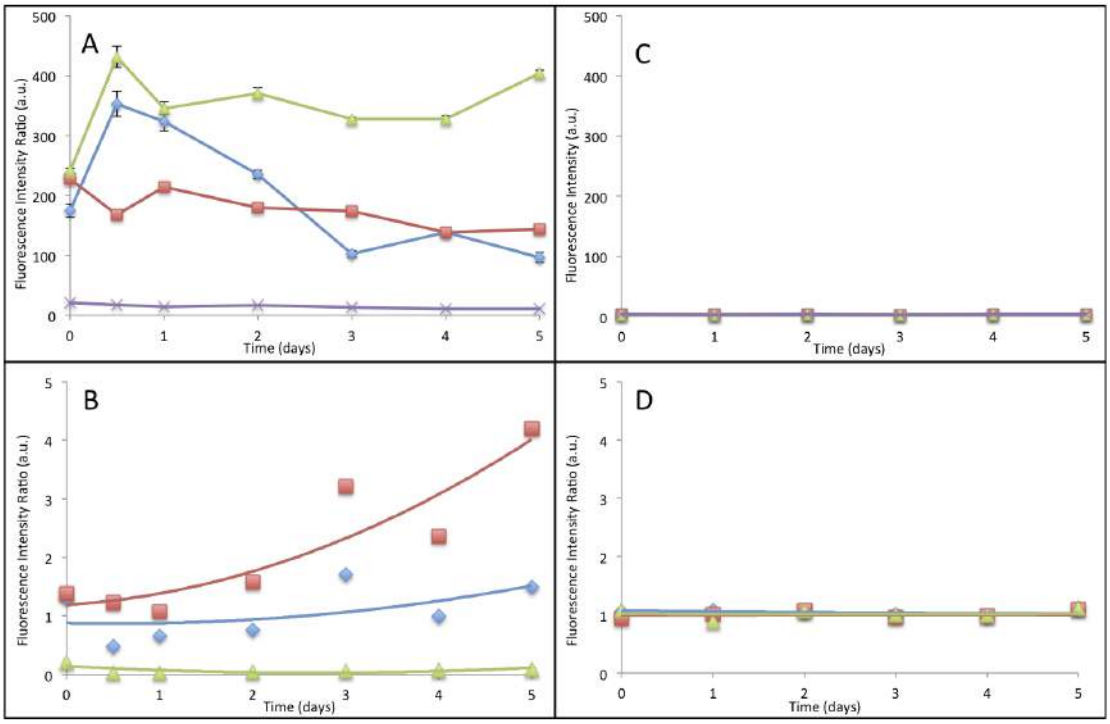

Figure 22. Fibrillisation kinetics of Aβ or BSA at 37ºC monitored thought changes in ThT fluorescence intensity.

(A) Aβ (0.5mg/ml) was incubated in the absence (blue) or the presence of 1.11 µM QD-OH (red), or 1.11 µM QD-COOH (green), or 1.11 µM QD-NH2 (violet) in a 10 mM sodium phosphate pH 7 buffer, at 37ºC, for 5 days with stirring at 300 rpm.

(B) Time course of ThT fluorescence of Aβ + QD over pure Aβ: QD-OH (blue), QD-COOH (red), or QD-NH2 (green). The trend curve for each condition has been calculated using a second order polynomial. The corresponding R-square are 0.8204 for QD-COOH, 0.59388 for QD-OH, and 0.9938 for QD-NH_2.

(C) Bovine serum albumin (0.1mg/ml) was incubated in the absence (blue) or the presence of 150 nM QD-OH (red), or 150 nM QD-COOH (green), or 150 nM QD-NH2 (violet) in a 10 mM sodium phosphate pH 7 buffer, at 37ºC, for 5 days with stirring at 300 rpm.

(D) Time course of ThT fluorescence of BSA + QD over pure BSA: QD-OH (blue), QD-COOH (red), or QD-NH2 (green). The trend curve for each condition has been calculated using a second order polynomial. The corresponding R-square are 0.75689 for QD-COOH, 0.66816 for QD-OH, and 0.64845 for QD-NH_2.

7.2.7. QD does not induce amyloid fibrillisation of BSA

Previous CD analysis of the effect of QD on BSA aggregation seems to show that aggregation is not related to amyloid fibrillisation but to a common protein aggregation pathway and that the presence of various QD does not change the mechanism of BSA aggregation, but only influences the rate of the process.

To ensure the absence of amyloid aggregates or fibers during BSA incubation in the absence or the presence of different QD we monitored the ThT fluorescence in BSA dispersions with or without QD. Figure 22C shows an absence of ThT fluorescence specific of amyloid aggregates when BSA was incubated in the absence of QD.

In the presence of different QD, the ThT fluorescence does not vary along the incubation and remains equal to the one of pure BSA (Figure 22C, D).

Thus we conclude that there are no amyloid aggregates of BSA formed during the incubation under physiological conditions even in the presence of QD. Variations in the BSA aggregation rate observed in Figure 20, when BSA is mixed with different QD, is not due to the induction of an amyloid process by QD but to an effect of QD on the common protein aggregation process.

7.3. The design of specifically generated PEGylated CdSe/ZnS quantum dots, invisible to insulin and capable of inhibiting Aβ amyloid fibrillisation under physiological conditions

Our previous results have demonstrated the effect of QD on peptides and proteins in their process to generate amyloid aggregates. Moreover this effect is due to charges at the QD surface and is specific for peptides or proteins. Our experiment with insulin has revealed that the QD effect is dependent on the distribution of charges at the surface of QD, rather than on total surface charges. Furthermore, we have shown that with a proper selection of chemical groups at the surface of QD one can create QD with a non-amyloid aggregation effect on amyloid-prone peptides. Thus, one could create QD with the capacity to remove amyloid-prone toxic peptide from the organism by aggregating them on the surface of QD in a non-amyloid way. This possibility was tested experimentally, as described below.

7.3.1. The generation of electrically-neutral QD, containing specific surface charges.

Previously displayed results have shown that the presence of specific charges at the QD surface can induce a non-amyloid aggregation of Aβ, a peptide whose amyloid aggregates are known to be directly responsible for some of symptoms of the Alzheimer's disease (AD). Thus it would be possible to allow the disposal of those peptides from the organism by macrophages and/or microglia.

Indeed, our analysis of the impact of QD on Aβ amyloid fibrillisation has shown that QD presenting at their surface positively charged NH_3^+ groups induce the non-amyloid aggregation of Aβ when incubated under physiological conditions (Figure 18C). Furthermore, QD-NH_2 have also shown that they do not induce either amyloid fibrillisation of potentially amyloid proteins like insulin (Figure 17). These QD do not induce either the non-amyloid aggregation of potentially amyloid proteins like insulin (Figure 9) and they seem to have a limited impact on strongly aggregating proteins like BSA (Figure 19H).

These data explain the need for positively-charged NH_2 groups at the surface of therapeutic QD (T-QD). Unfortunately QD-NH_2 have been shown in a previous study [130] to be relatively unstable in biological media at pH 7. In order to increase the lifespan of T-QD in extracellular fluids chemical groups must be added to its surface to increase the stability in liquid media at pH 7. Within this framework, we decided to

use the chemical group OH as a stabilizer for T-QD. The choice of hydroxyl groups originates from different data.

First, OH groups are known to increase the QD lifespan in biological media and to bring little or no charges at the QD surface and second, we have shown that OH groups at the QD surface reduces the rate of Aβ amyloid fibrillisation (Figure 18). However our previous results have also shown that the presence of OH groups at the QD surface could induce amyloid fibrillisation of insulin but we presume that the presence of NH_2 groups will be sufficient to avoid the amyloid-generating effect of OH groups on insulin.

Also important, while designing our T-QD, is the global charge of the particles. Previous studies have shown that QD carrying a global positive charge are easily incorporated inside cells and actively transported to the cell nucleus because of their global positive charge whereas neutral QD are hardly incorporated into cells [166]. To be optimally efficient our T-QD need to stay in the extracellular fluid where toxic amyloid Aβ aggregates are generated, thus we decided to add COOH, to neutralize positive charges from NH_2.

Four different ratios of NH_2, OH, and COOH groups were tested to generate individual T-QD that will be stable when incubated for one week in pH 7 buffer at 37ºC and have a nearly-neutral global charge (table 3). Only one combination of chemical groups reaches the targeted characteristics, this combination contains 30% NH_2 groups, 60% OH groups and 10% COOH groups. They present a larger proportion of OH groups than of NH_2 groups. Therefore, their efficiency as Aβ amyloid fibrillisation inhibitors, under physiological conditions, has to be investigated.

T-QD	PEG-NH2 contents	PEG-OH contents	PEG-COOH contents	Hydrodynamic radius (nm)	Zeta-Potential (mV)
1	71.25 %	5%	23.75 %	0.9 ± 0.1	13.8 ± 5.4
2	63.8 %	15 %	21.2 %	41.6 ± 18.1	12.9 ± 4.1
3	52.5 %	30 %	17.5 %	26.5 ± 5.5	9.1 ± 4.1
4	30 %	60 %	10 %	6.4 ± 1.6	-1.5 ± 3.1

Table 3. Hydrodynamic radius and zeta potential of CdSe/ZnS QD coated with various ratios of different PEG.

3.44 μM of CdSe/ZnS QD coated with various ratios of PEG-NH_2/PEG-OH/PEG-COOH were incubated in 10 mM sodium phosphate pH 7 buffer at 37ºC and analysed after 10 min incubation. Hydrodynamic radius was calculated from the intensity-based particle size distribution, using the Rayleigh's approximation, to reflect the number-based particle size distribution. Zeta potential was calculated using the Huckel's approximation. Data are average values ± S.D. (n=15)

7.3.2. The interaction of electrically-neutral QD with Aβ reduces amyloid fibrillisation

In order to measure the efficiency of our T-QD as Aβ amyloid inhibitors we decided to study their effect on Aβ under physiological conditions. One interesting pattern we were looking at was the capacity for T-QD to interact physically with Aβ and to form aggregates larger than pure Aβ.

7.3.2.1. Formation of Aβ/T-QD aggregates.

The effect of T-QD on Aβ aggregate formation size analysed by DLS shows that, contrary to what was expected, the effect of T-QD seems to be to slow down the amyloid aggregation of Aβ.

Figure 23 shows that even if under both conditions (with or without T-QD) aggregates are formed with a radius of 100 nm at the initiation step, the presence of T-QD seems to inhibit the presence of larger aggregates at this stage. Also while Aβ aggregates are rapidly growing to micrometric size when Aβ is incubated alone (Figure 23A), when T-QD are present aggregates of Aβ seem to be growing in size more slowly (Figure 23B). The effect of T-QD on Aβ aggregate size seems to be similar to the one observed when QD-OH are present (Figure 18B).

T-QD effect on Aβ aggregation shows that the aggregation rate is even slower than in the absence of QD. This does not support the possible therapeutic use of T-QD to generate Aβ aggregates large enough to be recognized and recycled by macrophages *in vivo*. Nevertheless, more information on the amyloid structure of aggregates is needed to define the potentiality of T-QD as a therapeutic agent. Indeed, if the observed aggregates have a non-amyloidal structure then T-QD could be considered as a stabilization agent for the pre-refolding form of Aβ, helping to decrease the toxic charge of Alzheimer's patients.

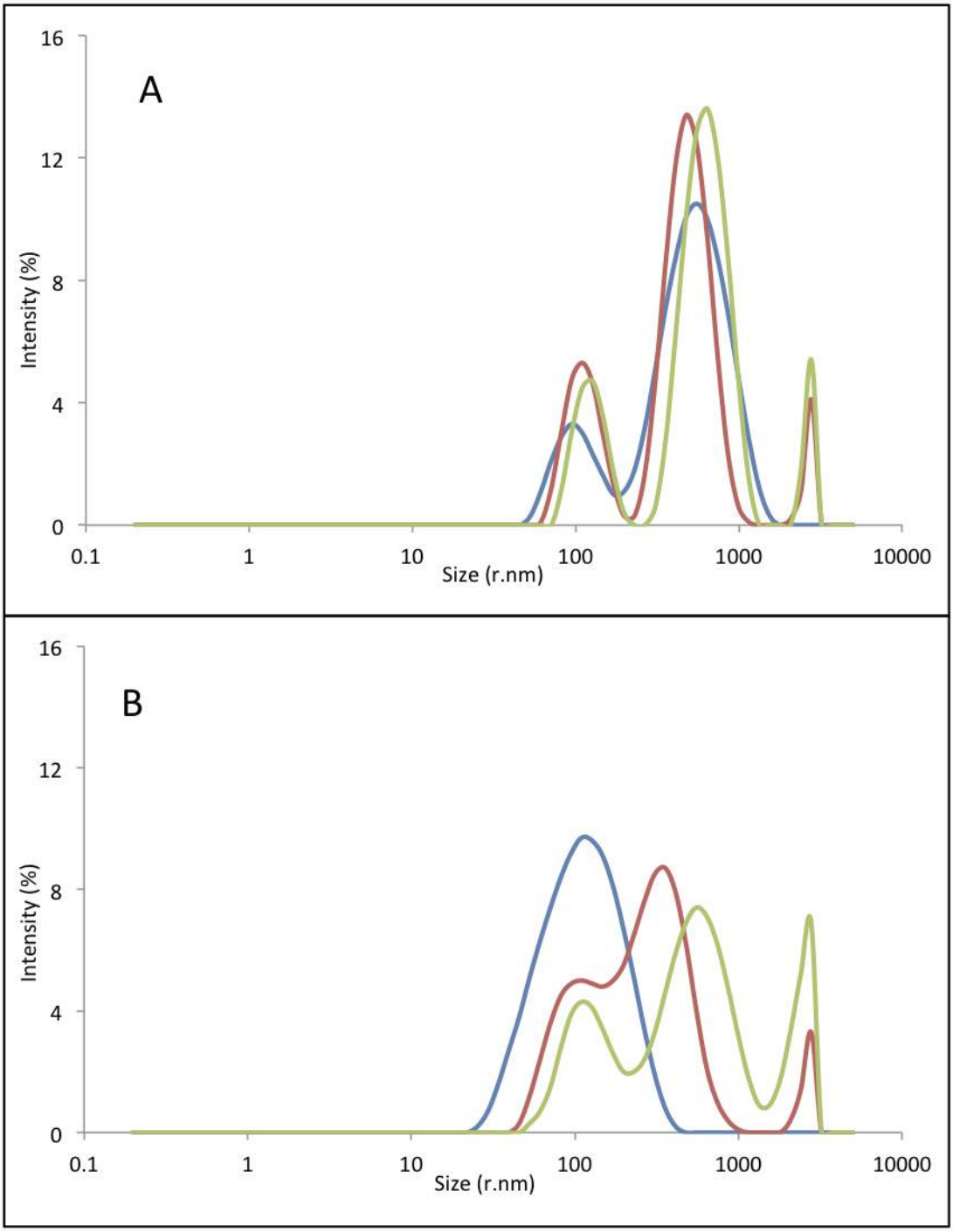

Figure 23. Changes in the Aβ size distribution frequency curve in the absence or the presence of QD, monitored for 6 days.

Size distribution of particles determined by DLS for Aβ (0.5 g/l) in the absence (A) or in the presence of 1.11 μM potentially therapeutic CdSe/ZnS QD (T-QD) (B). Measurements were performed after 0 (blue), 2 (red), 4 (green), and 6 days (violet) incubation. All dispersions were incubated in 10 mM sodium phosphate pH 7 buffer, 37ºC, and with 300-rpm agitation. (r.nm): hydrodynamic radius (in nm).

7.3.2.2. Aβ secondary structure changes due to T-QD.

The efficiency of T-QD as therapeutic agents depends as well on their capacity to limit the Aβ refolding from an α-helix-rich form to a β-sheet-rich form, a mandatory step for the generation of toxic amyloid aggregates of Aβ *in vivo*. In order to estimate the capacity of T-QD to limit Aβ refolding, we followed the effect of T-QD on the Aβ secondary structure through CD spectrometry and compared with the evolution of the Aβ secondary structure change observed when Aβ were incubated in the absence of QD.

CD analysis reveals that the presence of T-QD does not modify the sense of the Aβ CD spectrum evolution but seems to affect the rate of this evolution. Figure 24A shows that the pure Aβ CD spectrum signal disappears over 4 days incubation under physiological conditions. In the presence of T-QD, the Aβ CD signal also disappears over 4 days incubation under the same conditions (Figure 24B). However one can see that at the start of incubation (blue curve) the CD spectrum of Aβ in the presence of T-QD is more stable than in its absence. Furthermore, the CD spectrum of Aβ in the presence of T-QD corresponds more clearly to a β-sheet signal than the one of pure Aβ.

The disappearance of the CD signal can be correlated with the appearance of large aggregates and the Mie scattering previously explained, and the better definition of the Aβ CD signal in the presence of T-QD can be related to the stabilization of smaller aggregate populations observed in Figure 23B, these aggregates causing a limited light scattering, contrary to larger aggregates. The better definition would originate from the slower aggregation rate in the presence of T-QD.

In summary, results presented in Figure 24B do not allow us to clarify the amyloid nature of Aβ aggregates generated in the presence of T-QD. In order to enlighten this point we have used the amyloid-specific fluorescent dye, Thioflavin T.

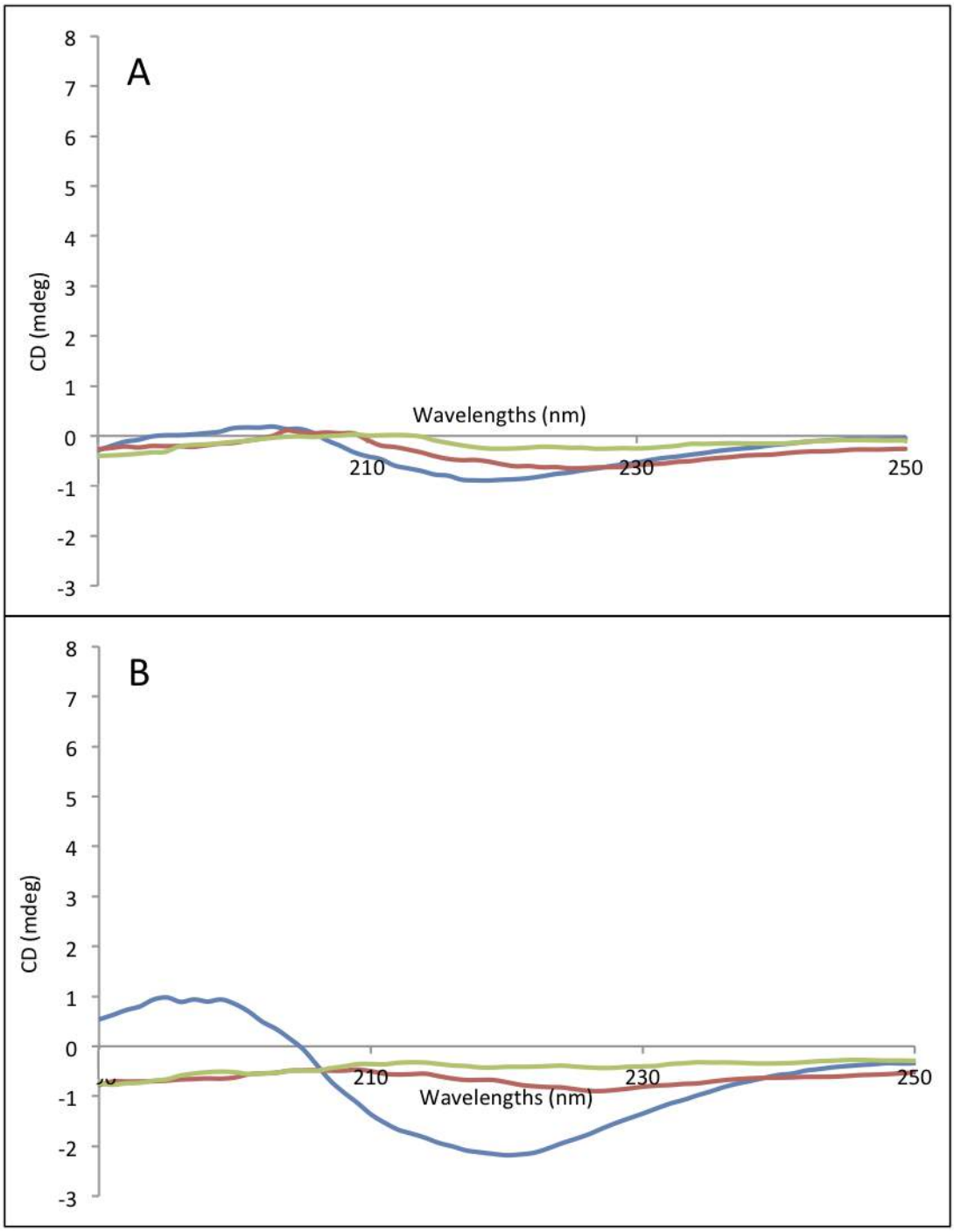

Figure 24. CD demonstrates changes in Aβ secondary structure in the presence of QD.

Far UV circular dichroism spectra of human amyloid β (0.5 g/l) were recorded in the absence (A) or in the presence of 1.11 μM of T-QD (B). Spectra were recorded after 0 (blue), 2 (red), 4 (green), and 6 days (violet) incubation. All dispersions were incubated in 10 mM sodium phosphate pH 7 buffer, 37ºC, and with 300-rpm agitation.

7.3.2.3. In the presence of T-QD, an amyloid-specific structure of Aβ is identified

The efficiency of T-QD as a therapeutic agent is dependent on its capacity to inhibit or to limit the formation of toxic amyloid aggregates of Aβ from its native non-toxic form. We have shown previously that the T-QD in incubation media limits the growing of Aβ aggregates, but we could not conclude whether aggregates formed in the presence of T-QD by Aβ were amyloid aggregates. In order to clarify this point we used the fluorescent dye ThT whose maximum emission is dependent on the presence of an amyloid β-cross structure.

Results of this experiment show that the presence of T-QD does not inhibit the formation of Aβ amyloid aggregates but slows down the rate of aggregate formation and growth. Figure 25A shows that the ThT amyloid-specific fluorescence is less intense in the presence of T-QD (red curve) than in its absence (blue curve) and decreases faster with pure Aβ. This effect is clearly visible when the ThT fluorescence of Aβ with T-QD is normalized with respect to Aβ alone (Figure 25B), then one can see that the effect of T-QD limits the amyloid-specific fluorescence of ThT.

Two explanations can be given for this phenomenon. One is that the strong decrease in ThT fluorescence observed with pure Aβ is due to the Mie scattering of the fluorescent light occurring when Aβ aggregates reach a certain size (Figure 25A). T-QD limits the growth of Aβ aggregates (Figure 25B). So it could also limit the Mie scattering and therefore explain the slower decrease observed in this case. The second explanation is that the presence of T-QD particles may slow down the process of amyloid fibrillisation of Aβ by "capturing" a certain quantity of Aβ molecules on their surface thus decreasing the effective concentration of Aβ in the dispersion and decreasing the rate of amyloid aggregate formation and growth. It is unfortunately not possible for us to conclude on which of these two explanations is valid here or, if both are valid, what is the impact of each one on the global effect.

After analysing the effect of T-QD on Aβ aggregation it appears clearly that these particles are able to slow down amyloid fibrillisation. T-QD revealed themselves as less efficient than QD-NH_2 but could still have a therapeutic interest to slow down the development of Alzheimer's disease by limiting the generation of toxic amyloid aggregates. Unfortunately the behaviour of T-QD seems to be really similar to the one observed with QD-OH (Figure 17). The issue is that these same QD have been shown to generate amyloid aggregates of human insulin under physiological conditions. In

order to demonstrate a potential therapeutic use of T-QD we would need to elucidate if T-QD generate amyloid aggregates under physiological conditions.

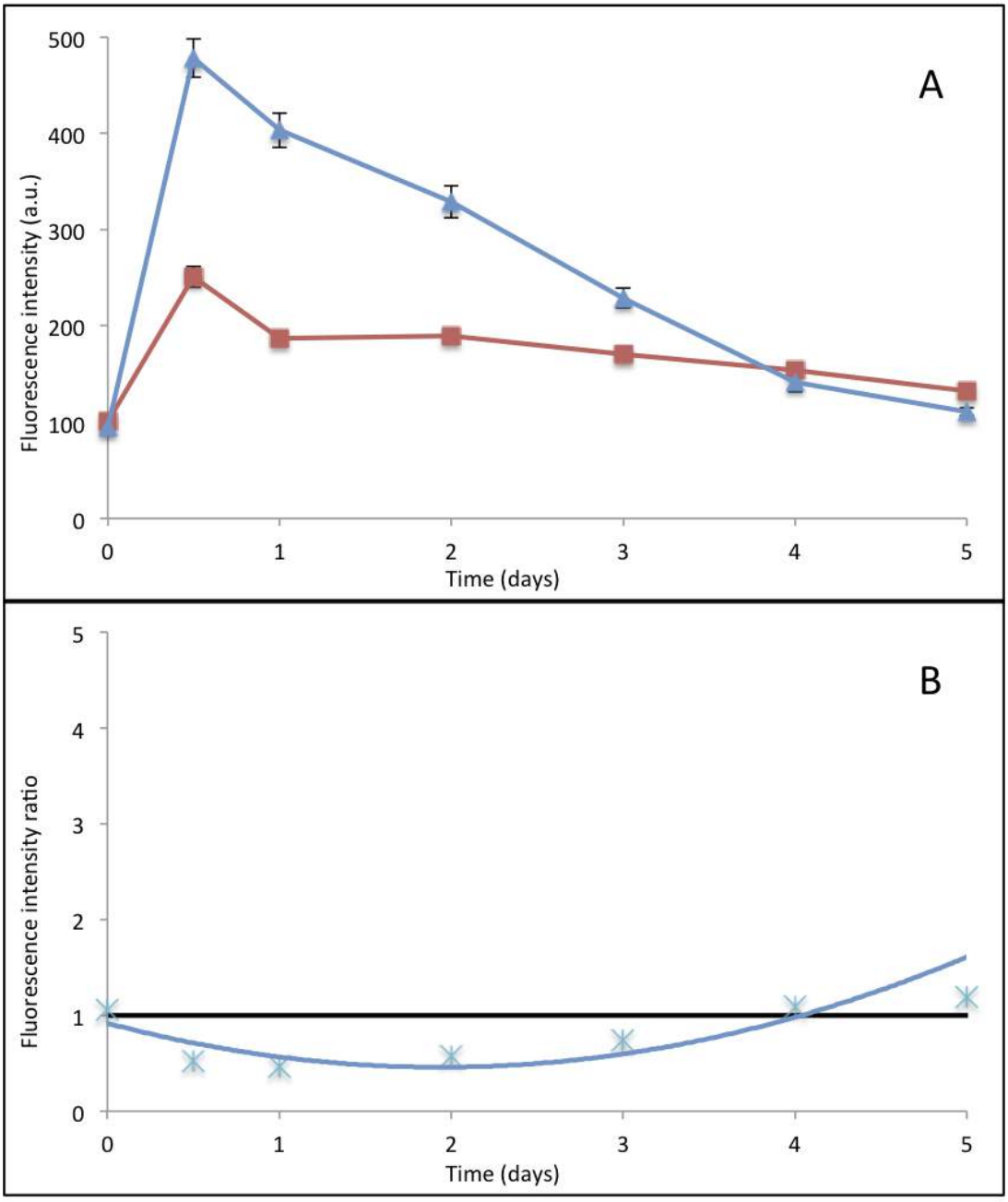

Figure 25. Fibrillisation kinetics of Aβ at 37ºC, monitored by ThT.

(A) Aβ (0.5 mg/ml) was incubated in the absence (blue) or the presence of 1.11 μM of T- QD (red) in a 10 mM sodium phosphate pH 7 buffer, 37ºC, with a 300-rpm agitation.

(B) Time course of ThT fluorescence of Aβ + T-QD over pure Aβ. The trend curve (blue) has been calculated using a second order polynomial. The corresponding R-square is 0.91071.

7.3.3. Interactions of electrically-neutral QD with insulin give rise to amyloid fibrillisation

Analysis of T-QD on Aβ amyloid fibrillisation has stressed the importance of the OH groups at the surface of T-QD. Our previous results have also shown that QD-OH are able to induce the aggregation of physiologically not amyloid-prone proteins, like insulin. In order to estimate the efficiency of T-QD as a therapeutic agent one needs to ensure that the latter do not induce the same amyloid process in insulin. We started by clarifying the capacity of T-QD to physically interact with insulin.

7.3.3.1. Identification of insulin/T-QD aggregates

To elucidate the capacity of T-QD to bind insulin we decided to use the DLS technique. Results appear to demonstrate that the presence of T-QD induces insulin aggregation. Figure 26A shows that during incubation under physiological conditions, pure insulin aggregates only slightly. The main population of molecules consists of monomers during the first 24 h and then become insulin hexamers. Over the incubation time one can see the appearance of sub micrometric-sized aggregates but the main population of particles remains below 10 nm.

On the contrary in the presence of T-QD one can see in Figure 26B that even at the start of incubation there are aggregates of T-QD and insulin. Aggregates grow during incubation until reaching the upper limit of detection of our tool after 3 days incubation under physiological conditions.

We propose that T-QD induces or largely accelerates the process of insulin aggregation.

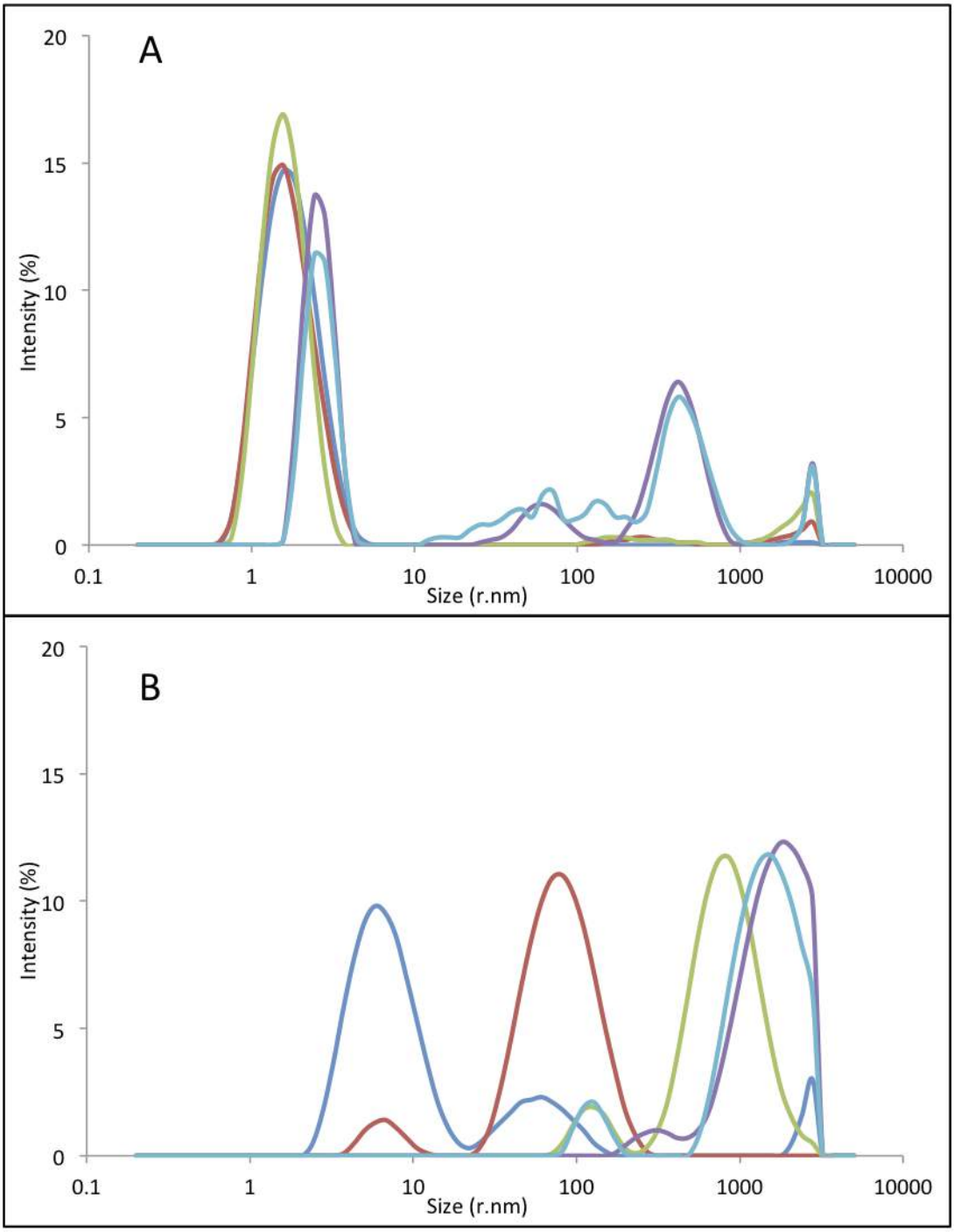

Figure 26. Insulin size distribution in the absence or the presence of T-QD, monitored over 3 days.

DLS distributions of particles as a function of size were recorded for insulin (2 g/l) in the absence (A) or the presence of 3.44 μM T-QD (B). Measurements were performed after 0 (blue), 0.5 (red), 1 (green), 2 (violet), and 3 days (cyan) incubation. Dispersions were incubated in 10 mM sodium phosphate pH 7 buffer at 37°C. (r.nm): hydrodynamic radius (in nm).

7.3.3.2. Slower secondary structure change of insulin in the presence of T-QD

Results displayed in figures 27A and 27B show that T-QD induces a change in insulin secondary structure. Figure 27A shows little variation in the insulin CD spectrum during incubation of pure insulin under physiological conditions. However, Figure 27B demonstrates important variations of the insulin CD spectrum when insulin are incubated with T-QD. The intensity of CD spectra seems to diminish over time of incubation. Nevertheless, even if the intensity of insulin CD spectra seems to decrease during incubation with T-QD, the CD spectrum shape does not vary, indicating that a transition from α-helix to β-sheet is not taking place.

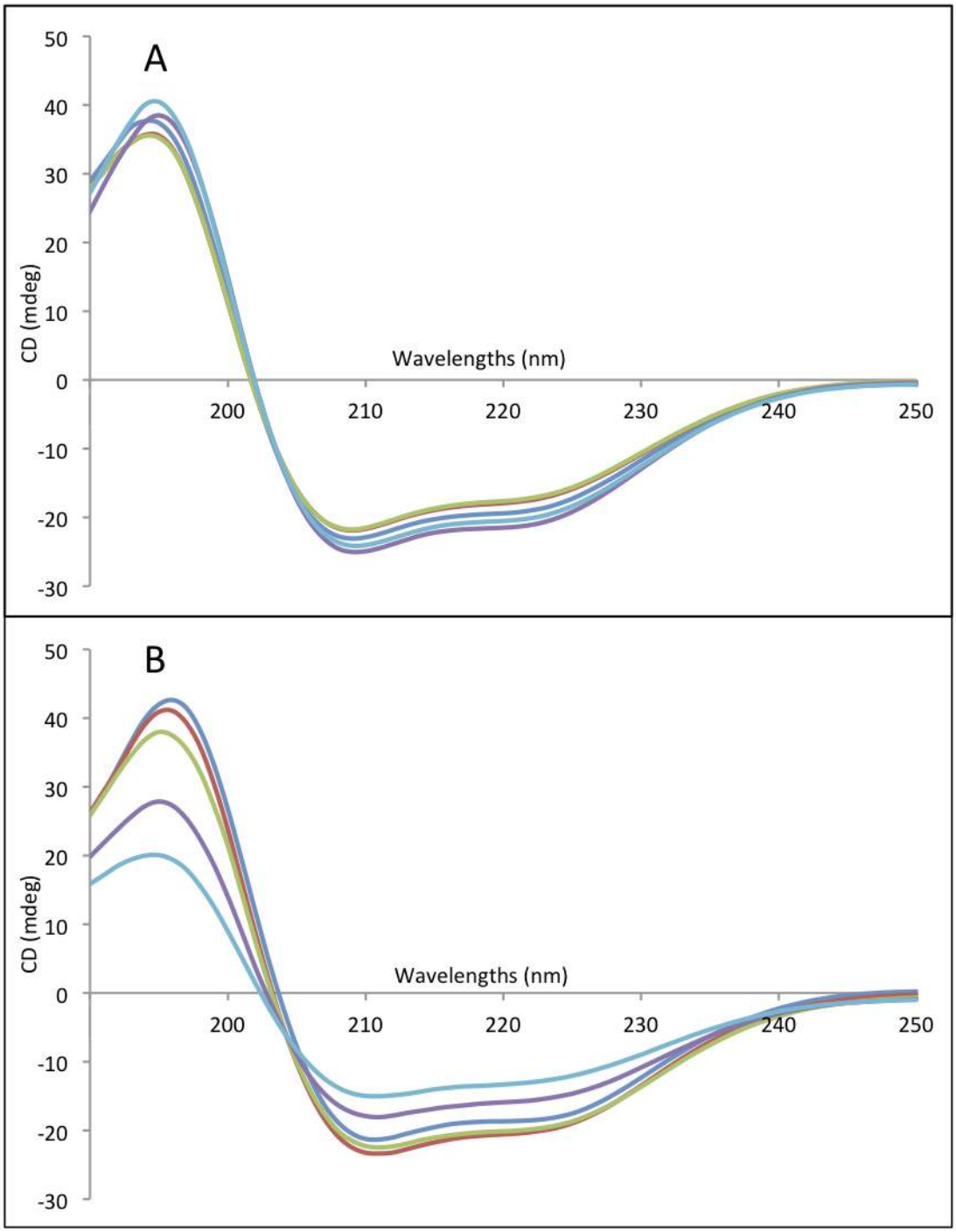

Figure 27. CD analysis demonstrates changes in the insulin secondary structure in the presence of QD.

Far UV circular dichroism spectra of insulin (2 g/l) were recorded in the absence (A) or in the presence of 3.44 μM of T-QD (B). Far UV circular dichroism spectra of insulin in the absence or in the presence of T-QD were recorded after 0 (blue), 0.5 (red), 1 (green), 2 (violet), and 3 days (cyan). All dispersions were incubated in 10 mM sodium phosphate pH 7 buffer at 37ºC.

7.3.3.3. Slower appearance of an amyloid-specific structure in the presence of T-QD

Figure 28A shows that pure insulin (blue curve) shows very little ThT emission over the time of incubation under physiological conditions. However, the presence of T-QD induces a rapid increase in the ThT amyloid specific fluorescence intensity.

By normalizing results one can observe, in Figure 28B, that the presence of T-QD generates amyloid fibrillisation of insulin. This amyloid fibrillisation seems to reach saturation after 2 days incubation.

The presence of T-QD clearly induces amyloid insulin aggregates under physiological conditions and this would be against their therapeutical use. The influence of OH groups present at the surface of T-QD appears higher than the one of NH_2 groups but surprisingly by comparing this result with the one obtained when insulin was incubated with QD-OH one can observe that the rate of amyloid formation induced by T-QD is lower than the one induced by QD-OH.

In order to develop an efficient Alzheimer's drug based on QD, new techniques of QD solubilisation based on other chemical groups or combinations of chemical groups at the surface of QD will be required.

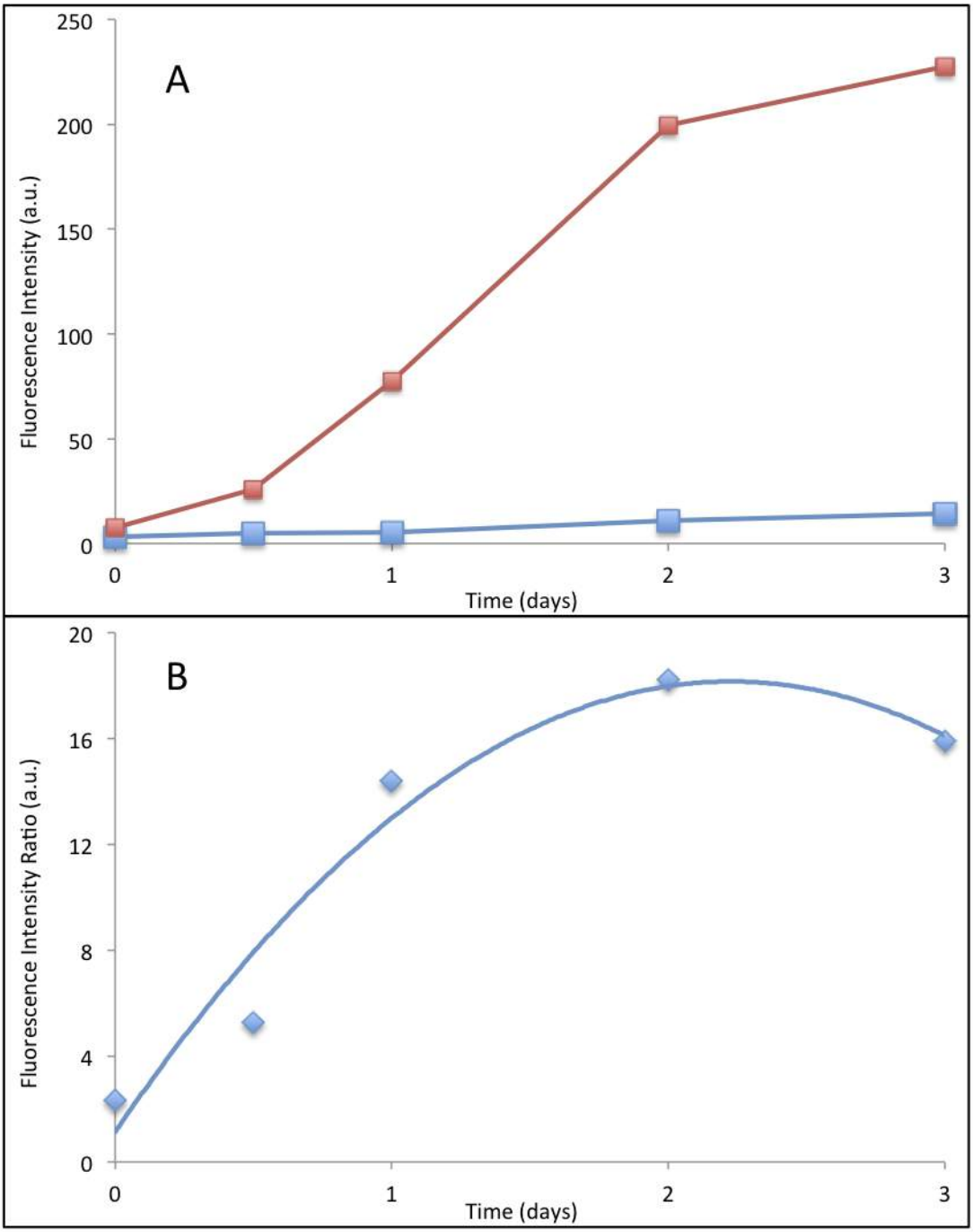

Figure 28. Fibrillisation kinetics of human insulin at 37ºC monitored by means of ThT fluorescence intensity.

(A) Insulin (2mg/ml) was incubated in the absence (blue) or the presence of 3.44 μM of T-QD (red) in 10 mM sodium phosphate a pH 7 buffer at 37ºC.

(B) Time course of ThT fluorescence of insulin + T-QD over pure insulin. The trend curve (blue) has been calculated using a second order polynomial. The corresponding R-square is 0.94599.

8. General Discussion

8.1. Surface charge distribution effect on biomaterials is dependent of and specific for the studied biomaterial and incubation conditions

The effect of nanomaterials on living organisms has been previously demonstrated as depending of their nature, shape, and size. Indeed some nanomaterials are directly toxic to cells due to their composition. Certain nanomaterials can generate damage in living tissues because of their shape. Some of them present a size-related reactivity, which generates toxic species in the biological media. Recently nanomaterials have also been suspected to induce molecular toxicity because of their capacity to disrupt the structure of certain biomolecules. Indeed some nanoparticles have been identified as able to interact with various biomolecules, particularly proteins, *in vitro* and *in vivo*. Two kinds of effects have been identified while investigating these phenomena, depending on the type of biomolecules present in the media with the nanomaterials, namely stable or amyloid-prone proteins.

8.1.1. NPs effect on stable proteins

The effect of nanoparticles on the internal stability of biomolecules has been investigated and is currently referred to as molecular toxicity of nanomaterials [167]. Indeed the study of the nanomaterials impact on biomaterials under physiological conditions has revealed that nanomaterials can change the structure of natively stable proteins. Within this thesis we presented the effect of two of the most used nanomaterials in bioscience: gold nanoparticles and carbon nanotubes.

8.1.1.1. Aggregation effect

As described by Klein and Lück, proteins in suspension under physiological conditions have a tendency to aggregate at the surface of nanoparticles [168, 169]. The resulting layer of protein at the surface of nanoparticles is called protein corona and can be a monolayer or a multilayer [170].

This aggregation could be the result of electrostatic forces, hydrophobic interactions, or Van der Waals forces [171]. The main hypothesis is that this phenomenon is due mainly to electrostatic interactions because the high global charge of nanomaterials

makes them extremely attractive for the charges carried by protein amino acid residues [124, 172].

The discovery of possible interaction of streptavidin protein with carbon nanotubes and of the aggregation of proteins at the surface of non-charged graphene sheets [173, 174] had weakened this hypothesis. Both phenomena of aggregation suppose the intervention of hydrophobic interactions between nanomaterials and proteins because pure carbon based nanostructures are hydrophobic and do not present any charge at their surfaces [175]. Also it appears that the kinetics of interaction analysed by Roth shows that the rate of aggregation is not correlated to electrostatic forces but to Van der Waals forces [176].

These observations do not support that aggregation phenomena are only limited to the electrostatic attraction between charge at the surface of nanomaterials and protein charges. Moreover during this thesis we have demonstrated that protein and peptides were interacting with QD covered with various chemical groups regardless of the electrostatic values displayed by these ones.

Our own understanding of this phenomenon is that protein aggregation at the surface of nanoparticles can be divided into two categories: one in which the proteins form a monolayer at the surface of nanoparticles, the other in which proteins form multiple layer at the nanoparticle surface.

In the first case the interaction between protein and nanoparticles can be related to Van der Waals attractions between surfaces. This interaction induces only one protein layer in nanoparticle protein corona because Van der Waals forces are not strong enough to induce structural changes of the proteins involved.

In the second one the interaction between nanoparticles and proteins is related to specific electrostatic or hydrophobic attraction. This type of interaction generates multiple layers of protein in the corona because they are strong enough to induce structural changes in the proteins involved.

Indeed as we will see in the next paragraph the impact of nanoparticles on proteins has been demonstrated to be destabilising for the internal structure of proteins under physiological conditions.

8.1.1.2. Structure destabilization

Structure destabilization has been observed in some case when nanomaterials are incubated with protein dispersions under physiological conditions [177]. Indeed CD spectrometry measurements performed by Scott Brewer have shown that the secondary structure of BSA can be influenced by the presence of gold nanoparticles. Interestingly this effect seems to be dependent on the charge present at the surface of gold nanoparticles [178, 179]. Also recent study by Gebauer *et al* present new possible way to assess the affinity of various protein for nanoparticles and the structural changes induces by this interaction [137]. In theory, only the layer of protein closest to the nanomaterial should be influenced by this denaturing phenomenon but then how to understand the existence of multilayer protein corona. Interestingly, so far no internal structure destabilisation was ever demonstrated for monolayer protein corona.

Our own results demonstrate that structural changes induced by nanomaterials are limited to multilayer protein coronas. In the case of insulin, only OH-covered QD were inducing secondary structure changes. Also size distribution analysis demonstrated that in this case, the mix of QD and insulin was generating multilayer aggregates. On the contrary, when mixed with NH_2-coated, or COOH-coated QD insulin proteins formed only a monolayer corona at the surface of QD and no secondary structure changes were recorded.

Our understanding of this phenomenon is that proteins under physiological conditions are pushed towards the surface of nanomaterials by Van der Waals forces and form a monolayer protein corona. In some conditions charge repartition at the surface of the nanomaterials induces a stronger interaction between nanomaterials and proteins causing a secondary structure refolding of the protein in contact with the nanomaterial. The presence of the refolded protein layer at the surface of nanomaterials will induce the aggregation of another layer of protein generating the multilayer protein corona observed in some cases.

This hypothesis can explain the results obtained previously on the interaction of proteins with charged nanoparticles and nanomaterials but some results obtained recently on the interaction of protein and other charged biomolecules with non-charged nanomaterials like carbon nanotubes are more difficult to understand (see below).

8.1.2. Nanoparticle effect on amyloid-prone peptide and protein

The other effect of nanomaterials observed in previous studies and investigated in this thesis is the impact of nanomaterials on amyloid-prone peptides and proteins. The identification by Engel and You of the molecular impact of nanomaterials on protein stability has raised the question of a possible impact of nanomaterials on structurally unstable amyloid-prone peptides and proteins [178, 180]. The implications of a destabilization of these peptides and proteins *in vivo* could be worrisome because of the role played by amyloid-prone peptides and proteins in various long-termed diseases like Alzheimer's. It is known that the unstable nature of amyloid-prone peptides and proteins facilitates their refolding upon changes in their environment, leading to the appearance of toxic protein aggregates. As described above, the effect of nanomaterials on BSA enhancing its aggregation has been suggested to induce the transition of amyloid-prone peptides and proteins from their physiological forms. Various amyloid-prone peptides and proteins have been studied. In this thesis we have presented the studies on the effect of nanomaterials on a natively unstable peptide, the Aβ, and on a natively stable amyloid-prone protein, insulin, using the inherently stable BSA as a control.

8.1.2.1. Effect of nanoparticles on Aβ

Amyloid β (1-42) fragment peptide (Aβ), because of its implication in Alzheimer's disease is certainly one of the most studied amyloid-prone peptides. The identification of the effect of nanomaterials on this peptide is fundamental because of potential breakthroughs in therapeutics against Alzheimer's disease. Studies on the presence of nanomaterials in biological media have demonstrated two possible effects depending on the nanomaterials tested, either a decreased or an enhanced rate of amyloid conversion of Aβ.

8.1.2.1.1. The presence of nanoparticles enhances the amyloid conversion of Aβ

The presence of nanomaterials on Aβ peptides has been initially shown as enhancing amyloid fibrillisation. Fu *et al.* have shown that the impact of carbon nanotubes on Aβ peptides was to enhance the kinetics of amyloid fiber formation under physiological conditions [181]. Similarly Wu *et al.* have shown that the presence of titanium dioxide nanoparticles induces an acceleration of fiber appearance under

physiological conditions [182]. Saraiva *et al.* have shown that nanoparticles presenting hydrogenated chemical groups at their surface induce faster kinetics of Aβ amyloid aggregate appearance [183].

The explanation initially developed to explain this enhancer effect was that the concentration of Aβ peptides at the surface was creating a recruitment effect on the peptide in solution [184]. It was previously demonstrated that an increase in Aβ concentration induces an increase in amyloid fiber formation [185]. This would be because the limiting element in amyloid fiber kinetics is the refolding of Aβ from α-helix to β-sheet conformations [186]. By concentrating the Aβ peptide at the surface of nanomaterials one can explain that the rate of refolding will be increased because of the capacity of β-sheet conformer to induce α to β transitions in the α-helix conformer [187].

Another explanation for the amyloid enhancing effect of nanomaterials on Aβ can be a destabilisation effect of nanomaterials on Aβ structure. We saw above that nanomaterials destabilise protein structure because of attraction of the amino acid residues by the nanomaterial surface. One can imagine that the effect of nanomaterials on Aβ could be similar.

Our own results show that the effect of differently coated QD on Aβ is dependent on the QD surface charge. QD coated with COOH, thus presenting negative charges at the surface, show the ability to induce faster amyloid fiber formation in Aβ, compared to a pure Aβ dispersion. This suggests that positively-charged amino acid residues of Aβ are attracted by the negatively-charged surface of QD.

8.1.2.1.2. Nanoparticles inhibit amyloid conversion of Aβ

The effect of nanomaterials on Aβ is not limited to a destabilisation. Indeed it had been demonstrated by Li and Kim that in the presence of respectively carbon nanotubes and fullerene, Aβ amyloid fiber formation was slow as compared to pure Aβ dispersion [188, 189]. Similarly Liao and Skaat have both shown that the presence of gold nanoparticles, or Fe_2O_3 nanoparticles inhibit Aβ amyloid fiber formation[190, 191]. This effect has been since demonstrated for a large number of nanomaterials and various explanatory hypotheses have been developed [192]. Interestingly Saraiva

et al. show that the presence of fluorinated chemical groups at the nanomaterial surface limit the amyloid fibrillisation of Aβ [183].

One of these hypotheses was centred on the protein corona formed by Aβ around nanomaterials. The idea was that this corona resulted from Van der Waals forces pushing Aβ peptides and nanomaterials together. Then the Aβ amino acids could interact with the nanomaterial surface depending on their specific affinities. If the connection between Aβ and nanoparticle surface was strong enough the secondary structure of Aβ aggregates at the nanomaterial surface could be stabilised in an α-helix form. By aggregating a certain quantity of Aβ and maintaining the α-helix form, the nanoparticles decrease the Aβ concentration in the media thus decreasing their probability of refolding. Therefore, nanomaterials would limit the rate of amyloid fiber formation by limiting the amount of their β-sheet forms.

Our own results obtained mixing OH-coated QD and Aβ peptides (Figure 20) show that the kinetics of amyloid fiber formation (Figure 22) and secondary structure refolding (Figure 21) are slowed down by the presence of this nanomaterial. Size distribution analysis (Figure 19&20) also demonstrated that the Aβ peptides were aggregating at the surface of OH-coated QD. Both elements support the hypothesis of a stabilisation effect of certain nanoparticles on Aβ unstable amyloid peptides.

In some cases the interaction between nanomaterial surfaces and Aβ amino acid residues is so strong that the nanomaterial can induce unfolding. Han and Skaat have shown that in the presence of respectively gold and Fe_2O_3 nanoparticles Aβ were aggregating at the surface and that peptides forming the first layer of the protein corona were partially or totally denatured [193, 194]. Aggregation of denatured peptides generates large multilayer protein coronas because of the recruitment of new Aβ peptide by the denatured peptide layer. The newly aggregated peptides are then denatured because of a cascade refolding effect.

This can be clearly seen in the results obtained when mixing NH_2-coated QD with Aβ under physiological conditions. Analysis of the secondary structure changes (Figure 21D) and of the particle charge distribution (Figure 20D) shows that these positively-charged QD induce Aβ denaturation and formation of micrometric aggregates of QD and denatured Aβ. Fluorescence (Figure 22) also demonstrates that these QD/Aβ

aggregates do not contain any amyloid structure, in agreement with the unfolded Aβ theory previously explained.

The effect of nanomaterials on Aβ seems to be dependent on surface charge thus explaining variations in results obtained by different groups. The unstable nature and short size of the Aβ peptide explain the strong impact of nanomaterials on its stability and its capacity to generate amyloid fibers.

8.1.2.2. Effect nanoparticles on insulin

Unstable peptides, such as Aβ are important because of their role in amyloidosis but other more stable protein can also undergo an amyloid fibrillisation process. These proteins are involved in cellular mechanisms under physiological conditions but can generate amyloid aggregates under pathological conditions. In some cases these aggregates are part of known amyloidosis mechanisms. In order to assess this possibility the effect of various nanoparticles has been investigated on insulin.

Because of its implication in nutrient cellular uptake, DNA replication, protein synthesis, and enzyme regulation insulin synthesis and release processes are carefully regulated. Insulin concentration in the bloodstream is highly controlled and formation of amyloid fibers could generate metabolic changes like hyperglycaemia. Insulin is known to be a very stable protein under physiological conditions but under destabilisation conditions it can refold and form amyloid fibers. The presence of certain nanomaterials was demonstrated to be able to induce this amyloid refolding under physiological conditions. Skaat *et al.* demonstrate that the presence of Fe_3O_4 nanoparticles induces formation of long insulin fibers [194]. These fibers were characterised as amyloid but the role of iron nanoparticles in their formation could not be demonstrated. Similarly nanoparticles coated with hydrophobic molecules have been shown to enhance the amyloid refolding of insulin under amyloid-prone conditions [195]. On the contrary nanoparticles presenting heptafluorobutyl acrylate chemical group at their surface have been shown to inhibit the amyloid refolding of insulin and limit the formation of amyloid fibers under amyloid-prone conditions [196]. These results seem to demonstrate that the presence of hydrophobic chemical groups at the surface of nanomaterials could induce amyloid fibrillisation of insulin and that the presence of hydrophilic chemical groups could inhibit the same mechanism.

Interestingly our own results have shown that the ability of nanomaterials to induce amyloid fibrillisation of insulin is not related to the type of chemical group present at the surface of nanoparticles but to the distribution of chemical groups on the nanoparticle surface.

Our data on the capacity of OH-coated QD to induce insulin amyloid fiber formation show that only certain distributions of OH are efficient (Figure 18). Higher or lower distributions of OH show no capacity to induce the formation of insulin amyloid fibers under physiological conditions.

Unfortunately in this thesis we could not demonstrate whether the inhibition effect of nanomaterials observed by other authors was also due to specific charge distributions because of a QD stability issue under amyloid-prone conditions. We could only demonstrate the inhibition effect of QD coated with either COOH or NH_2 under physiological conditions (Figure 17), perhaps more stable nanomaterials could be used to clarify this capacity under amyloid-prone conditions.

8.2. The use of nanomaterials as therapeutic agents against amyloidosis-related diseases

As we have demonstrated in this thesis (section 7.1 and 7.2), the effect of nanomaterials on protein structure depends on the charge distribution at the surface of the nanomaterials and on the type of protein tested. Some nanomaterial surfaces have revealed themselves as molecularly toxic for normally stable proteins under physiological conditions. Other nanomaterial surfaces have been demonstrated to slow down pathological peptide refolding, and therefore could be used to develop new therapeutic tools against pathological mechanisms previously considered as irreversible. Previously nanomaterials had raised hopes in the biomedical sciences. Sphere- and rode-shaped particles, of size below 20 nm, have demonstrated unique capacities to penetrate and distribute inside a living organism. These capacities coupled to their atypical optical and/or magnetic properties make them uniquely suited as imaging elements, drug delivery systems, siRNA carrier systems, or direct therapeutic agents.

8.2.1. Controlling nanomaterial surface to modulate effect on amyloid protein and peptide

Nanomaterials could be used as therapeutic agents, taking advantage of their high penetrance and distribution capacity, by making them target-specific. In order to make nanomaterials recognize a specific target either their surface must be coated with specific recognition molecules or nanomaterial surface charge distribution must be modified.

8.2.1.1. Nanoparticles coupled to recognition molecules

One of the possible ways to ensure that nanomaterials will encounter the targeted biomolecules *in vitro* or *in vivo* is to cover them with molecules that can specifically interact with the targeted biomolecules. Some of the most used recognition systems in bioscience are based on immune system antigen recognition mechanisms. Various systems have been developed based on the complement system or the MHC but here we will limit ourselves to systems based on the wildly used antibody recognition and on the newly developed nanobody recognition systems.

8.2.1.1.1. Antibodies

The first nanomaterial-based tagging agent, developed by Weissleder *et al.* using iron oxide superparamagnetic nanoparticles coupled to IgG antibodies, was shown as able to diffuse *in vivo* through the blood and to concentrate in liver, spleen, and bone marrow [197], demonstrating its capacity to pass physiological barriers. The recognition capacity was subsequently confirmed by other results showing a high tracking fidelity of nanoparticle/antibody hybrids [198], nanoparticle/antibody hybrids can efficiently mark and differentiate tagged-proteins inside a single cell and even inside the cell nucleus [199, 200]. Both the properties of nanoparticles and antibodies are not affected by the formation of the hybrid material. Antibodies that can target specific amyloid-prone forms of Aβ peptides were developed in order to target, bind and remove amyloid-prone Aβ from the human organisms using the magnetic properties of coupled nanoparticles [201]. The results obtained by Cimini *et al.* show that cerium oxide nanoparticles coupled to antibody against Aβ are able to specifically bind and remove β-sheet-rich Aβ from living organisms using magnet-coupled dialysis system [202]. Hybrids of nanomaterials and antibodies have proven

their efficiency but the large size of antibodies compared to nanomaterials limits the efficiency of such systems.

8.2.1.1.2. Nanobodies

In order to create efficient hybrid systems based on the coupling of nanoparticles with recognition molecules the latter must be of a size smaller than that of nanoparticles. Multiple recognition molecules can be attached to single nanoparticles, thus increasing the efficiency of such a system. Antibodies of mass 150-160 kDa present a size similar to that of most nanoparticle carriers. Their size limits the number of antibodies that can be efficiently coupled to the nanoparticle surface to 2 or 3 [203]. Therefore to enhance the binding power of nanoparticle/antibody hybrids smaller recognition molecules have been developed to replace antibodies [204]. One example of such attempts is the so-called nanobodies. Nanobodies, also called sdAb for single domain antibodies, are fragments of antibodies corresponding to a stable single monomeric antibody variable domain [205]. Nanobodies are directly expressed by dromedaries, camels, llamas, alpacas, or sharks or can be made from common murine or human IgG. Nanobodies have a size ranging around 12-15 kDa, one order of magnitude smaller than most carrier nanoparticles [206]. Recently Sukhanova *et al.* have been able to covalently bind nanobodies against carcinoembryonic antigen to the surface of CdSe/ZnS quantum dots with a ratio of 4 to 1 [207]. Therapeutics based on nanoparticle/nanobody hybrids are now been tested but the issue of the immunogenicity of such hybrids remains to be evaluated.

8.2.2. Modifying charge at the nanoparticle surface

As we have shown in this thesis (section 7.3) it is possible to induce the destabilization of biomaterials under physiological conditions by adding nanomaterials with a specific charge distribution at their surface. The outcome of this destabilization is dependent on the internal stability of the biomolecules and on charge distribution. By controlling the surface charge distribution one can engineer nanomaterials with the capacity to target specific biomaterials without having to couple them to recognition molecules, for example antibodies.

8.2.2.1. The effect of carboxylic groups at the nanoparticle surface on Aβ

Different studies have previously tried to develop nanoparticles targeted against peptides considered as pathological in order to enhance their removal from patient blood. One of the first examples of nano-therapeutics developed by Skaat *et al.* in 2009 was based on Aβ short amyloid aggregates covalently bound onto magnetic nanoparticle surfaces [208]. The idea was that Aβ amyloid aggregates present in the patient blood would aggregate at the surface of this hybrid material and that the latter could be later removed from the patient blood by a system of dialysis coupled with magnets.

One of the first drawbacks that were identified with this approach was that the chemical group used to couple the nanoparticles to the amyloid aggregates was COOH. Other research teams have identified that Aβ tend to have a higher affinity for COOH groups than for NH_2, CH_3, or OH groups. The aggregation of Aβ on COOH group could induce the amyloid transition of Aβ from the physiological to the pathological form [209].

Even if the capacity of the hybrid materials to aggregate Aβ on their surface was demonstrated *in vitro* it was never clear if this same hybrid would be able to impact the concentration of toxic aggregates *in vivo*. Indeed, its addition to the blood stream could induce the transition to their pathological forms of other amyloid-prone blood proteins (like insulin) in contact with the Aβ amyloid aggregates forming at the hybrid surface.

The main difference between the previous studies and the work developed in this thesis is that most research groups consider nanoparticles as a single homogeneous entity with properties similar to organic tagging agents of the same size. In this thesis (section 7.1) we have demonstrated that if the nature and structure of nanoparticle core is important to define nanoparticle optical and/or magnetic properties, the nature and structure of nanoparticle surface is determinant to understand the surface properties of nanoparticles and their impact on surrounding materials.

8.2.2.2. Development of anti-Alzheimer therapeutic nanoparticles based on our results on surface charge selection

Results obtained in this thesis (section 7.3) on the possible use of therapeutic QD (T-QD) to specifically aggregate the Aβ peptide in a non-pathological way have been partially successful. Results of size distribution analysis (Figure 23) have demonstrated that T-QD were able to slow down the amyloid fibrillisation of Aβ peptide but unable to stop fiber formation. Moreover the structural analysis of Aβ peptide distribution (Figure 24) in the presence of T-QD demonstrated their inability to inhibit the amyloid conversion of Aβ. Analysis of Aβ amyloid fiber formation in the presence of T-QD by the ThT fluorescence assay (Figure 25) has demonstrated a slowdown of the kinetics of fiber formation. Summarising these elements we are proposing that these data can be explained on the basis of Aβ aggregation at the T-QD surface. The absence of structural change and the lower size of QD-peptide aggregates make us assume that the interaction of T-QD and Aβ peptide is strong enough to capture part of the Aβ peptide population on the QD surface, effectively diminishing Aβ concentration in the medium and therefore slowing down fiber formation, but not effective enough to induce a cascade denaturation and aggregation of Aβ as observed for NH_2-coated QD. The results obtained with T-QD suggest a complex behaviour of QD surface due to the presence of three different types of chemical groups. We can make the assumption that the results obtained with T-QD are due to the joint influence of all chemical groups present at the surface of QD on protein structure stability.

Nevertheless, this thesis demonstrates clearly the possibility to develop nanoscale therapeutic agents against amyloidosis through the localised induction of toxic amyloid aggregates in order to facilitate their removal from the human body. Contrary to previously developed nanoparticles against Aβ amyloidosis our approach based on controlling nanoparticle surface to ensure non-amyloid aggregation of amyloid-prone peptide has the advantage of limiting the generation of secondary seeds, which could be the case in systems with Aβ linked to the nanoparticle surface [208]. Unfortunately our system presents drawbacks which seem to be connected to the presence of OH groups at the surface of QD. The presence of OH in the coating seems to predominate over that of NH_2. In order to improve the T-QD, reducing the proportion of OH

groups at the surface or replacing them with another solubilisation-prone neutral chemical group will be required.

Another limitation of nano-therapeutics identified in this thesis is due to the possible cross-inductions of amyloid aggregation of lowly amyloid-prone proteins (Section 7.3.3) or to the possible destabilisation of non-amyloid proteins by nanoparticles targeted against unstable peptides. Indeed, anti-amyloid nano-agents must avoid aggregating other protein and/or biomolecules to be considered as efficient *in vivo*.

In this thesis we have identified the role of charge distribution on the molecular toxicity of nanomaterials. Moreover we have demonstrated that a defined distribution of charges at the nanomaterial surface can induce different effects on different biomolecules. Therefore, any new nano-therapeutic agent should be tested against an extensive range of biomolecules found in human fluids even if its constituent atoms are classically considered as not toxic.

9. Perspective

Nanomaterial properties make them excellent drug delivery systems because of their capacity to penetrate and distribute in every living organism and cellular compartment. Coupling these passive properties of nanomaterials with their capacity to specifically interact with pathogenic proteins could make them very interesting tagging agents. Furthermore, by using superparamagnetic nanoparticles targeted against pathological proteins one could envisage to specifically remove these proteins from living organisms.

Using controlled charge distribution technologies specific nanoscale coating could be developed for implant, and other bionic systems. Indeed, the surface of implants could be treated to have a nanoscale-controlled charge distribution in order to enhance their immunostealth properties and to prevent formation of protein aggregates at their surface. This would improve the lifespan of bionic systems and prevent the formation of thrombus in patient blood.

10. Conclusions

1. The impact on protein structure of charge distribution at the nanomaterial surface demonstrates the capacity of proteins to interact in a specific manner with chemical groups at the nanomaterial surface. This phenomenon can be explained by electrostatic attraction between opposite charges.
2. Because of the high complexity and variety of proteins the effect of a given nanomaterial will change drastically from one protein to another.
3. Understanding the effect of nanoparticle charge distribution on proteins involved in the pathological mechanism of certain diseases could help design novel therapeutics, based on nanomaterials.

11.References

1. Brookmeyer, R., et al., *Forecasting the global burden of Alzheimer's disease.* Alzheimers & Dementia, 2007. **3**(3): p. 186-191.
2. Berrios, G.E., *Alzheimer's disease: A conceptual history.* International Journal of Geriatric Psychiatry, 1990. **5**(6): p. 355-365.
3. Parihar, M.S. and G.J. Brewer, *Amyloid-beta as a modulator of synaptic plasticity.* Journal of Alzheimers Disease, 2010. **22**(3): p. 741-763.
4. Parkinson, J., *An essay on the shaking palsy (Reprinted).* Journal of Neuropsychiatry and Clinical Neurosciences, 2002. **14**(2): p. 223-236.
5. Lees, A.J., *Unresolved issues relating to the shaking palsy on the celebration of James Parkinson's 250th birthday.* Movement Disorders, 2007. **22**(Suppl 17): p. 327-334.
6. Sipe, J.D. and A.S. Cohen, *Review: History of the amyloid fibril.* Journal of Structural Biology, 2000. **130**(2-3): p. 88-98.
7. Hardy, J., *Expression of normal sequence pathogenic proteins for neurodegenerative disease contributes to disease risk: 'permissive templating' as a general mechanism underlying neurodegeneration.* Biochemical Society Transactions, 2005. **33**(4): p. 578-581.
8. Chiti, F. and C.M. Dobson, *Protein misfolding, functional amyloid, and human disease.* Annual Review of Biochemistry, 2006. **75**: p. 333-366.
9. Dobson, C.M., *Protein misfolding, evolution and disease.* Trends in Biochemical Sciences, 1999. **24**(9): p. 329-332.
10. Hartmann, T., et al., *Distinct sites of intracellular production for Alzheimer's disease A beta 40/42 amyloid peptides.* Nature Medicine, 1997. **3**(9): p. 1016-1020.
11. Riddell, D.R., et al., *Compartmentalization of beta-secretase (Asp2) into low-buoyant density, noncaveolar lipid rafts.* Current Biology, 2001. **11**(16): p. 1288-1293.
12. Cookson, M.R., *alpha-Synuclein and neuronal cell death.* Molecular Neurodegeneration, 2009. **4**: p. 9.
13. Iwai, A., et al., *The precursor protein of non-A-beta component of Alzheimer's disease amyloid is a presynaptic protein of the central-nervous-system.* Neuron, 1995. **14**(2): p. 467-475.

14. Zhu, M., et al., *Alpha-synuclein can function as an antioxidant preventing oxidation of unsaturated lipid in vesicles.* Biochemistry, 2006. **45**(26): p. 8135-8142.
15. Bonini, N.M. and B.I. Glasson, *Snaring the function of alpha-synuclein.* Cell, 2005. **123**(3): p. 359-361.
16. Sandal, M., et al., *Conformational equilibria in monomeric alpha-synuclein at the single-molecule level.* Plos Biology, 2008. **6**(1): p. 99-108.
17. Kim, H.Y., et al., *Correlation of amyloid fibril beta-structure with the unfolded state of alpha-synuclein.* Chembiochem, 2007. **8**(14): p. 1671-1674.
18. Kedar, I., M. Ravid, and E. Sohar, *In vitro synthesis of amyloid fibrils from insulin, calcitonin and parathormone.* Israel Journal of Medical Sciences, 1976. **12**(10): p. 1137-1140.
19. Moore, R.A., et al., *Amyloid formation via supramolecular peptide assemblies Spectroscopic studies on native and protofibrillar insulin.* Biochemistry, 2007. **46**(24): p. 7079.
20. Wegiel, J., et al., *Promotion of synthetic amyloid beta-peptide fibrillization by cell culture media and cessation of fibrillization by serum.* Neuroscience Letters, 1996. **211**(3): p. 151-154.
21. Rosemberg, A. and J. Enberg, *Studies of hydrogen exchange in proteins 2: Reversible thermal unfolding of chymotrypsinogen A as studied by exchange kinetics.* Journal of Biological Chemistry, 1969. **244**(22): p. 6153-&.
22. Kusumoto, Y., et al., *Temperature dependence of amyloid beta-protein fibrillization.* Proceedings of the National Academy of Sciences of the United States of America, 1998. **95**(21): p. 12277-12282.
23. Mazor, Y., et al., *Identification and characterization of a novel molecular-recognition and self-assembly domain within the islet amyloid polypeptide.* Journal of Molecular Biology, 2002. **322**(5): p. 1013-1024.
24. Porat, Y., et al., *The human islet amyloid polypeptide forms transient membrane-active prefibrillar assemblies.* Biochemistry, 2003. **42**(37): p. 10971-10977.
25. Sellin, D., et al., *Suppression of IAPP fibrillation at anionic lipid membranes via IAPP-derived amyloid inhibitors and insulin.* Biophysical Chemistry, 2010. **150**(1-3): p. 73-79.

26. Sharp, J.S., J.A. Forrest, and R.A.L. Jones, *Surface denaturation and amyloid fibril formation of insulin at model lipid-water interfaces.* Biochemistry, 2002. **41**(52): p. 15810-15819.
27. Waxman, E.A., J.R. Mazzulli, and B.I. Giasson, *Characterization of hydrophobic residue requirements for alpha-synuclein fibrillization.* Biochemistry, 2009. **48**(40): p. 9427-9436.
28. Du, H.N., et al., *A peptide motif consisting of glycine, alanine, and valine is required for the fibrillization and cytotoxicity of human alpha-synuclein.* Biochemistry, 2003. **42**(29): p. 8870-8878.
29. Nilsberth, C., et al., *The 'Arctic' APP mutation (E693G) causes Alzheimer's disease by enhanced A beta protofibril formation.* Nature Neuroscience, 2001. **4**(9): p. 887-893.
30. Citron, M., et al., *Mutation of the beta-amyloid precursor protein In familial Alzheimer's disease increases beta-protein production.* Nature, 1992. **360**(6405): p. 672-674.
31. Go, N., *The consistency principle in protein-structure and pathways of folding.* Advances in Biophysics, 1984. **18**: p. 149-164.
32. Nguyen, J., et al., *Prion protein-peptides induce alpha-helix to beta-sheet conformational transitions.* Biochemistry, 1995. **34**(13): p. 4186-4192.
33. Zhu, L., et al., *Relationship between stability of folding intermediates and amyloid formation for the yeast prion Ure2p: A quantitative analysis of the effects of pH and buffer system.* Journal of Molecular Biology, 2003. **328**(1): p. 235-254.
34. Kayed, R., et al., *Permeabilization of lipid bilayers is a common conformation-dependent activity of soluble amyloid oligomers in protein misfolding diseases.* Journal of Biological Chemistry, 2004. **279**(45): p. 46363-46366.
35. Reches, M., Y. Porat, and E. Gazit, *Amyloid fibril formation by pentapeptide and tetrapeptide fragments of human calcitonin.* Journal of Biological Chemistry, 2002. **277**(38): p. 35475-35480.
36. Pace, C.N. and J.M. Scholtz, *A helix propensity scale based on experimental studies of peptides and proteins.* Biophysical Journal, 1998. **75**(1): p. 422-427.
37. Zhang, S., et al., *The Alzheimer's peptide A beta adopts a collapsed coil structure in water.* Journal of Structural Biology, 2000. **130**(2-3): p. 130-141.

38. Pastor, M.T., A. Esteras-Chopo, and L. Serrano, *Hacking the code of amyloid formation the amyloid stretch hypothesis.* Prion, 2007. **1**(1): p. 9-14.
39. Padrick, S.B. and A.D. Miranker, *Islet amyloid: Phase partitioning and secondary nucleation are central to the mechanism of fibrillogenesis.* Biochemistry, 2002. **41**(14): p. 4694-4703.
40. Senguen, F.T., et al., *Clarifying the influence of core amino acid hydrophobicity, secondary structure propensity, and molecular volume on amyloid-beta 16-22 self-assembly.* Molecular Biosystems, 1984. **7**(2): p. 497-510.
41. Schmechel, A., et al., *Alzheimer beta-amyloid homodimers facilitate A beta fibrillization and the generation of conformational antibodies.* Journal of Biological Chemistry, 2003. **278**(37): p. 35317-35324.
42. Vaden, T.D., S.A.N. Gowers, and L.C. Snoek, *Observation of beta-sheets aggregation in a gas-phase Tau-peptide dimer.* Journal of the American Chemical Society, 2009. **131**(7): p. 2472-2474.
43. Chauhan, V.P.S., et al., *Binding of gelsolin, a secretory protein, to amyloid beta-protein.* Biochemical and Biophysical Research Communications, 1999. **258**(2): p. 241-246.
44. Lomakin, A., et al., *On the nucleation and growth of amyloid beta-protein fibrils: Detection of nuclei and quantitation of rate constants.* Proceedings of the National Academy of Sciences of the United States of America, 1996. **93**(3): p. 1125-1129.
45. Harper, J.D., et al., *Assembly of A beta amyloid protofibrils: An in vitro model for a possible early event in Alzheimer's disease.* Biochemistry, 1999. **38**(28): p. 8972-8980.
46. Ohnishi, S., A. Koide, and S. Koide, *The roles of turn formation and cross-strand interactions in fibrillization of peptides derived from the OspA single-layer beta-sheet.* Protein Science, 2001. **10**(10): p. 2083-2092.
47. Blackley, H.K.L., et al., *Morphological development of beta(1-40) amyloid fibrils.* Experimental Neurology, 1999. **158**(2): p. 437-443.
48. Blackley, H.K.L., et al., *In-situ atomic force microscopy study of beta-amyloid fibrillization.* Journal of Molecular Biology, 2000. **298**(5): p. 833-840.

49. Jones, E.M. and W.K. Surewicz, *Fibril conformation as the basis of species- and strain-dependent seeding specificity of mammalian prion amyloids.* Cell, 2005. **121**(1): p. 63-72.
50. Gobbi, M., et al., *Gerstmann-Strarussler-Scheinker disease amyloid protein polymerizes according to the "dock-and-lock" model.* Journal of Biological Chemistry, 2006. **281**(2): p. 843-849.
51. Avidan-Shpalter, C. and E. Gazit, *The early stages of amyloid formation: Biophysical and structural characterization of human calcitonin pre-fibrillar assemblies.* Amyloid: Journal Of Protein Folding Disorders, 2006. **13**(4): p. 216-225.
52. DeMarco, M.L. and V. Daggett, *From conversion to aggregation: Protofibril formation of the prion protein.* Proceedings of the National Academy of Sciences of the United States of America, 2004. **101**(8): p. 2293-2298.
53. Zampagni, M., et al., *Lipid rafts are primary mediators of amyloid oxidative attack on plasma membrane.* Journal of Molecular Medicine, 2010. **88**(6): p. 597-608.
54. Giasson, B.I., et al., *Initiation and synergistic fibrillization of tau and alpha-synuclein.* Science, 2003. **300**(5619): p. 636-640.
55. Necula, M. and J. Kuret, *Pseudophosphorylation and glycation of tau protein enhance but do not trigger fibrillization in vitro.* Journal of Biological Chemistry, 2004. **279**(48): p. 49694-49703.
56. Butterfield, D.A., *Amyloid beta-peptide (1-42)-induced oxidative stress and neurotoxicity: Implications for neurodegeneration in Alzheimer's disease brain. A review.* Free Radical Research, 2002. **36**(12): p. 1307-1313.
57. Rosen, G.M., M.J. Barber, and E.J. Rauckman, *Disruption of erythrocyte membranal organization by superoxide.* Journal of Biological Chemistry, 1983. **258**(4): p. 2225-2228.
58. Tabner, B.J., J. Mayer, and D. Allsop, *Hypothesis: Soluble Ab oligomers in association with redox-active metal ions are the optimal generators of reactive oxygen species in Alzheimer's disease.* International Journal of Alzheimer's Disease, 2011. **2011**(2011).
59. Tayler, H., et al., *Oxidative balance in Alzheimer's disease: Relationship to APOE, Braak tangle stage, and the concentrations of soluble and insoluble amyloid-beta.* Journal of Alzheimers Disease, 2010. **22**(4): p. 1363-1373.

60. Kruman, I., et al., *Evidence that 4-hydroxynonenal mediates oxidative stress-induced neuronal apoptosis.* Journal of Neuroscience, 1997. **17**(13): p. 5089-5100.
61. Lowell, M.A. and W.R. Markesbery, *Amyloid β peptide, 4-hydroxynonenal, and apoptosis.* Current Alzheimer Research, 2006. **3**(4): p. 359-364.
62. Mattson, M.P. and S.L. Chan, *Neuronal and glial calcium signaling in Alzheimer's disease.* Cell Calcium, 2003. **34**(4-5): p. 385-397.
63. Pedersen, W.A., et al., *Corticotropin-releasing hormone protects neurons against insults relevant to the pathogenesis of Alzheimer's disease.* Neurobiology of Disease, 2001. **8**(3): p. 492-503.
64. Pacher, P., J.S. Beckman, and L. Liaudet, *Nitric oxide and peroxynitrite in health and disease.* Physiological Reviews, 2007. **87**(1): p. 315-424.
65. Poole, C.P. and F.J. Owens, *Introduction to nanotechnology*. 2003: Wiley-interscience, Hoboken, United States of America. 388.
66. Molitor, F., et al., *Electronic properties of graphene nanostructures.* Journal of Physics: Condensed Matter, 2011. **23**(24): p. 243201.
67. Yu, M.-F., et al., *Strength and breaking mechanism of multiwalled carbon nanotubes under tensile load.* Science 2000. **287**(5453): p. 637-640.
68. Tang, Z.K., et al., *Superconductivity in 4 angstrom single-walled carbon nanotubes.* Science 2001. **292**(5526): p. 2462-24-65.
69. Sinha, S., et al., *Off-axis thermal properties of carbon nanotube films.* Journal of Nanoparticle Research, 2005. **7**(6): p. 651-657.
70. Pop, E., et al., *Thermal conductance of an individual single-wall carbon nanotube above room temperature.* Nano Letters, 2005. **6**(1): p. 96-100.
71. Thostenson, E., C. Li, and T. Chou, *Nanocomposites in context.* Composites Science and Technology, 2005. **65**(3-4): p. 491-516.
72. Prato, M., V. Lucchini, and M. Maggini, *Energetic preference in 5,6 and 6,6 ring junction adducts of C60: fulleroids and methanofullerenes.* Journal of the American Chemical Society, 1993. **115**(18): p. 8479.
73. Wallace, P.R., *The band theory of graphite.* Physical Review, 1947. **71**(9): p. 622.
74. Buhro, W.E. and V. Colvin, *Semiconductor nanocrystals: Shape matters.* Nature Materials, 2003. **2**(3): p. 138-139.

75. Eustis, S. and M.A. el-Sayed, *Why gold nanoparticles are more precious than pretty gold: Noble metal surface plasmon resonance and its enhancement of the radiative and nonradiative properties of nanocrystals of different shapes.* Chemical Society Reviews 2006. **35**(3): p. 209-217.
76. Gubin, S.P., *Magnetic nanoparticles*. 2009: Wiley-VCH Weinheim Germany.
77. Zhong, X.L., W.L.E. Wong, and M. Gupta, *Enhancing strength and ductility of magnesium by integrating it with aluminum nanoparticles.* Acta Materialia, 2007. **55**(18): p. 6338-6344.
78. Cao, A. and G. Veser, *Exceptional high-temperature stability through distillation-like self-stabilization in bimetallic nanoparticles.* Nature Materials, 2010(9): p. 75-81.
79. Binks, B.P. and T.S. Horozov, *Colloidal Particles at Liquid Interfaces*. 1 ed. 2006: Cambridge University Press. . 518.
80. Avouris, P., Z. Chen, and V. Perebeinos, *Carbon-based electronics.* Nature Nanotechnology 2007. **2**(10): p. 605-615.
81. Britnell, L., et al., *Field-effect tunneling transistor based on vertical graphene heterostructures.* Science, 2012. **335**(6071): p. 947-950.
82. Stoller, M.D., et al., *Graphene-based ultracapacitors.* Nano Letters, 2008. **8**(10): p. 3498-3502.
83. Ni, G.X., et al., *Graphene-ferroelectric hybrid structure for flexible transparent electrodes.* ACS Nano, 2012. **6**(5): p. 3935-3942.
84. Giovanni, M., A. Bonanni, and M. Pumera, *Detection of DNA hybridization on chemically modified graphene platforms.* The Analyst 2012. **137**(3): p. 580-583.
85. Tan, Y.W., et al., *Measurement of scattering rate and minimum conductivity in graphene.* Physical Review Letters, 2007. **99**(24): p. 246803.
86. Liu, M., et al., *A graphene-based broadband optical modulator.* Nature, 2011. **474**(7349): p. 64-67.
87. Hsu, C.L., et al., *Layer-by-layer graphene/TCNQ stacked films as conducting anodes for organic solar cells.* ACS Nano, 2012. **6**(6): p. 5031–5039.
88. Mannoor, M.S., et al., *Graphene-based wireless bacteria detection on tooth enamel.* Nature Communications, 2012. **3**(763).
89. Arora, A. and G.W. Padua, *Review: nanocomposites in food packaging.* Journal of Food Science, 2010. **75**(1): p. 43-49.

90. Rawson, P.S., *Ceramics*. 1984: University of Pennsylvania Press, Philadelphia, United States of America.
91. Faraday, M., *Experimental relations of gold (and other metals) to light.* Philosophical Transactions of the Royal Society of London, 1857. **147**: p. 145-181.
92. Norris, D.J. and M.G. Bawendi, *Measurement and assignment of the size-dependent optical spectrum in CdSe quantum dots.* Physical Review B: Condensed Matter 1996. **53**(24): p. 16338-16346.
93. Nagarajan, R. and A.T. Hatton, *Nanoparticles: Synthesis, stabilization, passivation, and functionalization*. Vol. 996. 2008: American Chemical Society, Washington D.C., United States of America.
94. Birdi, K.S., *Handbook of surface and colloid chemistry*. 3 ed. 2008: CRC Press, Boca Raton, United States of America. 756.
95. Yang, P., A.R. Tao, and S. Habas, *Shape control of colloidal metal nanocrystals.* Small, 2008. **4**(3): p. 310-325.
96. Gur, I., et al., *Air-stable all-inorganic nanocrystal solar cells processed from solution.* Science, 2005. **310**(5745): p. 462-465.
97. Xu, L.P., S. Pradhan, and S. Chen, *Adhesion force studies of Janus nanoparticles.* Langmuir, 2007. **23**(16): p. 8544-8548.
98. Paulo, C.S., R. Pires das Neves, and L. Ferreira, *Nanoparticles for intracellular-targeted drug delivery.* Nanotechnology, 2011. **22**(49): p. 494002.
99. Rao, J., *Shedding light on tumors using nanoparticles.* ACS nano, 2008. **2**(10): p. 1984-1986.
100. Vanmaekelbergh, D. and P. Liljeroth, *Electron-conducting quantum dot solids: novel materials based on colloidal semiconductor nanocrystals.* Chemical Society Reviews, 2005. **34**(4): p. 299-312.
101. Joung, S., et al., *Facile synthesis of uniform large-sized InP nanocrystal quantum dots using tris(tert-butyldimethylsilyl)phosphine.* Nanoscale Research Letters, 2012. **7**(1): p. 93.
102. Maune, B.M., et al., *Coherent singlet-triplet oscillations in a silicon-based double quantum dot.* Nature, 2012. **481**(7381): p. 344-347.
103. De Franceschi, S., et al., *Hybrid superconductor-quantum dot devices.* Nature Nanotechnology, 2010. **5**(10): p. 703-711.

104. Cheng, G., et al., *Sketched oxide single-electron transistor.* Nature Nanotechnology, 2011. **6**(6): p. 343-347.
105. Usami, N., et al., *Simultaneous enhanced photon capture and carrier generation in Si solar cells using Ge quantum dot photonic nanocrystals.* Nanotechnology, 2012. **23**(18): p. 185401.
106. Wang, X., et al., *Doped quantum dots for white-light-emitting diodes without reabsorption of multiphase phosphors.* Advanced Materials, 2012. **24**(20): p. 2742-2747.
107. Dang, C., et al., *Red, green and blue lasing enabled by single-exciton gain in colloidal quantum dot films.* Nature Nanotechnology, 2012. **7**(5): p. 335-339.
108. Muller-Borer, B.J., et al., *Quantum dot labeling of mesenchymal stem cells.* Journal of Nanobiotechnology, 2007(5): p. 9.
109. Singh, N., et al., *Effect of nanoparticle conjugation on gene silencing by RNA interference.* Journal of the American Chemical Society, 2010. **132**(24): p. 8241-8243.
110. Herzing, A.A., et al., *Identification of active gold nanoclusters on iron oxide supports for CO oxidation.* Science, 2008. **321**(5894): p. 1331-1335.
111. Miyagawa, H., M. Misra, and A.K. Mohanty, *Mechanical properties of carbon nanotubes and their polymer nanocomposites.* Journal of Nanoscience and Nanotechnology, 2005. **5**(10): p. 1593-1615.
112. Morimoto, Y., et al., *Hazard assessments of manufactured nanomaterials.* The Journal of Occupational Health, 2010. **52**(6): p. 325-334.
113. Labille, J. and J. Brant, *Stability of nanoparticles in water.* Nanomedicine 2010. **5**(6): p. 985-998.
114. Quadros, M.E. and L.C. Marr, *Environmental and human health risks of aerosolized silver nanoparticles.* Journal of the Air & Waste Management Association, 2010. **60**(7): p. 770-781.
115. Schade, R., et al., *Biomimetic organic-inorganic nanocomposite coatings for titanium implants. In vitro and in vivo biological testing.* Journal of Biomedical Materials Research Part A, 2010. **95**(3): p. 691-700.
116. Labouta, H.I., et al., *Mechanism and determinants of nanoparticle penetration through human skin.* Nanoscale, 2011. **3**(12): p. 4989-4999.
117. Andujar, P., et al., *Respiratory effects of manufactured nanoparticles.* Revue des Maladies Respiratores 2011. **28**(8): p. 66-75.

118. Fröhlich, E. and E. Roblegg, *Models for oral uptake of nanoparticles in consumer products.* Toxicology, 2012. **291**(1-3): p. 10-17.
119. Powell, J.J., et al., *Origin and fate of dietary nanoparticles and microparticles in the gastrointestinal tract.* Journal of Autoimmunity, 2010. **34**(3): p. 226-233.
120. Almeida, J.P., et al., *In vivo biodistribution of nanoparticles.* Nanomedicine 2011. **6**(5): p. 815-835.
121. Sharma, H.S. and A. Sharma, *Nanoparticles aggravate heat stress induced cognitive deficits, blood-brain barrier disruption, edema formation and brain pathology.* Progress in Brain Research, 2007. **162**: p. 245-273.
122. Zahmakiran, M. and S. Ozkar, *Metal nanoparticles in liquid phase catalysis; from recent advances to future goals.* Nanoscale, 2011. **3**(9): p. 3462-3481.
123. Sau, T.K., et al., *Properties and applications of colloidal nonspherical noble metal nanoparticles.* Advanced Materials, 2010. **22**(16): p. 1805-1825.
124. Chen, N., et al., *The cytotoxicity of cadmium-based quantum dots.* Biomaterials, 2012. **33**(5): p. 1238-1244.
125. Kane, A.B. and R.H. Hurt, *Nanotoxicology: The asbestos analogy revisited.* Nature Nanotechnology, 2008. **3**(7): p. 378-379.
126. Boraschi, D., L. Costantino, and P. Italiani, *Interaction of nanoparticles with immunocompetent cells: Nanosafety considerations.* Nanomedicine, 2012. **7**(1): p. 121-131.
127. Goncalves, D.M., R. de Liz, and D. Girard, *Activation of neutrophils by nanoparticles.* ScientificWorldJournal, 2011. **11**: p. 1877-1885.
128. Abdelhalim, M.A. and B.M. Jarrar, *Histological alterations in the liver of rats induced by different gold nanoparticle sizes, doses and exposure duration.* Journal of Nanobiotechnology. , 2012. **10**: p. 5.
129. Gaunt, J.A., et al., *Stability and quantum yield effects of small molecule additives on solutions of semiconductor nanoparticles.* Journal of Colloid and Interface Science, 2005. **290**(2): p. 437-443.
130. Kirchner, C., et al., *Cytotoxicity of colloidal CdSe and CdSe/ZnS nanoparticles.* Nano Lett. , 2005. **5**(2): p. 331-338.
131. Fubini, B., M. Ghiazza, and I. Fenoglio, *Physico-chemical features of engineered nanoparticles relevant to their toxicity.* Nanotoxicology, 2010. **4**: p. 347-363.

132. Vanlangenakker, N., et al., *Molecular mechanisms and pathophysiology of necrotic cell death.* Current Molecular Medicine, 2008. **8**(3): p. 207-220.
133. Toyokuni, S., *Reactive oxygen species-induced molecular damage and its application in pathology.* Pathology International, 1999. **49**(2): p. 91-102.
134. Simbula, G., et al., *Increased ROS generation and p53 activation in alpha-lipoic acid-induced apoptosis of hepatoma cells.* Apoptosis, 2007. **12**(1): p. 113-123.
135. Song, M.F., et al., *Metal nanoparticle-induced micronuclei and oxidative DNA damage in mice.* Journal of Clinical Biochemistry and Nutrition, 2012. **50**(3): p. 211-216.
136. Dominguez-Medina, S., et al., *In situ measurement of bovine serum albumin interaction with gold nanospheres.* Langmuir, 2012. **28**(24): p. 9131-9139.
137. Gebauer, J.S., et al., *Impact of the Nanoparticle–Protein Corona on Colloidal Stability and Protein Structure.* Langmuir, 2012: p. 9673-9679.
138. Skaat, H., et al., *Effect of maghemite nanoparticles on insulin amyloid fibril formation: selective labeling, kinetics, and fibril removal by a magnetic field.* J. Biomed. Mater. Res. A., 2009. **91**(2): p. 342-351.
139. Xiao, L., et al., *Inhibition of beta 1-40 amyloid fibrillation with N-acetyl-L-cysteine capped quantum dots.* Biomaterials, 2010. **31**(1): p. 91.
140. Wu, W.H., et al., *TiO2 nanoparticles promote beta-amyloid fibrillation in vitro.* Biochem. Biophys. Res. Commun. , 2008. **373**(2): p. 315-318.
141. Peng, A.Z. and X. Peng, *Formation of high-quality Cdte, CdSe and CdS nanocrystals using CdO as precursor.* J. Am. Chem. Soc., 2001. **123**(1): p. 183-184.
142. Talapin, D.V., et al., *Highly luminescent monodisperse CdSe and CdSe/ZnS nanocrystals synthesized in a hexadecylamine-trioctylphosphine oxide-trioctylphosphine mixture.* Nano Lett., 2001. **1**(4): p. 207-211.
143. Fasman, G.D., *Circular dichroism and the conformational analysis of biomolecules*. 1996: Plenum press.
144. Meierhenrich, U.J., et al., *Circular dichroism of amino acids in the vaccum-ultraviolet region.* Angewandte Chemie (International Edition in English), 2010. **49**(42): p. 7799-7802.
145. Sehgal, R.K., et al., *Synthesis and biological properties of actinomycin D chromophoric analogues substitutes at the 7-carbon with aziridine and*

aminopropoxy functions. Journal of Medicinal Chemistry, 1987. **30**(9): p. 1626-1631.

146. Fiallo, M.M., et al., *Circular dichroism studies on anthracycline antitumor compounds. Relationship between the molecular structure and the spectroscopic data.* Journal of Pharmaceutical Sciences, 1998. **87**(8): p. 967-975.
147. Benditt, E.P., N. Eriksen, and B. C., *Congo red dichroism with dispersed amyloid fibrils, an extrinsic cotton effect.* Proceedings Of The National Academy Of Sciences Of The United States Of America, 1970(66): p. 1044-51.
148. Dzionara, M., *Ribosomal proteins. Secondary structure of individual ribosomal proteins of E. coli studied by circular dichroism.* FEBS Letters, 1970. **8**(4): p. 197-200.
149. Greenfield, N.J., *Using circular dichroism spectra to estimate protein secondary structure.* Nature Protocols, 2006. **1**(6): p. 2876-2890.
150. Whitmore, L. and B.A. Wallace, *Protein secondary structure analyses from circular dichroism spectroscopy: methods and reference databases.* Biopolymers, 2007. **89**(5): p. 392-400.
151. Berner, B.J. and R. Pecora, *Dynamic light scattering: with applications to chemistry, biology, and physics*. 2000: Dover edition.
152. Liu, T. and B. Chu, *Light-scattering by proteins*, in *Encyclopedia of Surface and Colloid Science,* A.T. Hubbard, Editor. 2002, Marcel Dekker. p. 3023-3043.
153. Frisken, B.J., *Revisiting the method of cumulants for the analysis of dynamic light-scattering data.* Applied Optics, 2001. **40**(24): p. 4087-4091.
154. Provencher, S.W., *CONTIN: a general purpose constrained regularization program for inverting noisy linear algebraic and integral equations.* Computer Physics Communications, 1982(27): p. 229-242.
155. Philo, J.S., *Is any measurement method optimal for all aggregate sizes and types?* The AAPS Journal, 2006. **8**(3): p. 564-571.
156. Nobbmann, U., et al., *Dynamic light scattering as a relative tool for assessing the molecular integrity and stability of monoclonal antibodies.* Biotechnology and Genetic Engineering Reviews, 2007. **24**: p. 117-128.

157. O'Brien, R.W. and L.R. White, *Electrophoretic mobility of a spherical colloidal particle.* Journal of the Chemical Society, Faraday Transactions 2, 1978(74): p. 1607-1626.
158. Doane, T.L., et al., *Nanoparticles ζ-potentials.* Accounts of Chemical Research, 2011. **45**(3): p. 317-326.
159. Sukhanova, A., et al., *Highly stable fluorescent nanocrystals as a novel class of labels for immunohistochemical analysis of paraffin-embedded tissue sections.* Lab. Invest., 2002. **82**(9): p. 1259-1261.
160. Rakovich, A., et al., *Resonance energy transfwer improves the biological function of Bacteriorhodopsin within a hybrid material built from purple membranes and semiconductor quantum dots.* Nano Lett., 2010. **10**: p. 2640-2648.
161. Loksztejn, A. and W. Dzwolak, *Chiral bifurcation in aggregating insulin: an induced circular dichroism study.* Journal of Molecular Biology, 2008. **379**(1): p. 9.
162. LeVine, H., *Thioflavin T interaction with synthetic Alzheimer's disease beta-amyloid peptides: detection of amyloid aggregation in solution.* Protein Science, 1993. **2**(3): p. 404-10.
163. Bouchard, M., J. Zurdo, and E.J. Nettleton, *Formation of insulin amyloid fibrils followed by FITR simultaneously with CD and electron microscopy.* Protein Science, 2000(10): p. 1960-7.
164. Wagner, S.C., M. Roskamp, and M. Pallerla, *Nanoparticles-induced folding and fibril formation of coiled-coil-based model peptides.* Small, 2010(6): p. 1321-8.
165. Yoo, E.J., et al., *Size-dependent flocculation behavior of colloidal Au nanoparticles modified with various biomolecules.* Ultramicroscopy, 2008. **108**(10): p. 1273-1277.
166. Nabiev, I., et al., *Nonfunctionalized nanocrystals can exploit a cell's active transport machinery delivering them to specific nuclear and cytoplasmic compartments.* Nano Lett., 2007. **7**(11): p. 3452-3461.
167. Elsaesser, A. and C.V. Howard, *Toxicology of nanoparticles.* Adv Drug Deliv Rev, 2012. **64**(2): p. 129-137.

168. Klein, J., *Probing the interactions of proteins and nanoparticles.* Proceedings of the National Academy of Sciences, 2007. **104**: p. 2029-2030.
169. Lück, M. and B. Paulke, *Analysis of plasma protein adsorption on polymeric nanoparticles with different surface characteristics.* Journal of biomedical …, 1998: p. 478-485.
170. W., N., *Adsorption of proteins from solution at the solid-liquid interface.* Adv Colloid Interface Sci., 1986. **25**(4): p. 267-340.
171. Haynes, C.A. and W. Norde, *Globular proteins at solid/liquid interfaces.* Colloid. Surface. B. , 1994. **2**(6): p. 517–566.
172. Yang, Q., J. Liang, and H. Han, *Probing the interaction of magnetic iron oxide nanoparticles with bovine serum albumin by spectroscopic techniques.* The Journal of Physical Chemistry B, 2009. **113**: p. 10454-10458.
173. Balavoine, F., P. Schultz, and C. Richard, *Helical crystallization of proteins on carbon nanotubes: a first step towards the development of new biosensors.* Angewandte Chemie …, 1999: p. 1912-1915.
174. Ohno, Y., et al., *Electrolyte-gated graphene field-effect transistors for detecting pH and protein adsorption.* Nano letters, 2009. **9**: p. 3318-3322.
175. Zorbas, V., et al., *Importance of Aromatic Content for Peptide / Single-Walled Carbon Nanotube Interactions list of prospective applications of SWNTs to biophysical and.* J. Am. Chem. Soc, 2005. **127**: p. 12323-12328.
176. Roth, C.M., B.L. Neal, and A.M. Lenhoff, *Van der Waals interactions involving proteins.* Biophysical journal, 1996. **70**: p. 977-87.
177. Brewer, S.H., et al., *Probing BSA binding to citrate-coated gold nanoparticles and surfaces.* Langmuir, 2005. **21**(20): p. 9303-9307.
178. You, C.-c., et al., *Tunable Inhibition and Denaturation of a-Chymotrypsin with Fabrication of Amino Acid-Functionalized Gold Nano-*. J. Am. Chem. Soc, 2005. **127**: p. 12873-12881.
179. Aubin-Tam, M. and K. Hamad-Schifferli, *Gold nanoparticle-cytochrome c complexes: the effect of nanoparticle ligand charge on protein structure.* Langmuir, 2005: p. 12080-12084.
180. Engel, M.F., A.J. Visser, and C.P.M. van Mierlo, *Adsorption of Bovine a-Lactalbumin on Suspended Solid Nanospheres and Its Subsequent Displacement Studied by NMR Spectroscopy.* Langmuir, 2004. **20**: p. 5530-5538.

181. Fu, Z., et al., *Induced beta-barrel formation of the Alzheimer's Abeta25-35 oligomers on carbon nanotube surfaces: implication for amyloid fibril inhibition.* Biophysical journal, 2009. **97**: p. 1795-803.
182. Wu, W.-H., et al., *TiO2 nanoparticles promote beta-amyloid fibrillation in vitro.* Biochemical and biophysical research communications, 2008. **373**: p. 315-8.
183. Saraiva, A.M., et al., *Randomization of amyloid-ß-peptide(1-42) conformation by sulfonated and sulfated nanoparticles reduces aggregation and cytotoxicity.* Macromol. Biosci., 2010. **10**(10): p. 1152-1163.
184. Linse, S., et al., *Nucleation of protein fibrillation by nanoparticles.* Proceedings of the National Academy of Sciences of the United States of America, 2007. **104**(21): p. 8691.
185. Hortschansky, P., et al., *The aggregation kinetics of Alzheimer's b-amyloid peptide is controlled by stochastic nucleation.* Protein Science, 2005. **14**: p. 1753-1759.
186. Lee, C.-C., et al., *A three-stage kinetic model of amyloid fibrillation.* Biophysical journal, 2007. **92**: p. 3448-58.
187. Kim, J. and D.M. Holtzman, *Medicine. Prion-like behavior of amyloid-beta.* Science (New York, N.Y.), 2010. **330**: p. 918-9.
188. Li, H., et al., *Carbon nanotube inhibits the formation of ß-sheet-rich oligomers of the Alzheimer's amyloid-ß(16-22) peptide.* Biophysical Journal, 2011. **101**(9): p. 2267-2276.
189. Kim, J.E. and M. Lee, *Fullerene inhibits β-amyloid peptide aggregation.* Biochemical and Biophysical Research Communications, 2003. **303**: p. 576-579.
190. Skaat, H. and S. Margel, *Synthesis of fluorescent-maghemite nanoparticles as multimodal imaging agents for amyloid-beta fibrils detection and removal by a magnetic field.* Biochemical and Biophysical Research Communications, 2009. **386**(4): p. 645-9.
191. Liao, Y.H., et al., *Negatively charged gold nanoparticles inhibit Alzheimer's amyloid-β fibrillization, induce fibril dissociation, and mitigate neurotoxicity.* Small, 2012. **8**(23): p. 3631-3639.
192. Lynch, I. and K. Dawson, *Protein-nanoparticle interactions.* Nano Today, 2008. **3**: p. 40-47.

193. Han, S.-H., et al., *Effective screen for amyloid β aggregation inhibitor using amyloid β-conjugated gold nanoparticles.* International Journal of Nanomedicine, 2011. **6**: p. 1-12.
194. Skaat, H., et al., *Effect of maghemite nanoparticles on insulin amyloid fibril formation: selective labeling, kinetics, and fibril removal by a magnetic field.* Journal of Biomedical Materials Research. Part A, 2009. **91**(2): p. 342.
195. Nayak, A., A.K. Dutta, and G. Belfort, *Surface-enhanced nucleation of insulin amyloid fibrillation.* Biochemical and biophysical research communications, 2008. **369**: p. 303-7.
196. Skaat, H., G. Belfort, and S. Margel, *Synthesis and characterization of fluorinated magnetic core-shell nanoparticles for inhibition of insulin amyloid fibril formation.* Nanotechnology, 2009. **20**: p. 225106.
197. Weissleder, M., et al., *Polyclonal human immunoglobulin G labeled with polymeric iron oxide: antibody MR imaging.* Radiology, 1991. **181**(1): p. 245-249.
198. Hwang, W.S. and S.J. Sim, *A strategy for the ultrasensible detection of cancer biomarkers based on the LSPR response of a single AuNP.* J. Nanosci. Nanotechnol., 2011. **11**(7): p. 5651-5656.
199. Iyer, G., et al., *Tracking single proteins in live cells using single-chain antibody fragment-fluorescent quantum dot affinity pair.* Methods Enzymol., 2010. **475**: p. 61-79.
200. Wu, X., et al., *Immunofluorescent labeling of cancer marker Her2 and other cellular targets with semiconductor quantum dots.* Nat. Biotechnol. , 2003. **21**(1): p. 41-46.
201. Panza, F., et al., *Immunotherapy for Alzheimer's disease: from anti-beta-amyloid to tau-based immunization strategies.* Immunotherapy, 2012. **4**(2): p. 213-238.
202. Cimini, A., et al., *Antibody-conjugated PEGylated cerium oxide nanoparticles for specific targeting of Aβ aggregates modulate neuronal survival pathways.* Acta biomaterialia, 2012. **8**: p. 2056-67.
203. Mahmoud, W., et al., *Advanced procedures for labeling of antibodies with quantum dots.* Analytical biochemistry, 2011. **416**: p. 180-5.

204. Hao, R., et al., *Synthesis, functionalization, and biomedical applications of multifunctional magnetic nanoparticles.* Adv Mater., 2010. **22**(25): p. 2729-42.
205. Dumoulin, M., et al., *Single-domain antibody fragments with high conformational stability.* Protein Sci., 2002. **11**(3): p. 500-15.
206. Harmsen, M.M. and H.J. De Haard, *Properties, production, and applications of camelid single-domain antibody fragments.* Appl Microbiol Biotechnol., 2007. **77**(1): p. 13-22.
207. Sukhanova, A., et al., *Oriented conjugates of single-domain antibodies and quantum dots: toward a new generation of ultrasmall diagnostic nanoprobes.* Nanomedicine. , 2012. **8**(4): p. 516-525.
208. Skaat, H. and S. Margel, *Synthesis of fluorescent-maghemite nanoparticles as multimodal imaging agents for amyloid-beta fibrils detection and removal by a magnetic field.* Biochemical and biophysical research communications, 2009. **386**: p. 645-9.
209. Wang, Q., et al., *Alzheimer Abeta(1-42) monomer adsorbed on the self-assembled monolayers.* Langmuir : the ACS journal of surfaces and colloids, 2010. **26**: p. 12722-32.